The Imaging Properties of A Transformation Optics Designed Cooke Triplet

by

Saul Joseph Wiggin

A thesis submitted to the University in partial fulfilment of the requirements for the degree of

Electronic and Electrical Engineering **MPhil**

School of Electronic Engineering and Computer Science

Queen Mary University of London

United Kingdom

Abstract

This thesis proposes to design a Triplet lens using Metamaterials (MTM) and Discrete Transformation Optics (DCT) modelled on the three lens Cooke Triplet. MTMs are artificially engineered materials with values of permittivity and permeability outside the range of naturally occurring materials. Metamaterials suffer from inherent losses and narrowband operation. To overcome these limitations Discrete Coordinate Transformation Optics has been used to design an all-dielectric DCT Triplet. The proposed MTM triplet is matched to free space and it suffers less reflections from the incident waves. The MTM and DCT Triplet can be designed to have a flat surface which would allow greater interoperability with other optical systems. The field of view in the MTM triplet is not limited as it is in the original Cooke Triplet suggesting there is a place for MTM lenses with larger than typical field of view. In this thesis a Cooke Triplet designed using Metamaterials and the Discrete Coordinate Transformation method is analysed as a potential replacement for the original Cooke Triplet lens.

A coordinate system is modelled using grid generation software and ray propagation in optical designers software is used to model the geometry of the MTM Cooke Triplet. An FDTD simulation models the electromagnetic field of the Cooke Triplet, MTM Triplet and All-Dielectric lens with a plane wave, an off axis source and a Gaussian pulse. The lenses are analysed in terms of Seidel aberrations in order to determine the suitability for optical imaging of the MTM Triplet. The lenses are subjected to Zernike analysis of their wavefront aberration to yield further information on the optics of the different lenses. The FDTD simulation, focal lengths, wavefront aberration function and Zernike aberration function on a unit disk and Zernike aberration coefficients show good agreement between the original Cooke Triplet, MTM Triplet and DCT Triplet.

This thesis is a presentation of my original research work. Wherever contributions of others are involved, every effort is made to indicate this clearly, with due references to the literature, and acknowledgement of collaborative research and discussions. This thesis has not been submitted for any degree or other purposes.

Acknowledgements

I'd like to thank the metamaterials community and the antennas and electromagnetics group: Dr. Rui Yang, Dr. Oscar Quevedo-Teruel, Dr. Khalid Rajab, Dr Di Bao, Dr Rhiannon Mitchell-Thomas, Dr Anestis Katsounaros, Dr. Quammer Abbasi, Dr Lianhong Zhang, Dr Yifeng Fan, Dr Tuba Yilmaz, Dr. Alice Pellegrini, Mrs Zhijiao Chen, Mr Alexander Sushko, Dr Rostslav Dubrovka and Dr Rob Donnan. My experience of them during my PhD were extremely positive and a group of people who work tirelessly on a subject which they are passionate about and which promises real benefits to our society. I would also like to thank my friends and family for supporting me spiritually and financially through the process of writing this thesis. This research was funded by a 4 year PhD Cooperative Awards in Science and Technology (CASE) Stipend into Metamaterials and Transformation Optics funded by The Defence Science and Technology Laboratory (DSTL) in partnerships with the Antennas and Electromagnetic Theory Group in the School of Electronic Engineering and Computer Science at Queen Mary, University of London.

Publications

- **Saul J. Wiggin**, Zernike Aberration Deconvolution from the Wavefront in Finite Difference Time Domain Simulations", IET Microwaves, Antennas & Propagation (under submission).

- **Saul J. Wiggin**, Wenxuan Tang, Yang Hao, Rob Foster and Ian Youngs "Multi-Element Optical Systems using Transformation Optics and Metamaterials", Optics Express (under submission).

- **S. J. Wiggin**, W. Tang, Y. Hao and I. Youngs 'A Flat Profile Microwave Lens without Metamaterials using Transformation Optics' META 2012, 19-22 April, Paris, France

- **Saul J. Wiggin**, Wenxuan Tang, Yang Hao and Ian Youngs, 'A Low Aberration Microwave 2D GRIN Lens Antenna Realizable with Dielectrics', DSTL internal conference, Oct 23rd 2011.

Contents

List of Tables

List of Figures

Chapter 1

Introduction

Metamaterials are a new paradigm in materials science which offer the possibility to reshape many current engineering solutions. They are artificially engineered materials which are tailored according to the shape or geometry of there individual elements rather than the traditional chemical composition which naturally occurring materials are made. This make metamaterials particular of interest to electromagnetic engineers who study similar materials used in antennas, frequency selective surfaces and artificial dielectrics. Metamaterials has exploded in recent times as an active research topic following publication of various findings demonstrating fascinating properties such as invisibility (1) and negative refractive index materials (2).

1.1 Negative Index Metamaterials

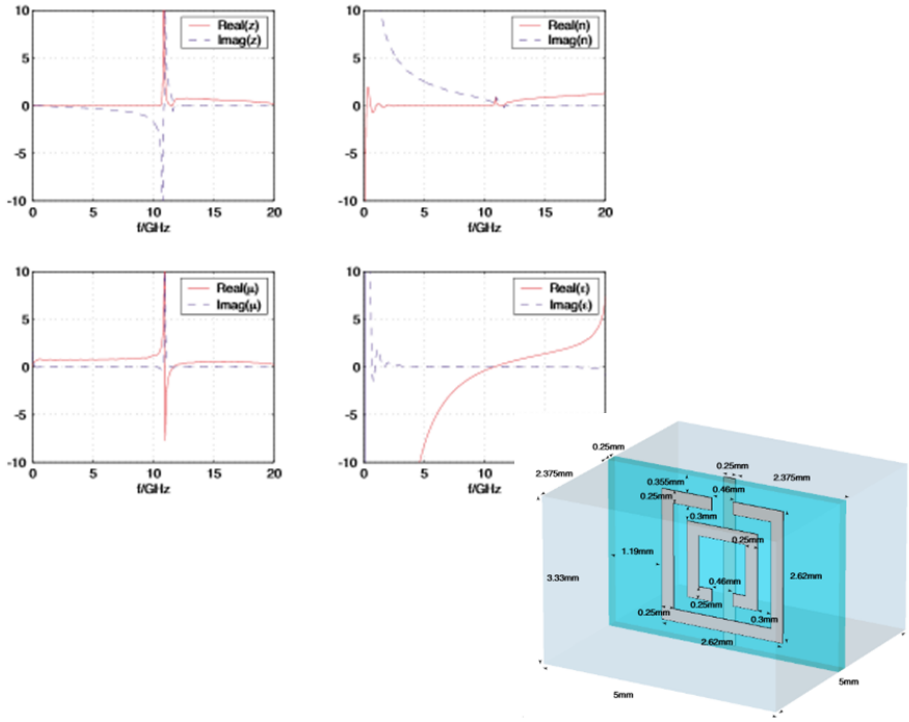

Figure 1.1: This figure shows the real (top-left) and imaginary part (top-right) of the refractive index and the real (bottom-left) and imaginary part (bottom-right) of the Permeability and Permittivity. The Permittivity and Permeability are functions of frequency causing dispersion where this measurement is in the microwave regime centred on 10 GHz. The Metamaterial unit cell has the form of a Split Ring Resonator (SRR) with dimensions: 5 mm by 3.33 mm. The metallic structure is Silver and is placed on a dielectric FR4 and backed with a gold rod (0.25 mm x 3.33 mm). This is a sample SRR Metamaterial used in CST antenna simulations (4).

The first metamaterial was demonstrated, in 2000, by combining a negative permittivity medium, the wire medium, and a negative permeability medium, the split ring resonator (2). An example of a split ring resonator is visible in section 1.1. Pendry's work re-assessed the merits of the wire medium (5) in addition to artificial magnetism from split ring resonators (6). This initiated a long list of novel structures for the construction of Negative impedance materials (NIM) and their applications such as perfect lens section 1.1 of which the omega-structure is the preferred for gain enhancement in low profile antennas (7) compared with traditional split ring resonators. Anisotropic metamaterials made from metallic nano-wire structures also enables negative refraction and focusing (8). Opposing chiral effects in bi-

anisotropic metamaterials such as the omega particles can achieve negative refractive index (9).

The major limitation with bulk NIM metamaterials, which are typically split ring resonators combined with a wire medium, is that it has a very narrow bandwidth. It can only work at a limited band of frequencies. This is due to the fact that the negative permittivity and permeability can only be achieved while the bodies are resonating at a specific frequency. At the resonant frequencies, the material possesses negative permeability and also has a large loss factor. This is sometime known as anomalous resonance, section 1.1. This resonance means that all metamaterials are lossy and operate in a very limited bandwidth around the resonance and this is a key limitation in the technology.

Metamaterials have their origins in the 1960s, when a lot of research was done on artificial dielectrics. A wire medium was demonstrated at RF frequencies leading to a negative refraction below the cut off frequency (10). Lens antennas used artificial dielectrics to focus electromagnetic rays and were used as an alternative for parabolic reflector antennas (11). This was the origin of the wire medium which was then added to by the split ring resonator in the design of a NIM metamaterial. Modern metamaterials research pushes towards the optical regime and relies on the addition of artificial magnetism to provide the combined negative permittivity and permeability to give a negative refractive index.

NIMs can be also designed based on composite right/left-handed transmission line structures (12) which can be achieved with a combination of capacitor and inductor which has been used to experimentally verify perfect imaging in TL-NIM (13). Metamaterials created in transmission lines are not prone to being narrow-band and lossy. Negative Refractive index metamaterials therefore allow demonstration of negative index behaviour without the losses present in bulk materials (14). Evanescent wave growth (15), NIM lens focusing (16) and negative refraction in 2D waves (17) has been experimentally verified in TL-MTM.

A negative index slab of MTM has been simulated and quantified in terms of the Seidel aberrations to define the image quality of an optical system (18; 19). These produce perfect images in negative index optical MTM lenses. This is not perfect in terms of beating the diffraction limit which is a physical law but in the sense that aberrations are minimised. Specifically: a negative index slab lens is able to create an aplanatic image, one with min-

imised Spherical aberration and Coma (20). A perfect lens can magnify using curved boundaries rather than the planar slab and tailoring these curved boundaries (21) to tailor the subwavelength imaging effect.

A lens made from a slab of negative refractive index makes a perfect lens (22). Other methods of achieving subwavelength imaging using metamaterials and transformation optics design techniques include using canalisation (23) and using transformation optics only (24). The first sub-wavelength imaging device (22) used negative index material as opposed to using transformation optics and is made from a combination of split ring resonator arrays and metallic wire arrays to generate the combined negative permittivity and negative permeability required for negative refractive index (25). The negative refractive index lens also known as a perfect lens. A superlens is a similar lens made from transformation optics and metamaterials but it is able to create a focal point far from the surface of the lens which is similar to how a typical glass lens focuses (26). MTMs allows the creation of a perfect imager, without the losses and narrow bandwidth of metamaterials, by controlling the flow of electromagnetic radiation at will. It would improve on existing microscopes and optics and allow the user to see small objects such as real DNA molecules or viruses with the naked eye through a microscope. Another limitation of the NIM superlens is that it operates in the near field. A transformation has allowed focusing in the far-field for a lens known as an optical hyper-lens (27). A perfect imager has been fabricated using only transformation optics and a drain placed at the source (28). Transformation optics can be used for designing superlenses (24) without the need for the metamaterial slab. This super lens which used transformation optics to focus in the far field was developed by the US navy (26) and would overcome the limitations of the NIM superlens which is intrinsically near field.

Plasmonics is the study of the interactions of electromagnetic radiation with metals. These which excite surface particles called plasmons and these offer a way to create metamaterials at optical frequencies. Plasmonics can also offer a route to perfect imaging (30) and time reversal methods have been used to achieve perfect imaging in plasmonic structures (31). A Sievenpiper surface is a artificial surface plasmon (32). A plasma can be classified as a metamaterial and therefore a wire medium can be called an artificial plasma. A silver device was shown to be able to resolve sub-wavelength images (33) in the optical part of the spectrum and the device resolution is wideband. A metal, silver, has a negative permittivity below a certain plasma frequency as does gold 1.1. For optical frequencies this

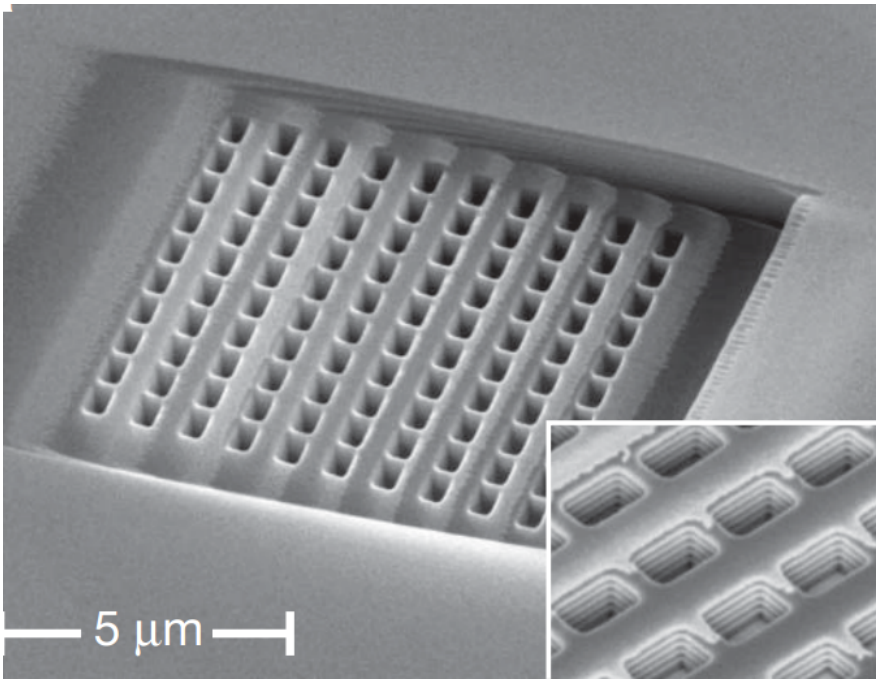

Figure 1.2: A SEM image of a three dimensional optical Metamaterial with a fishnet structure with a unit cell of 860 nm and containing twenty one layers. The structure consists of alternating layers of 30 nm Silver Ag and 50 nm Magnesium Fluoride (MgF_2).
(29)

occurs in silver at wavelengths around 800 nm. Plasmonics offer a route to using resonant metamaterial type structures for optical perfect imaging and energy harvesting devices (34). Transformation optics techniques have been used to transform plasmonic structures to allow for light harvesting applications (35). One group of optical negative index metamaterials are called fish-net structures. This fish-net is made up of dielectric-metal layers with negative refractive index through layers achieved with low loss. The structures overcome the lossiness of bulk metamaterials and are valid at light frequencies for achieving negative refraction using silver.

1.2 The Motivation of Research and Original Contribution

The Cooke Triplet was first designed and patented in 1893 by Dennis Taylor who sold the patent to TT&H Cooke and sons of York. The Cooke Triplet minimises all the primary Seidel aberrations: spherical, coma, astigmatism, distortion and field curvature as well as the chro-

matic aberration. The Cooke triplet uses a combination of two converging lenses of crown glass surrounding a diverging lens of flint glass. The TT&H Cooke lens catalog of 1897 states: Lack of sharp definition at the margins, and blackness and lack of detail in the shadows, are among the commonest defects of photographs. The introduction of lenses which, without the use of stops, yield definition uniformly fine throughout their plates, marks quite a new era in photography, referring to the distortion and vignetting which is reduced in the Cooke triplet.

The Cooke triplet minimises all five Seidel aberrations. In a single structure spherical aberration can be reduced using a combination of concave and convex lenses, off axis aberrations: coma and astigmatism can be reduced by tailoring the lens spacing and field curvature can be reduced by adjusting the lens spacing and use of a stop. Distortion can be controlled by use of a symmetrical system but all can not be minimised without adding more components and this is true generally for optical lens designers. The Cooke triplet is still used to capture images and reduce optical aberrations in a variety of applications today from mass-produced cameras to expensive ones used by the film industry. Aberration-free imaging is achieved theoretically using gradient index lenses such as the Luneburg Lens or Maxwell's fisheye. The range of varying indexes in fish eyes is $\triangle$n = 0.22 compared to $\triangle$n = 0.03 in the human eye. Gradient index manufacturability has lagged behind theoretical developments, the largest gradient index which can be achieved using common ion exchange diffusion technique is $\triangle$n = 0.05, meaning that while in theory gradient index optics (GRIN) might allow aberration free imaging the real GRIN lenses are often not as good in terms of aberrations and standard refractive optical systems such as the Cooke triplet.

Aberrations in a lens image using NIM in optical design might allow mitigation of aberrations easier than with conventionally available materials (40). Gradient index with negative index materials have also been explored (41). A group used meta-surfaces to create a lens with no aberrations at telecom frequencies (42). These researchers at Havard have developed a distortion free flat lens using engineered metasurfaces (42) and have demonstrated the nano sized lens which eliminate distortion by tailoring the meta-elements on the surface. Another group used transformation optics to extend the flat negative index perfect lens and magnify the image into the far-field (27). This hyper-lens has been demonstrated using graphene and dielectric layers (43).

Transformation Optics can be used to improve existing optical systems such as a flat-

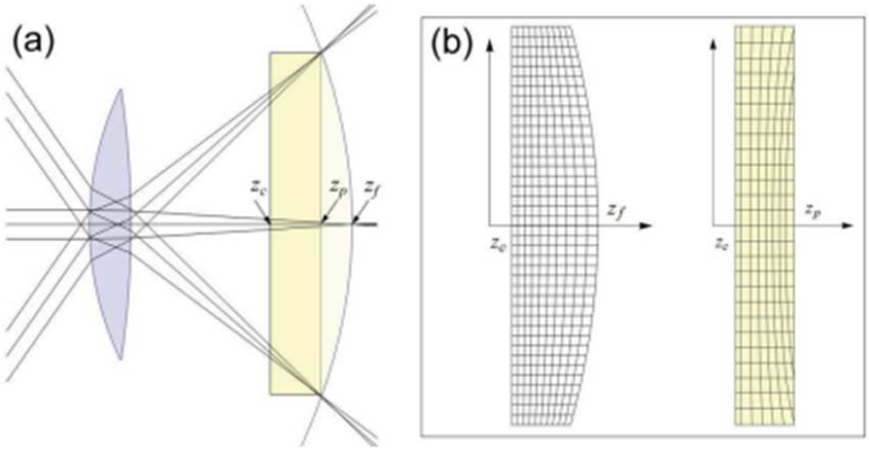

Figure 1.3: A lens designed using transformation optics which improves the Field Curvature in the image (44). (a) The ray diagram for on-axis rays and off-axis rays passing through the lens and then corrected using the transformation media. The focal surface is curved when field curvature is present and results in the focus being different for different angles of incidence on the lens. z_f shows the focal length for the paraxial ray and z_p shows the focal length for the meridional ray and z_c shows where the transformation media will be placed to flatten the surface. Panel (b) shows the inverse transformation grid (yellow) which possess the same electromagnetic properties as the original lens (white) (44).

tened Fisheye lens and a lens with reduced field curvature by flattening the focal surface (44), fig. 1.3. Many transformation optical devices possess large variations in permittivity. The invisibility cloak for example possesses infinity regions which can be smoothed away to provide working examples such as an Eaton lens or invisible sphere (45).

The major novel contributions presented of this work are summarised as follows:

- A ray tracing method is used to characterise an optical system for transformation into a transformation optics engineering optical system. This uses ray tracing of a Cooke triplet in ZEMAX and imports the rays to use as boundaries in a grid generation software package called Pointwise.

- A triplet lens is engineered using a reduced transformation optics map which requires no metamaterials. The discrete coordinate transformation method is used to calculate the permittivity of individual grid cells in a triplet device. The metamaterial values are then removed around the edges and simulated.

- A system for calculating the Zernike Aberrations in terms of a FDTD simulation. The source is placed at the centre of the focus and the distorted wavefront exiting the lens

is sampled, interpolated using a polynomial and fitted to the Zernike polynomial set to give coefficients for the Zernike aberrations of the lens and these are compared to the results of a Cooke triplet in Zemax.

- A Ray Tracing program for calculating a 2D distribution of refractive index is created. This is based on Bucahrel's quasi-invariant method (46) which is used to calculate the Seidel aberrations in an inhomogeneous material and this is applied to the Reduced MTM lens. This combines an axial gradient with a radial gradient.

1.3 The Structure of the Thesis

This thesis introduces the novel concept of transformation optics (TO) in the design of gradient index lenses. The aim is to present evidence of the improvement achieved using a TO designed Lens. It reduces the aberrations, size, weight, cost and improving the manufacturability and performance compared with existing optical systems. Research in this field has shown that a flat lens of negative refractive index of one will produce theoretically a resolution unlimited by the wavelength. For designers of optical systems the availability of refractive indices lower than one increases the design parameter space. This allows aplanatic single lenses (20) and sub-wavelength resolution has been extended to a far-field lens using a transformation optics magnification (27). This thesis's novel goal is to examine the aberrations in a single, flat lens designed using transformation optics which can be manufactured with no metamaterial values of permittivity and optimise the lens for aberrations to give an improvement in imaging for defence and civilian applications.

In this thesis, we propose to apply transformation optics to design a single lens which preserves the optical property of the original Cooke triplet. Exotic material properties are usually generated from a transformation therefore metamaterials are required in the design of the proposed lens. The model is verified based on an in-house dispersive Finite-Difference Time-Domain software as having the same DNA as the original Cooke triplet by analysing the Seidel aberrations for the MTM lens compared with a conventional triplet. The lens is in the quasi-optical regime. Additionally, we compare the MTM lens with a simplified one, where MTMs are replaced with an all-dielectric reduced map. This reduced map will be valid for the TM mode. The lens designed will remain the same size as the Cooke triplet and will in fact be slightly larger due to extending the lines of light propagation before and behind to account for the curved surface. The lens will be flat and therefore allow increased

compatibility with optical and optoelectronic system components.

This thesis breaks down into the following chapters:

- **Chapter 2** explains the theory of transformation optics derived from the theory of invisibility. The key concept of carpet cloaking and how this allows more practical devices to be designed using dielectric materials. This chapter then examines some of the uses of transformation optics in antennas. electromagnetic and optical engineering applications.

- **Chapter 3** This chapter looks at the engineering of a low aberration triplet engineered using discrete transformation optics. It explains a virtual space and associated distorted grid was generated based on a Cooke triplet design, the theory behind the coordinate transformation based on this grid in order to compute a permittivity map and finally the layout of the FDTD simulation which computed the electromagnetic response of the lens. The novel concept of ray tracing to specify the virtual space and the verification in terms of focal point.

- **Chapter 4** The FDTD simulation of the MTM triplet is presented in terms of the aberrations of the lens. The method for calculating each aberration is described and a comparison between the MTM lens, a simplified lens and the conventional Cooke triplet based on FDTD simulations. The MTF a key optical parameter presents the performance of the lenses. The RMS wavefront error is also calculated showing good results for the all-dielectric triplet design. The novel concept of calculating aberrations for lenses in FDTD is also described based on sampling a wavefront aberration function.

- **Chapter 5** contains the derivation of the Seidel aberrations for the Cooke Triplet, MTM and All-Dieletric Lenses using the results of the FDTD simulation. The Spherical aberration, Coma, Field Curvature and Distortion are all calculated. A discussion of these results and a comparison between the performance of the different lenses are offered and conclusions drawn on the validity of using metamaterials for lens design and what improvements the discrete coordinate transformation approach offers lens designers.

- **Chapter 6** examines the wavefront abberation, RMS error and PV ratio using FDTD simulation results for the main lenses. The Zernike aberrations and the Modulation

Transfer Function are calculated for each of the lenses from the wavefront error. Conclusions in terms of the validity and performance of metamaterials and coordinate transformation is made in the design of a Cook Triplet lens.

Bibliography

[1] D. Smith, D. Vier, T. Koschny, and C. Soukoulis, "Electromagnetic parameter retrieval from inhomogeneous metamaterials," *Physical Review E*, vol. 71, no. 3, p. 036617, 2005.

[2] D. R. Smith, W. J. Padilla, D. C. Vier, S. C. Nemat-Nasser, and S. Schultz, ""Composite medium with simultaneously negative permeability and permittivity"," *Phys. Rev. Lett.*, vol. 84, no. 18, pp. 4184–4187, May 2000.

[3] V. G. Veselago, ""The Electrodynamics of substances with simultaneously negative values of epsilon and mu"," *Soviet Physics Uspekhi*, vol. 10, no. 4, p. 509, 1968. [Online]. Available: http://stacks.iop.org/0038-5670/10/i=4/a=R04

[4] K. B. Alici and E. Özbay, "Radiation properties of a split ring resonator and monopole composite," *physica status solidi (b)*, vol. 244, no. 4, pp. 1192–1196, 2007.

[5] J. Pendry, A. Holden, D. Robbins, and W. Stewart, "Low frequency plasmons in thin-wire structures," *Journal of Physics: Condensed Matter*, vol. 10, no. 22, p. 4785, 1998.

[6] J. B. Pendry, A. J. Holden, D. Robbins, and W. Stewart, "Magnetism from conductors and enhanced nonlinear phenomena," *Microwave Theory and Techniques, IEEE Transactions on*, vol. 47, no. 11, pp. 2075–2084, 1999.

[7] B.-I. Wu, W. Wang, J. Pacheco, X. Chen, T. M. Grzegorczyk, and J. A. Kong, "A study of using metamaterials as antenna substrate to enhance gain," *Progress In Electromagnetics Research*, vol. 51, pp. 295–328, 2005.

[8] A. Fang, T. Koschny, and C. M. Soukoulis, "Optical anisotropic metamaterials: Negative refraction and focusing," *Physical Review B*, vol. 79, no. 24, p. 245127, 2009.

[9] Z. E. Djeffal, H. Talleb, D. Lautru, and V. Fouad-Hanna, "Negative refractive index behavior through magneto-electric coupling in split ring resonators," *Progress In Electromagnetics Research Letters*, vol. 22, pp. 155–163, 2011.

[10] W. Rotman, "Plasma simulation by artificial dielectrics and parallel-plate media," *Antennas and Propagation, IRE Transactions on*, vol. 10, no. 1, pp. 82–95, 1962.

[11] W. Kock, "Path-length microwave lenses," *Proceedings of the IRE*, vol. 37, no. 8, pp. 852–855, 1949.

[12] A. Alù and N. Engheta, "Guided modes in a waveguide filled with a pair of single-negative (sng), double-negative (dng), and/or double-positive (dps) layers," *Microwave Theory and Techniques, IEEE Transactions on*, vol. 52, no. 1, pp. 199–210, 2004.

[13] A. Grbic and G. V. Eleftheriades, "Experimental verification of backward-wave radiation from a negative refractive index metamaterial," *Journal of Applied Physics*, vol. 92, no. 10, pp. 5930–5935, 2002.

[14] G. V. Eleftheriades, "Enabling rf/microwave devices using negative-refractive-index transmission-line (nri-tl) metamaterials," *Antennas and Propagation Magazine, IEEE*, vol. 49, no. 2, pp. 34–51, 2007.

[15] A. Grbic and G. V. Eleftheriades, "Growing evanescent waves in negative-refractive-index transmission-line media," *Applied Physics Letters*, vol. 82, no. 12, pp. 1815–1817, 2003.

[16] A. K. Iyer, P. C. Kremer, G. V. Eleftheriades *et al.*, "Experimental and theoretical verification of focusing in a large, periodically loaded transmission line negative refractive index metamaterial," *Opt. Express*, vol. 11, no. 7, pp. 696–708, 2003.

[17] A. K. Iyer and G. V. Eleftheriades, "Negative refractive index metamaterials supporting 2-d waves," in *Microwave Symposium Digest, 2002 IEEE MTT-S International*, vol. 2. IEEE, 2002, pp. 1067–1070.

[18] J. Chen, C. Radu, and A. Puri, "Aberration-free negative-refractive-index lens," *Applied Physics Letters*, vol. 88, no. 7, pp. 071 119–071 119–3, 2006.

[19] K. Mantel, D. Bachstein, and U. Peschel, "Perfect imaging of hypersurfaces via transformation optics," *Optics letters*, vol. 36, no. 2, pp. 199–201, 2011.

[20] J. P. D. Schurig and D. R. Smith, ""negative index lens aberrations"," *Optics express*, vol. 14, p. 9794, 2006.

[21] J. Pendry, "Perfect cylindrical lenses," *Opt. Express*, vol. 11, no. 7, pp. 755–760, 2003.

[22] R. Pendry, ""Negative refraction makes a perfect lens"," *New journal of physics*, 2000.

[23] P. A. Belov and Y. Hao, "Subwavelength imaging at optical frequencies using a transmission device formed by a periodic layered metal-dielectric structure operating in the canalization regime," *Physical Review B*, vol. 73, no. 11, p. 113110, 2006.

[24] M. Qiu, M. Yan, J. Hao, W. Yan, and J. Wang, "Transformation optics for designing superlenses," in *Electromagnetics in Advanced Applications, 2009. ICEAA'09. International Conference on.* IEEE, 2009, pp. 944–947.

[25] X. Rao and C. Ong, "Subwavelength imaging by a left-handed material superlens," *Physical Review E*, vol. 68, no. 6, p. 067601, 2003.

[26] Z. Jacob, L. V. Alekseyev, and E. Narimanov, "Optical hyperlens: far-field imaging beyond the diffraction limit," *Optics express*, vol. 14, no. 18, pp. 8247–8256, 2006.

[27] Z. Jacob, L. Alekseyev, and E. Narimanov, "Optical hyperlens: far-field imaging beyond the diffraction limit," in *NanoScience+ Engineering.* International Society for Optics and Photonics, 2007, pp. 66 380W–66 380W.

[28] U. Leonhardt, "Perfect imaging without negative refraction," *New Journal of Physics*, vol. 11, no. 9, p. 093040, 2009.

[29] J. Valentine, J. Li, T. Zentgraf, G. Bartal, and X. Zhang, ""An optical cloak made of dielectrics"," *Nature Materials*, vol. 8, no. 7, pp. 568–571, April 2009. [Online]. Available: http://dx.doi.org/10.1038/nmat2461

[30] W. L. Barnes, A. Dereux, and T. W. Ebbesen, "Surface plasmon subwavelength optics," *Nature*, vol. 424, no. 6950, pp. 824–830, 2003.

[31] G. Bartal, G. Lerosey, and X. Zhang, "Subwavelength dynamic focusing in plasmonic nanostructures using time reversal," *Physical Review B*, vol. 79, no. 20, p. 201103, 2009.

[32] D. Sievenpiper, L. Zhang, R. F. Broas, N. G. Alexopolous, and E. Yablonovitch, "High-impedance electromagnetic surfaces with a forbidden frequency band," *Microwave Theory and Techniques, IEEE Transactions on*, vol. 47, no. 11, pp. 2059–2074, 1999.

[33] N. Fang, ""Subdiffraction-limited optical imaging with a silver superlens"," *Science*, 2005.

[34] A. Aubry, D. Y. Lei, A. I. Fernández-Domínguez, Y. Sonnefraud, S. A. Maier, and J. B. Pendry, "Plasmonic light-harvesting devices over the whole visible spectrum," *Nano letters*, vol. 10, no. 7, pp. 2574–2579, 2010.

[35] A. I. Fernández-Domínguez, Y. Luo, A. Wiener, J. Pendry, and S. A. Maier, "Theory of three-dimensional nanocrescent light harvesters," *Nano letters*, vol. 12, no. 11, pp. 5946–5953, 2012.

[36] U. L. Andrea Di Flaco, Susanne C Kehr, ""Luneburg lens in silicon photonics"," *arXiv.org*, 2011.

[37] Z. Wang and L. You, "Design and analysis of double negative binary diffractive lens," in *Microwave and Millimeter Wave Technology (ICMMT), 2010 International Conference on.* IEEE, 2010, pp. 1502–1505.

[38] K. Buell, H. Mosallaei, and K. Sarabandi, "A substrate for small patch antennas providing tunable miniaturization factors," *Microwave Theory and Techniques, IEEE Transactions on*, vol. 54, no. 1, pp. 135–146, 2006.

[39] R. Ziolkowski and A. Erentok, "At and below the chu limit: passive and active broad bandwidth metamaterial-based electrically small antennas," *IET Microwaves, Antennas & Propagation*, vol. 1, no. 1, pp. 116–128, 2007.

[40] J. Chen, C. Radu, and A. Puri, "Aberration-free negative-refractive-index lens," *Applied physics letters*, vol. 88, no. 7, p. 071119, 2006.

[41] A. O. Pinchuk and G. C. Schatz, "Metamaterials with gradient negative index of refraction," *JOSA A*, vol. 24, no. 10, pp. A39–A44, 2007.

[42] F. Aieta, P. Genevet, M. A. Kats, N. Yu, R. Blanchard, Z. Gaburro, and F. Capasso, "Aberration-free ultrathin flat lenses and axicons at telecom wavelengths based on plasmonic metasurfaces," *Nano letters*, vol. 12, no. 9, pp. 4932–4936, 2012.

[43] T. Zhang, L. Chen, and X. Li, "Graphene-based tunable broadband hyperlens for far-field subdiffraction imaging at mid-infrared frequencies," *Optics express*, vol. 21, no. 18, pp. 20 888–20 899, 2013.

[44] D. R. Smith, Y. Urzhumov, N. B. Kundtz, and N. I. Landy, "Enhancing imaging systems using transformation optics," *Optics express*, vol. 18, no. 20, pp. 21 238–21 251, 2010.

[45] T. Tyc and U. Leonhardt, "Transmutation of singularities in optical instruments," *New Journal of Physics*, vol. 10, no. 11, p. 115038, 2008.

[46] H. A. Buchdahl, *An introduction to Hamiltonian optics*. Courier Dover Publications, 1993.

Chapter 2

Transformation Optics

2.1 Invisibility Cloaks

This section examines a classic example of the invisibility cloak and the latest in the field of transformation optics including quasi-conformal mapping method which allows extremely simple of transformation media. It looks at the transformation optics method for deriving a set of permittivity and permeability tensors from the metric tensor and Jacobian matrices. We look at the application of this in the design of a 3D invisibly cloak. The idea of an invisibility cloak sounds like it is from the pages of Harry Potter however we seriously look at the design of a practical cloak of invisibility. A 2D carpet cloak is designed with simplified material parameters which allows fabrication. We look at the application to flat antennas and lenses and extraordinary transmission devices. Finally we look at other novel transformation optics such as the optical black hole.

2.1.1 Conformal Mapping

Transformation optics has been derived using a mathematical framework based on complex numbers known as conformal mapping which was originally used in one of the designs of the invisibility cloak (1). It is based on conformal mapping where different coordinate systems,

w and z typically can be transformed maintaining their orthogonality between angles of the grid cells. An example of a Conformal mapping is the Mercator projection, where the spherical surface of the world is mapped onto a cylindrical surface to give the atlas or rectangular map of the world we are familiar with. Conformal mapping can be used to design invisibility cloaks which preserve angles and hide objects inside an electromagnetic field distorted by a transformation media. This is not the mathematical formulation we follow in the remaining thesis but this method can be used as an alternative to yield the same experimental results.

It is possible to design a single lens which transforms a plane wave to a point source using the conformal mapping Mobius transformation.

$$z = i\frac{i+w}{i-w} \tag{2.1}$$

for example and from the theory of optical conformal mapping we find the refractive index is

$$n_z = |n_w \frac{dw}{dz}| \tag{2.2}$$

therefore the refractive index in this case is

$$n(x,y) = \frac{2n_0}{x^2 + (1+y)^2} \tag{2.3}$$

This concept has been extended to include non-Euclidean geometries and multiple dimensions which allow one to minimise the singularities in the original cloak (2). This technique was later generalised to mapping to Riemann sheets (3).

2.1.2 The Principle of Invariance

Invariance of Maxwell's equations states that a physical law should be the same independent of the frame of reference or coordinate system which the observer happens to be observing

from. The principle of Invariance in Maxwell's equations means that the electromagnetic field must be independent of the co-ordinate system. Typical examples are Cartesian (x,y,z), cylindrical (z,r,θ) and spherical (r,θ,ϕ) co-ordinate systems. Covariance means that the electromagnetic field must be scaled in different coordinate systems in order to maintain the same result in each of the different coordinate systems.

The metric tensor, g, is a measure of distance which is coordinate invariant and therefore very useful in the mathematics of general relativity which possess curved space-time and also in coordinate transformation theory g^{ij} is the symbol for the metric tensor where the tensor coordinates are defined in terms of i and j. This is a matrix of differentials between the basis coordinate vectors (x, y, z). g is a coordinate system independent length scale taken from Einstein's Genereral Theory of Relativity.

The permittivity and permeability are also covariant matrices which denotes an inhomogeneous and anisotropic material. Covariance and contravariance describe how a geometry responds to a change in basis vectors. A covariant properties such as the length scale results in a transformation proportional to the length scale. A contravariant variable such as gradient results in an inverse transformation under a change in basis vector.

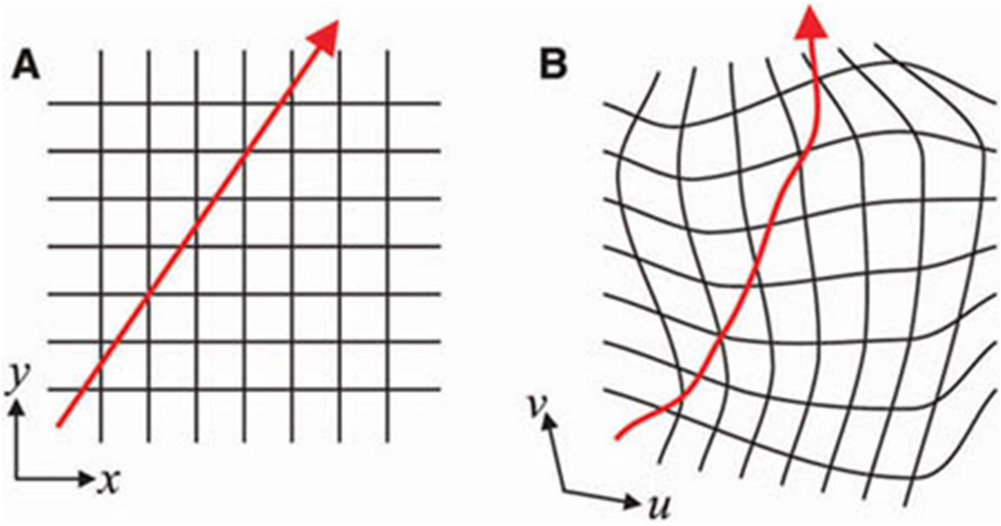

Figure 2.1: Figure (A) is a flat Cartesian coordinate system (x,y) with a ray travelling through it. This is how light typically propagates in a vacuum. Figure (B) is the original coordinate system (x,y) has been transformed into a new coordinate system (u,v). The rays travels as a ray of light. Due to the distorted space the trajectory of a ray of light is changed.

The invariance of Maxwell's equations when applied to a material rather than the abstract coordinate system has large implications called the materials interpretation, see fig. 2.1 in Transformation optics. It states that this process can be used as a design approach to yield a permittivity tensor which gives the same propagation characteristics for electromagnetism of a given coordinate system in terms of permittivity and permeability (4). Instead of interpreting this coordinate transformation as a change in topology we can interpret it as a change in material. This means that we can control the shape of the electromagnetic field by changing the background material properties, the permittivity and permeabilty of the material, and yield comparable results to if we have used the invariance of Maxwell's equations to yield a change in electromagnetic field distribution in terms of changing the geometry or coordinate system.

2.1.3 A Design of the Cloaking Device

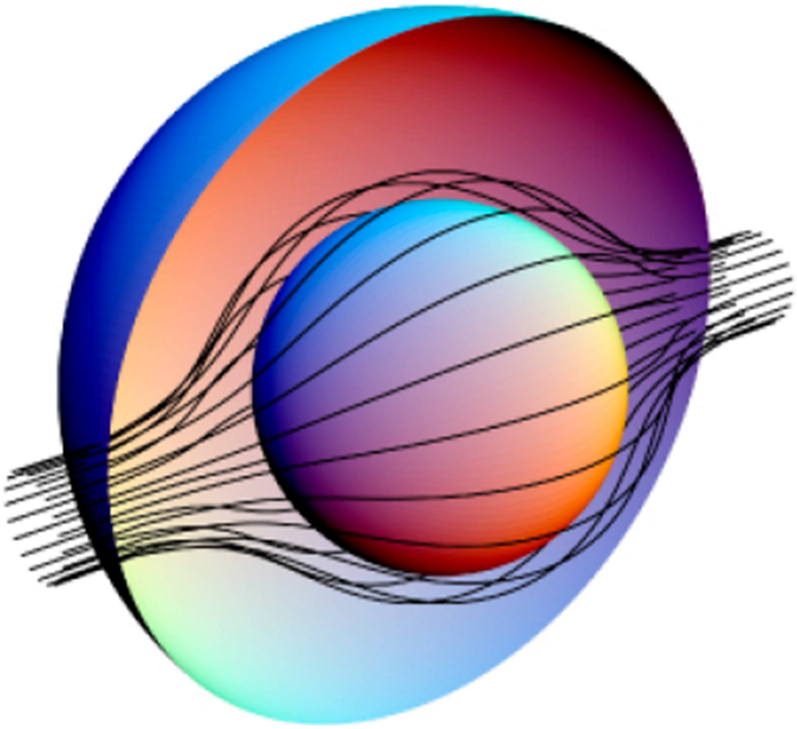

Figure 2.2: The spherically symmetric cloak designed by Sir J. Pendry (5). The inner sphere is the cloaked region radius, R1, and the outer sphere the radius of the cloak, R2. The lines show the ray propagation in the invisibility cloak being diverted around the cloaked region like water around a stone.

In order to create a cloaking device it is necessary to divert the field lines away from a region. This is achieved by stretching the coordinate system from a point in space to a sphere. The distorted coordinate system (u,v,w) is recorded in terms of the original coordinates system (x,y,z).

$$u(x, y, x), v(x, y, z), w(x, y, z). \tag{2.4}$$

The point in virtual space is distorted in comparison to original real space which gives a vector for the distorted grid which can be expressed across the whole grid as a metric tensor. The change in coordinate system results is a change in permittivity or permeability of the

medium to maintain covariance of Maxwell's equations.

$$\epsilon' = \epsilon \frac{Q_u Q_v Q_w}{Q_u^2} \tag{2.5}$$

$$\mu' = \mu \frac{Q_u Q_v Q_w}{{Q_u}^2}, \tag{2.6}$$

where Q is the length of the differential of the basis vector. This is a special case when the grid is orthogonal. We choose to cloak a spherical region, $r < R1$ and the cloak be an annulus $R1 < r < R2$, fig. 2.2.

The coordinate transformation to compress the region $r < R2$ into the annulus is in spherical coordinates is

$$r' = R1 + r(R2 - R1)/R2 \tag{2.7}$$

$$\phi' = \phi \tag{2.8}$$

$$\theta' = \theta \tag{2.9}$$

Applying the transformation, eq. (2.4), for the annulus, $R1 < r < R2$, the permittivity and permeability are

$$\epsilon'_r = \mu'_r = \frac{R2}{R2 - R1} \frac{(r' - R1)^2}{r2} \tag{2.10}$$

$$\epsilon'_\theta = \mu'_\theta = \frac{R2}{R2 - R1} \tag{2.11}$$

$$\epsilon'_\phi = \mu'_\phi = \frac{R2}{R2 - R1} \tag{2.12}$$

The region $r < R1$ is now cloaked and no electromagnetic field can enter or exit the region. It is worth noting that the outer layer of the cloak is reflection-less and have the conditions which allow it to be compared to a perfectly matched layer

$$\epsilon'_\theta = \epsilon'_\phi = \frac{1}{\epsilon_r} \mu'_\theta = \mu'_\phi = \frac{1}{\mu'_r} \tag{2.13}$$

The electric permittivity and magnetic permeability are in terms of the geometry denoted by the metric tensor. Electromagnetic interaction with a medium is analogous to interaction with a geometry. This is the fundamental concept to transformation optics known as the materials interpretation (6). The materials interpretation states that the propagation in a material can be transformed in the equivalent way to a coordinate system by changing the permittivity and permeability tensor. This transformation can be given in terms of the metric tensor, g. This typically defines a metric of distance in Non-Euclidean geometries such as the Mobius strip of the geometry of space time. It is a measure of distance which can exist independent of the coordinate system.

$$\epsilon^{ij} = \mu^{ij} = \pm\sqrt{g}g^{ij}. \tag{2.14}$$

or in another more common, tensor form, (4) in terms of the Jacobian Transformation matrix

$$\epsilon' = \frac{\Lambda\epsilon\Lambda^T}{det(\Lambda)} \tag{2.15}$$

$$\mu' = \frac{\Lambda\mu\Lambda^T}{det(\Lambda)} \tag{2.16}$$

The Jacobian matrix contains the first order partial derivatives of two coordinate systems ϕ.

$$\Lambda(x,y) = \begin{vmatrix} \frac{d\phi}{dx} & \frac{d\theta}{dy} \\ \frac{d\phi}{dx} & \frac{d\theta}{dy} \end{vmatrix} \tag{2.17}$$

In a coordinate transformation this would be followed by a change in basis vectors and variables to account for the change in coordinate system and maintain the same electromagnetic behaviour as before maintaining the invariance of Maxwell's equations (7). This coordinate transformation gives us a permeability tensor and permittivity tensor describing the material in which for example a Cartesian plane wave flowed like a cylindrical wave. This equation can be further simplified and the inhomogeneity and anisotropy of the permittivity and per-

meability reduced as long as we are always transforming to a flat Cartesian space.

The Discrete Transformation Optics (DTC) method, All-Dieletric or Dieletric-Only approach was developed by (8) as a response to the cloak design fabricated by (9) which suffered the possession of a limiting factor such as highly anisotropic materials, in the form of highly anisotropic permittivity distributions with prohibitive ranges reaching infinity at the inner cloak boundary. If we choose our transformation so that it is almost orthogonal the design can be simplified (8). This allows the transformation optics equation to be used but resulting in a medium with permittivity and permeabilty which can be fabricated by naturally occuring materials such as dielectrics rather than resorting to lossy metamaterials.

2.1.4 Carpet Cloaks

The Carpet Cloak is an innovation in the original cloak design where instead of designing to cloak a point in space a cloak is designed to hide a bump on a plane. For a 2D E_z-polarised light we have a simplified case where using only one polarisation simplifies the device design in terms of material parameters. The material is invariant in the z direction and only $\epsilon_{zz}, \mu_{xx}, \mu_{xy}, \mu_{yy}, \mu_{yx}$ contribute in the case where we have TE mode electromagnetic field. In addition to this the transformation tensor is simplified so we only require the 2D Jacobian matrix Λ. All of this results in a simplification of the canonical equations which govern transformation optics media where the determinate of the metric tensor is only required because we have a scalar response which scales the electromagnetic field property.

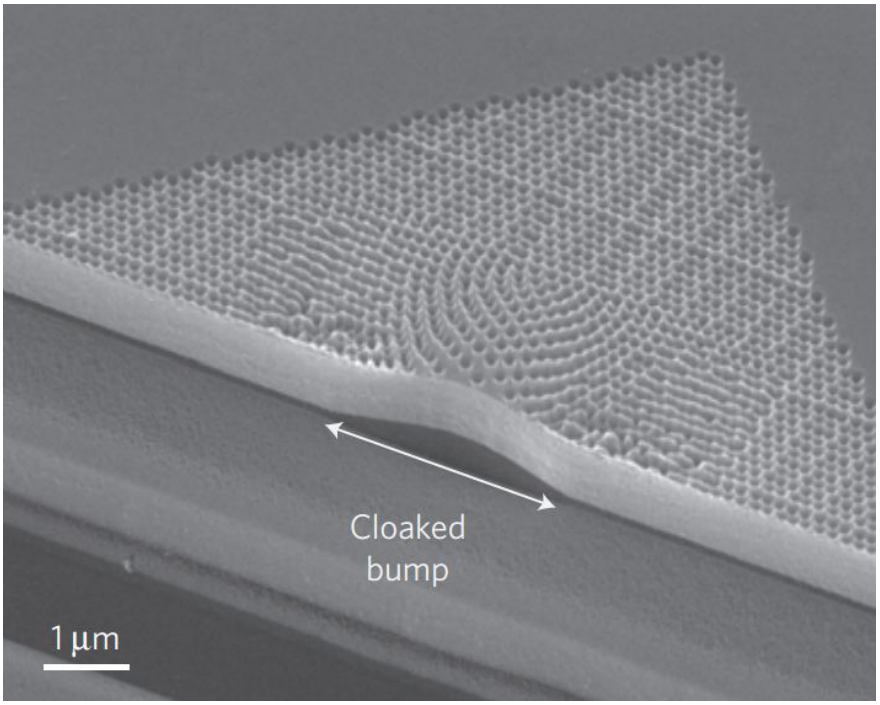

Figure 2.3: A nano fabricated carpet cloak (10). It has been placed in a Silicon Nitride waveguide on a nano porous Silicon Oxide substrate with very low refractive index for testing. The spatial index variation is realised by etching holes of various sizes in the nitride layer at deep wavelength scale which creates a local effective medium index (10) cloaking the bump region.

If the grid is quasi-orthogonal then this transformed medium can now be fabricated using dielectric lego blocks. This description in terms of refractive index and anisotropy of the transformation makes sense if transforming a square cell δ by δ to a distorted parallelogram $\vec{x} \cdot \delta$ by $\vec{y} \cdot \delta$ where δ is used as an infinitesimally small distance equivalent to taking a differential δE/dt infinitely small distance in E over t as a mathematical abstraction for the preceding integral or differential equation. A larger compression leads to a smaller area $\sqrt{det(g)}\delta^2$ and a larger refractive index. An expansion leads to a refractive index less than the original background medium and hence a metamaterial requirement.

$$n^2 \approx \frac{\epsilon_z}{\epsilon_0} = \frac{1}{det(\sqrt{g})} \tag{2.18}$$

The Permittivity and Permeability can be normalised in terms of the refractive index to remove the problem of variation of permeability. The permeability equals unity and the refractive index is a function of permittivity. This eliminates the complicated permeability function, eq. (2.25) which requires materials with a permeability less than one, which does not occur in nature. If we treat the effective refractive index as a function of the permeability in the transverse and longitudinal direction

$$n_t = \sqrt{\mu_l \epsilon} \tag{2.19}$$

the permittivity and permeability of the distorted space can be totally described by the refractive index.

$$n_l = \sqrt{\mu_t \epsilon} \tag{2.20}$$

From this definition if the relative permeability of the material is equal to free space

$$\mu_l \mu_t = 1 \tag{2.21}$$

then the effective refractive index of the cell where we are splitting the larger material down into individual cells defined by the original coordinate system we used to define the real and virtual geometry which is defined as

$$n^2 = \frac{\sqrt{n_l n_t}}{\sqrt{\epsilon_0}} = \frac{1}{det(g)} \tag{2.22}$$

This device has material parameters, that all varied as a function of radial distance being r and this direction only. The cloak only has the permittivity variation in the z direction, ϵ_{zz}. The other two parameters in the x and y tensors of permittivty remain constant in the carpet cloak. The permeabilty in the x and y are functions of distance. This was possible so long as the effective medium condition was satisfied and the material parameters changed

slowly as a function of wavelength. The parameters were transformed into a single function of refractive index and calculated for ϵ_{zz}.

The anisotropy of the material is an important property in defining the transformation media. It is defined as the inverse of the metric tensor and gives a measure of how much the distorted cell diverges from the original flat Cartesian space. A key measure of the performance of a transformation optics device is to reduce the anisophy of the designed material. It is a key approximation in the design of the carpet cloak that the anisophy is minimized.

$$\alpha = \frac{1}{det(g)} \tag{2.23}$$

The carpet cloak can be fabricated without the need for metamaterials using only dielectrics. An all dielectric cloak has been designed using only dielectric and an optimisation method creating an eye type cloak as using multilayer cladding with material with a single constant value of permittivity but varying the thickness and constancy of the material (11). One group has engineered a cloak which works in a gradually changing medium (12) including arbitrary boundaries (13). This rather basic cloak might be further moved towards fabrication by using a layered approach (14). The cloak could be replaced by a waveguiding structure diverting the rays around an object using a grooved metallic cylinder(15).

$$\epsilon = \frac{\epsilon_{ref}}{\sqrt{det(g)}} \tag{2.24}$$

$$\mu^{ij} = \frac{\Lambda\Lambda^T}{\sqrt{det(g)}} \tag{2.25}$$

Metamaterials and transformation optics can be used to create illusion devices which replace an image with an illusion (16). This process can be used to cloak a cup and replace it with an image of a spoon (17). This concept of illusion optics has also been applied to the projection of an image onto a physical cloak (16).

2.1.5 Other Forms of Cloaking

Transformation Optics is a mathetical framework which extends beyond electromagnetism along and allows cloaking to be designed for sound and heat. An example of this is an earthquake shield can be produced using transformation optics. It is theoretically possible to build a cloak for other waves as well as electromagnetic and this has been applied to acoustics. A cloak which guides an earthquake around the future city has been imagined and predicted (18). The cloak varies with the parameters density instead of permittivity as the wave in question, sound, is affected by density. This seismic cloak is able to divert an earthquake around a region in space.

Metafluids offer an implementation of the metamaterial concept to fluids. Fluids which are tailored to possess properties not typically found in nature. Fluid waves fundamentally work the same as Maxwell's equations and the invariance in them used to derive the transformation optics equations can equally be applied to the equation which govern sound wave propagation in matter (19).

2.2 Transformation Optics Imaging Devices

Electromagnetic modelling is available in all sorts of commerical packages for metamaterials research. CST and HFSS are common packages which have been used to model split ring resonator arrays to give negative permeability. COMSOL is a commercial solver which can solve PDE's and therefore has been used to model the invisibility cloak and plasmonic

antennas. Outside of this, custom modelling has been done using the finite difference time domain method extensively as well as with finite element methods. Photonic crystals can be simulated using FDTD or with plane wave expansion yielding scattering parameters (20). There are several ways commonly used to model Electromagnetic Band Gap Materials (EBG) using Bloch waves and method of moments (MoM) and the Finite Difference Time Domain (FDTD) method. FDTD has been demonstrated to be the best application for modelling metamaterials due to its ability to easily implement inhomogeneous material properties. FDTD is a time domain method which means that it gives a better physical understanding of the electromagnetic behaviour inside materials with a negative index of permittivity and permeability.

Frequency selective surfaces are artificially constructed surfaces to engineer interaction properties with electromagnetic radiation. This may seem very similar to metamaterials and it is. The key text book being by the authoritative Munk (21). This well established field of research is reviewed well in (22). Transformation optics and metamaterials can be applied to the study of wave propagation on surfaces. Here the wave is controlled on the surface by varying the impedance or resistivity rather than the permittivity and permittivity in bulk metamaterials. Variation in these surfaces takes place by changing the inclusions and shapes of the mushrooms. This is a standard metamaterial technique of engineering the sub-wavelength inclusions structurally by using different shapes in order to create macroscopic effects. Using structural variations rather than chemical ones typically found in nature. Colleagues in the group here at Queen Mary have published work on a surface wave cloak (23). Directivity or the ability to control the beam direction of an antenna is important for antenna engineers. A material with a refractive index of zero (ENZ) refracts incoming radiation into a plane wave perpendicular to the surface. An ENZ material could be used to direct a beam of radiation very effectively. Gradient index lenses are a hot topic in metamaterials and transformation optics. These are lenses with a refractive index which varies radially. They

are very hard to fabricate with current techniques which involve diffusion with chemicals to create the gradient or by drilling holes or varying spaces or by using concentric shells. Metamaterials have been shown to improve the directivity of antennas using matching techniques (24).

2.2.1 Other Novel Devices

Transformation Optics can manipulate an EM wave to allow it to propagate through a hole smaller than its wavelength without diffracting. An example of transformation media is the extraordinary transmission device which allows electromagnetic waves to propagate through a region smaller than its wavelength without suffering diffraction. This device has been verified experimentally. It has been fabricated without metamaterials. It is therefore broadband. This device design (25) has proposed an idea for a sub-wavelength cavity made from metamaterials due to compression.

Novel optical devices which control the propagation of electromagnetic waves have been suggested based on the TO method using metamaterials. The manipulation of electromagnetic wave propagation is a key feature in many lenses and optical systems. For example the single lens focuses a plane wave to a single point. Many classic optical devices such as beamsplitters and lenses (28) have been redesigned using the methods of transformation optics. New types of absorber have been introduced such as the optical black hole. These transformation designed devices are simple optical instruments and can therefore be understood in terms of quantum optics which is a fascinating topic all by itself and gets to the heart of the optical question by looking at it on a quantum level (29). Integrating optical systems into a single metamaterial device such as in optical modulators for communications modulators integrates three lenses for low aberrations into one metamaterial lens (30).

Metamaterials share an analogy with general relativity which can be used to gener-

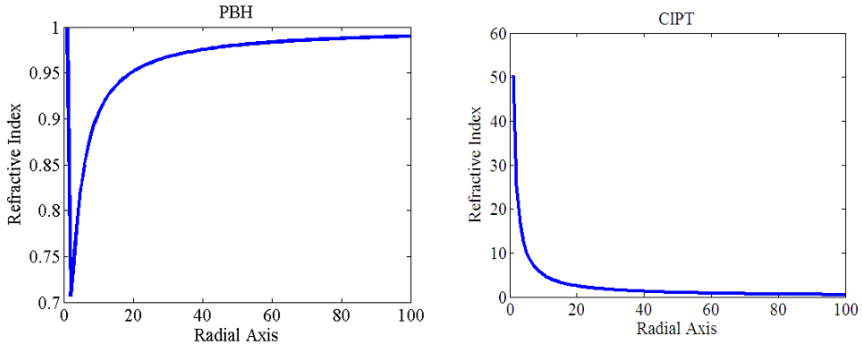

Figure 2.4: The refractive index distribution from the Photonic Black Hole (31) with a index of distribution less than one satisfied with Metamaterials. The Continuous Index Photon Trap (CIPT) with a high permittivity can be achieved with high permittivity microwave ferrite material.

ate table top copies of astrophysical phenomenon. The continuous index photon trap is a model of a planet orbiting a star and transformation optics. A table top photonic black hole (PBH) would allow an experimental study of this phenomenon to test some of Stephan Hawking's among others theories (31). FDTD simulation of these black hole structures have been carried out by the Antennas and Electromagnetics group at Queen Mary, University of London (32). Continuous Index Photonic Trap's (CIPT's) allow light confinement for optical computing and telecommunications, for example in on-demand time delay or optical memories (33). The refractive index distribution as a function of radius for a CIPT and PBH are given in fig. 2.4.

2.3 Summary

Transformation Optics has led to many interesting and practical devices such as invisibility cloaking at microwave and optical frequency bands. The original designs for the invisibility cloaks were fascinating and made deliverable by the use of Discrete Coordinate Transformation and using the Carpet Cloak design approach. The innovation of carpet cloaking provided a way to realise these devices more effectively using more achievable values for permittivity and permeability. The design of the invisibility cloak and carpet cloak has meant that this

method for designing exotic equipment such as invisibility cloaks. It also has far reaching effects for engineering in other fields such as thermal, acoustic and even quantum. Useful devices which this change in thinking could bring about where able to surpass fundamental limited such as using negative index metamaterials to surpass the resolution limit in imaging or overcome wave transmission through small holes in the extraordinary transmission device. The transformation optics method could be applied to many fields of science for cloaking in heat, quantum and seismic wave scenarios. In the following chapter we will attempt to design a Cooke Triplet, a fundamental lens used in photography, using the principles of Transformation Optics.

Bibliography

[1] U. Leonhardt, "Optical conformal mapping," *Science*, vol. 312, no. 5781, pp. 1777–1780, 2006.

[2] U. Leonhardt and T. Tyc, "Broadband invisibility by non-euclidean cloaking," *Science*, vol. 323, no. 5910, pp. 110–112, 2009.

[3] L. Xu and H. Chen, "Transformation optics with artificial riemann sheets," *New Journal of Physics*, vol. 15, no. 11, p. 113013, 2013. [Online]. Available: http://stacks.iop.org/1367-2630/15/i=11/a=113013

[4] D. Schurig, J. Pendry, and D. R. Smith, "Calculation of material properties and ray tracing in transformation media," *arXiv preprint physics/0607205*, 2006.

[5] D. J. B. Pendry, D. Schurig, ""Controlling Electromagnetic Fields"," *Science*, vol. 321, June 2006.

[6] A. J. Ward, "Refraction and geometry in Maxwell's equations," *Journal of Modern Optics*, vol. 43, pp. 773–793, Apr. 1996.

[7] J. B. P. D. S. Schurig and D. R. Smith, “”calculation of material properties in transformation media”,” *Optics Express*, vol. 14, 2006.

[8] J. Li and J. B. Pendry, “”Hiding under the carpet: a new strategy for cloaking”,” *ArXiv*, 2008.

[9] D. Smith, D. Vier, T. Koschny, and C. Soukoulis, “Electromagnetic parameter retrieval from inhomogeneous metamaterials,” *Physical Review E*, vol. 71, no. 3, p. 036617, 2005.

[10] J. V. Majid Gharghi and X. Zhang, “A carpet cloak for visible light,” *Nano lett*, 2011.

[11] C. A. Valagiannopoulos and P. Alitalo, “Electromagnetic cloaking of cylindrical objects by multilayer or uniform dielectric claddings,” *Physical Review B*, vol. 85, no. 11, p. 115402, 2012.

[12] J. Zhang, J. Huangfu, Y. Luo, H. Chen, J. A. Kong, and B.-I. Wu, “Cloak for multilayered and gradually changing media,” *Physical Review B*, vol. 77, no. 3, p. 035116, 2008.

[13] C. Li, K. Yao, and F. Li, “Invisibility cloaks with arbitrary geometries for layered and gradually changing backgrounds,” *Journal of Physics D: Applied Physics*, vol. 42, no. 18, p. 185504, 2009.

[14] C.-W. Qiu, L. Hu, X. Xu, and Y. Feng, “Spherical cloaking with homogeneous isotropic multilayered structures,” *Physical Review E*, vol. 79, no. 4, p. 047602, 2009.

[15] S. Tretyakov, P. Alitalo, O. Luukkonen, and C. Simovski, “Broadband electromagnetic cloaking of long cylindrical objects,” *Physical review letters*, vol. 103, no. 10, p. 103905, 2009.

[16] Y. Lai, J. Ng, H. Chen, D. Han, J. Xiao, Z.-Q. Zhang, and C. Chan, “Illusion optics: the optical transformation of an object into another object,” *Physical review letters*, vol. 102, no. 25, p. 253902, 2009.

[17] C. T. C. Yun Lai, Jack Ng, "Creating illusion effects using transformation optics," in *Transformation Electromagnetics and Metamaterials Fundamental Principles and Applications*, K. D.-H. Werner, Douglas H., Ed. Oxford: Springer, 2014.

[18] P. Sheng, "A step towards a seismic cloak," *Physics Online Journal*, vol. 7, p. 34, 2014.

[19] G. W. Milton, M. Briane, and J. R. Willis, "On cloaking for elasticity and physical equations with a transformation invariant form," *New Journal of Physics*, vol. 8, no. 10, p. 248, 2006.

[20] *"FDTD Modeling of Metamaterials: Theory and Applications"*. Artech house, 2009.

[21] B. A. Munk, *Frequency selective surfaces: theory and design*. John Wiley & Sons, 2005.

[22] E. Parker, "The gentleman's guide to frequency selective surfaces," in *17th QMW Antenna Symposium*. London, UK, Queen Mary and Westfield College, 1991, pp. 1–18.

[23] R. C. Mitchell-Thomas, T. M. McManus, O. Quevedo-Teruel, S. A. R. Horsley, and Y. Hao, "Perfect surface wave cloaks," *Phys. Rev. Lett.*, vol. 111, p. 213901, Nov 2013. [Online]. Available: http://link.aps.org/doi/10.1103/PhysRevLett.111.213901

[24] B.-I. Wu, W. Wang, J. Pacheco, X. Chen, T. M. Grzegorczyk, and J. A. Kong, "A study of using metamaterials as antenna substrate to enhance gain," *Progress In Electromagnetics Research*, vol. 51, pp. 295–328, 2005.

[25] N. Engheta, "An idea for thin subwavelength cavity resonators using metamaterials with negative permittivity and permeability," *Antennas and Wireless Propagation Letters, IEEE*, vol. 1, no. 1, pp. 10–13, 2002.

[26] S.-H. L. Sang-Hoon Kim, "Air transparent soundproof window," *pre-print*, 2013.

[27] D. Bao, K. Z. Rajab, W. Tang, and Y. Hao, "Experimental demonstration of broadband transmission through subwavelength aperture," *Applied Physics Letters*, vol. 97, no. 13, pp. 134 105–134 105–3, 2010.

[28] J. B. P. D. Schurig and D. R. Smith, “”Transformation-designed optical elements”,” *Optics Express*, 2007.

[29] U. Leonhardt, “”Quantum physics of simple optical instruments”,” *Reports on progress in physics*, 2003.

[30] X. Xu, Y. Feng, and T. Jiang, “Electromagnetic beam modulation through transformation optical structures,” *New Journal of Physics*, vol. 10, no. 11, p. 115027, 2008.

[31] X. Z. D. A. Genov, S. Zhang, “”Mimicking Celestial Mechanics in Metamaterials,” *Nature*, vol. 5, p. 687, 2009.

[32] Christos Argyropoulos, Efthymios Kallos, and Yang Hao, “”FDTD analysis of the optical black hole”,” *J. Opt. Soc. Am. B*, 2010.

[33] D. P. San-Román-Alerigi, A. B. Slimane, T. K. Ng, M. Alsunaidi, and B. S. Ooi, “A possible approach on optical analogues of gravitational attractors,” *Optics express*, vol. 21, no. 7, pp. 8298–8310, 2013.

Chapter 3

A Flat Single Lens Using Coordinate Transformation

The motivation for this section is to use the Discrete Transformation Optics method to design a single lens and move from this simple application of Transformation Optics to the more complicated example of the three lens Cooke Triplet in the following chapter. We hope that moving gradually from a single lens to a Cooke Triplet then it should be able to implement many optical systems for example sight finders on a rifle or periscopes which might have military applications. In this section we use Discrete Coordinate Transformation to design a single flat lens. The flat lens and the original Concave lens are then simulated using the FDTD method.

3.1 The Discrete Coordinate Transformation Method

The Discrete Coordinate transformation method provides a simplification in terms of materials parameters from the general case which allows the fabrication of achievable devices. The general equations for transformation optics are

$$\epsilon' = \frac{J\epsilon J^T}{det(J)} \tag{3.1}$$

$$\mu' = \frac{J\mu J^T}{det(J)} \tag{3.2}$$

The problem with the devices permittivity and permeability which these are very general create such as have we applied them to a general invisibility cloak in the previous chapter is that they are highly anisotropic and inhomogeneous. This means that they may have negative permittivity values and or permeability values different to 1 which is the typically observed permeability of naturally occurring materials. This problem makes these devices therefore very difficult to fabricate and create practically. In order to create devices we can fabricate we must simplify the coordinate transformation. In this chapter we apply some key assumptions and simplify the materials parameters using the discrete coordinate transformation.

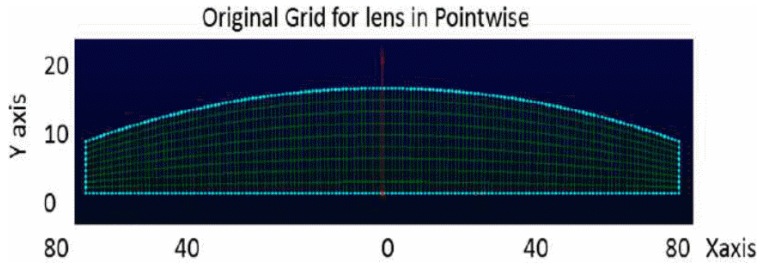

Figure 3.1: The grid generated in Pointwise for the single convex lens. The grid cells get larger towards the centre. When these are mapped to the flat Cartesian coordinate space they will undergo a compression and generate larger permittivity values than those at the edge. The units are in mm.

The single lens is one of the fundamental building blocks of optical systems and in this chapter we look at creating a single lens using discrete coordinate transformation optics. Flat lenses have applications in optical frequencies and at microwave and radio frequencies. Some published research in this field have created planar antennas using transformation optics to make curved surfaces such as the Luneburg lens flat (2; 3; 4) and curved reflectors such as parabolic antennas flat (3). Planar antennas could be used to reduce the size of

satellite communications systems such as devices created by Kymeta. The flat lens possesses advantageous qualities to the parabolic reflector (3; 2) for mm wave communications (6). In this section we describe in detail how the discrete coordinate transformation method is used to create a flat lens. Flat lenses have been designed which remove the distortion present in curved refractive lenses to create an aberration-free flat camera lens where one has been demonstrated at Havard where Capasso has pioneered using metamaterials in optical reflect and transmit arrays (7). Flat lenses have been combined to create a flat achromatic doublet lens which were then compared with the original lens and Seidel aberrations were analytically calculated (1).

The grid is generated for the single lens, see Fig. 3.1, initially to determine the geometry for the coordinate transformation. The parameters for this single lens are taken from the Zemax lens library. The dimensions of the lens are 16 cm by 1 cm for operation at visible light frequencies 400nm to 700nm and the lens is concave. The grid generation suite Pointwise is used to generate the mesh of the virtual space. This involves setting the boundaries of the grid and applying a gridding algorithm with a predetermined cell spacing.

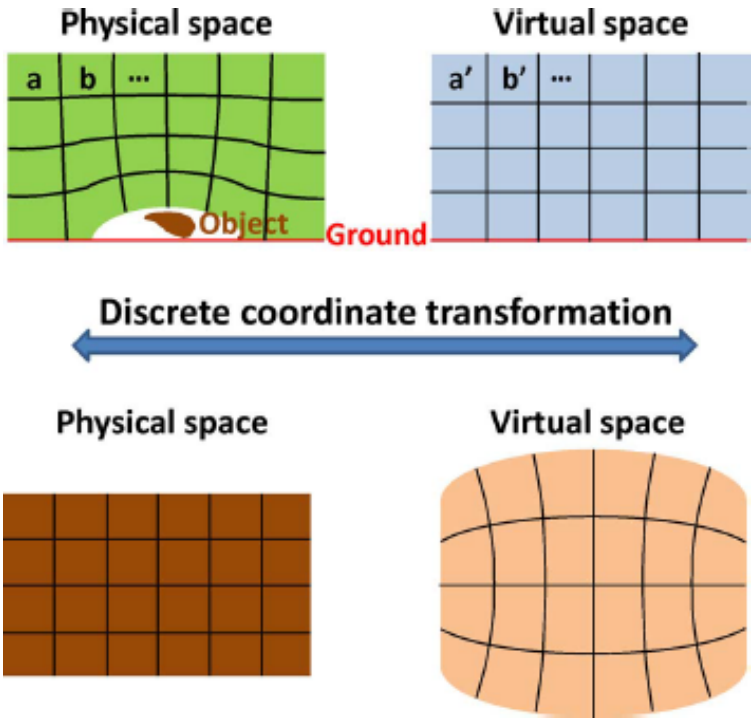

Figure 3.2: The transformation of coordinate systems of the Carpet Cloak is on either side of the top level. The transformation is between each pair of local coordinate systems: a and a', b and b', etc in the physical and virtual space. This process can be applied in either direction. An inverse coordinate transformation can be used as seen on the bottom part of the diagram to transform a curved body such as a lens to a flat body (3).

Coordinate transformation is a transformation between either a distorted real space and a flat virtual space or vis-a-versa, Fig. 3.1. The calculation is independent on which way round this distinction is made. The Transformation Optics equations for the permittivity and permeability tensor in physical space are given by

$$\epsilon' = \frac{J\epsilon J^T}{det(J)} \tag{3.3}$$

$$\mu' = \frac{J\mu J^T}{det(J)} \tag{3.4}$$

where J is the Jacobian transformation matrix, defined as

$$J = \begin{pmatrix} \frac{\delta x'}{\delta x} & \frac{\delta x'}{\delta y} & \frac{\delta x'}{\delta z} \\ \frac{\delta y'}{\delta x} & \frac{\delta y'}{\delta y} & \frac{\delta y'}{\delta z} \\ \frac{\delta z'}{\delta x} & \frac{\delta z'}{\delta y} & \frac{\delta z'}{\delta z} \end{pmatrix} \tag{3.5}$$

We assume that the object is surrounded by free space in the virtual space and the original permittivity and permeability tensors are

$$\epsilon = \epsilon_0 \mathbf{I} \tag{3.6}$$

$$\mu = \mu_0 \mathbf{I} \tag{3.7}$$

where $\mathbf{I}$ is the unitary matrix.

We simplify this and assume that the transformation is 2D. We also assume that the device is infinite in the z direction normal to the xy plane. In this case the Jacobian matrix simplifies to

$$J = \begin{pmatrix} \frac{\delta x'}{\delta x} & \frac{\delta x'}{\delta y} & 0 \\ \frac{\delta y'}{\delta x} & \frac{\delta y'}{\delta y} & 0 \\ 0 & 0 & 1 \end{pmatrix} \tag{3.8}$$

Here equation 3.3 can be rewritten as

$$\epsilon' = \epsilon_0 \begin{pmatrix} \frac{\delta x'}{\delta x}^2 + \frac{\delta x'}{\delta y}^2 & \frac{\delta x'}{\delta x}\frac{\delta y'}{\delta x} + \frac{\delta x'}{\delta y}\frac{\delta y'}{\delta y} & 0 \\ \frac{\delta y'}{\delta x}\frac{\delta x'}{\delta x} + \frac{\delta x'}{\delta y}\frac{\delta y'}{\delta y} & \frac{\delta y'}{\delta x}^2 + \frac{\delta y'}{\delta y}^2 & 0 \\ 0 & 0 & 1 \end{pmatrix} / det(J) \tag{3.9}$$

$$\mu' = \mu_0 \begin{pmatrix} \frac{\delta x'}{\delta x}^2 + \frac{\delta x'}{\delta y}^2 & \frac{\delta x'}{\delta x}\frac{\delta y'}{\delta x} + \frac{\delta x'}{\delta y}\frac{\delta y'}{\delta y} & 0 \\ \frac{\delta y'}{\delta x}\frac{\delta x'}{\delta x} + \frac{\delta x'}{\delta y}\frac{\delta y'}{\delta y} & \frac{\delta y'}{\delta x}^2 + \frac{\delta y'}{\delta y}^2 & 0 \\ 0 & 0 & 1 \end{pmatrix} /det(J) \tag{3.10}$$

For an E-polarized incident wave the electric field is along the z direction. This means that the only components that contribute are μ_{xx}, μ_{xy}, μ_{yy}, μ_{yx} and ϵ_{zz}. In this case the permittivity and permeability become

$$\epsilon'_z \equiv \epsilon'_{zz} = \epsilon_0 det(J)^{-1} \tag{3.11}$$

$$\mu' = \mu_0 \begin{pmatrix} \frac{\delta y'}{\delta x}^2 + \frac{\delta y'}{\delta y}^2 & \frac{\delta x'}{\delta x}\frac{\delta y'}{\delta x} + \frac{\delta x'}{\delta y}\frac{\delta y'}{\delta y} \\ \frac{\delta y'}{\delta x}\frac{\delta x'}{\delta x} + \frac{\delta x'}{\delta y}\frac{\delta y'}{\delta y} & \frac{\delta y'}{\delta x}^2 + \frac{\delta y'}{\delta y}^2 \end{pmatrix} /det(J) \tag{3.12}$$

Based on the theoretical study for anisotropic materials an effective refractive index can be defined as

$$n'^2 = n'_{xx}n'_{yy}/(\epsilon_0\mu_0) = \sqrt{\mu'_{yy}\epsilon'_z}\sqrt{\mu'_{xx}\epsilon'_z}/(\epsilon_0\mu_0 = \sqrt{\mu'_{yy}\mu'_{xx}}\epsilon'_z/(\epsilon_0\mu_0) \tag{3.13}$$

Equation 3.13 indicates that is $\mu'_{xx}\mu'_{yy} = \mu_0^2$ which is equivalent to there being no magnetic dependence then the refractive index n' which determines the trace of the wave could be realized *by the permittivity alone* leading to an all dielectric device. Next we show that this condition is satisfied if a certain grid is properly selected in the coordinate transformation. The explicit value of $\mu'_{xx}\mu'_{yy}$ from Eq. 3.12 is

$$\mu'_{xx}\mu'_{yy} = \mu_0^2(\frac{\delta x'}{\delta x}^2)(\frac{\delta y'}{\delta x}^2) + (\frac{\delta x'}{\delta x}^2)(\frac{\delta y'}{\delta y}^2) + (\frac{\delta x'}{\delta y}^2)(\frac{\delta y'}{\delta x}^2) + (\frac{\delta x'}{\delta y}^2(\frac{\delta y'}{\delta y}^2]/[(\frac{\delta x'}{\delta x})^2(\frac{\delta y'}{\delta y})^2 - 2\frac{\delta x'}{\delta x}\frac{\delta y'}{\delta y}\frac{\delta x'}{\delta y}\frac{\delta y'}{\delta x} + (\frac{\delta x'}{\delta y})^2(\frac{\delta y'}{\delta x})^2 \tag{3.14}$$

The approximate condition $\mu'_{xx}\mu'_{yy} \simeq \mu_0^2$ is satisfied when simultaneously

$$\frac{\delta x'}{\delta y'} \simeq 0 \tag{3.15}$$

$$\frac{\delta y'}{\delta x} \simeq 0 \tag{3.16}$$

Since x' and y' are functions of both x and y, Eq. 3.15 and Eq. 3.16 can also be written using the chain rule

$$\frac{\delta x'}{\delta y'} = \frac{\delta x'}{\delta x}\frac{\delta x}{\delta y} \simeq 0 \tag{3.17}$$

$$\frac{\delta y'}{\delta x} = \frac{\delta y'}{\delta y}\frac{\delta y}{\delta x} \simeq 0 \tag{3.18}$$

However, the above condition can indeed be satisfied because we can generate a grid in the virtual space with near orthogonal cells such as

$$\frac{\delta x}{\delta y} \simeq 0 \tag{3.19}$$

$$\frac{\delta y}{\delta x} \simeq 0 \tag{3.20}$$

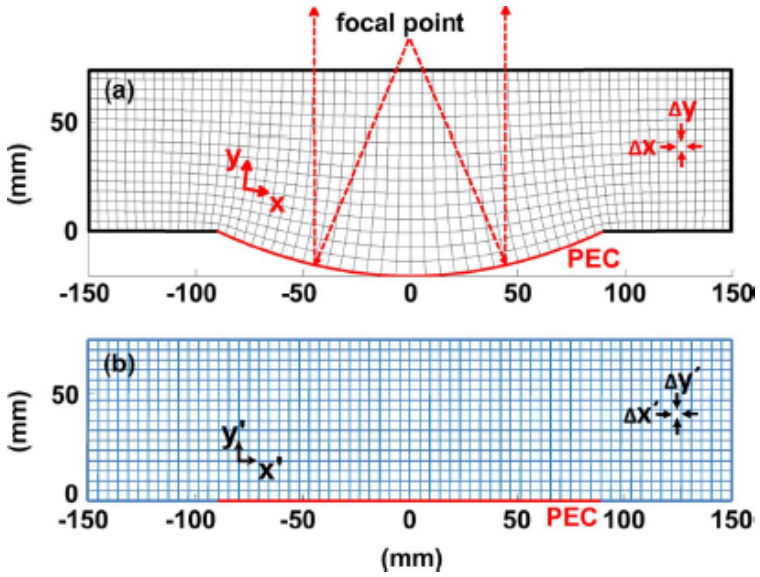

Figure 3.3: In figure (a) is the virtual space with distorted coordinates. A reflector is set in the air. This is illustrated by the bottom curve. Figure (b) is the physical space with Cartesian coordinates. The curved reflector is replaced with a flat PEC sheet at the bottom (3).

To illustrate how this orthogonality restriction can be approximately satisfied we use the example of the flat parabolic reflector. The top grid in Fig. 3.1 shows the distorted virtual space which defines the device and the bottom grid shows the flat real device grid for illustration. A sample distorted cell is drawn in Fig. 3.1 which is characterized by the co-variant metric, g

$$g = \begin{pmatrix} g_{11} & g_{12} \\ g_{21} & g_{22} \end{pmatrix} \tag{3.21}$$

$$g_{i,j} = \overrightarrow{a_i} \cdot \overrightarrow{a_j} (i, j = 1, 2) \tag{3.22}$$

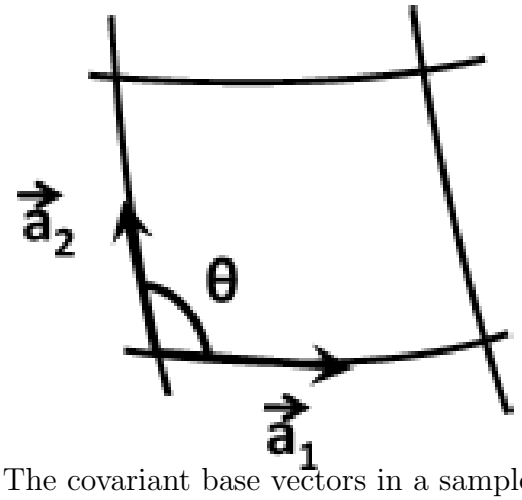

Figure 3.4: The covariant base vectors in a sample distorted cell (3).

where $\overrightarrow{a_1}$ and $\overrightarrow{a_j}$ are the co-variant base vectors defined in Fig. 3.1 and θ is the angle in between. We quantify the orthogonality of the grid using the parameter θ for each cell defined as

$$cos(\theta)\sqrt{\frac{g_{12}g_{21}}{g_{11}g_{22}}} \tag{3.23}$$

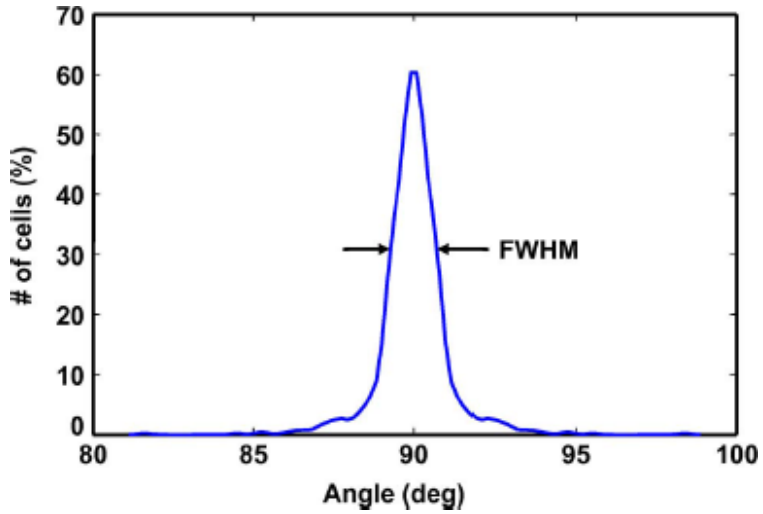

Figure 3.5: The distribution of the degrees between two local coordinates in every grid of the virtual space. The orthogonal property is quantified by the full width half maximum (FWHM) index. When the FWHM index is approaching zero, the local coordinates are near-orthogonal. In this case the index is only 1°, indicating that the local coordinates are near-orthogonal (3).

In Fig. 3.1 the distribution of the angle parameter θ is plotted for the grid shown in the flat reflector shown in Fig. 3.1 We observe that most cells are near-orthogonal and are distributed around the 90° point with a smaller number away from the 90°. The FWHM is measured from this distribution. For a perfectly orthogonal grid, $\cos\theta = 0, FWHM = 0$ and ultimately $\mu'_{xx}\mu'_{yy} = \mu_0^2$. However, for the near orthogonal grid such as the example, section 3.1, these conditions can be approximately satisfied yielding an all-dielectric device with a very minor sacrifice in performance. The near-orthogonal property ensures the approximation of Eq. 3.12 that

$$\mu' = \mu_0 \begin{pmatrix} (\frac{\delta x'}{\delta x})^2 & 0 \\ 0 & (\frac{\delta y'}{\delta y})^2 \end{pmatrix} / det(J) \tag{3.24}$$

Because all meshes are generated to be approximately square shaped μ'_{xx} and μ'_{yy} have similar values and the permeability matrix has equal tensor elements which are equal to unity, as that in free space. The relative permeability of the device is assumed to be isotropic and unity and the effective relative refractive index in Eq. 3.13 is only dependent on ϵ'_z

$$n'^2 \simeq \epsilon'_z/\epsilon_0 = \frac{1}{det(J)} \tag{3.25}$$

Under the orthogonal condition of Eq. 3.15 and Eq. 3.1, the refractive index profile of the device can be directly retrieved from the cells of the generated grid using Eq. 3.8

$$n'^2 \simeq \frac{1}{\frac{\delta x'}{\delta x}\frac{\delta y'}{\delta y}} \simeq \frac{\triangle x \triangle y}{\triangle x' \triangle y'} \tag{3.26}$$

where $\triangle x, \triangle y, \triangle x', \triangle y'$ are the dimensions of each cell in the two coordinate systems shown in section 3.1.

For the case of H polarization similar results are obtained. In this case the contributing components of the permittivity and permeabilty are $\epsilon_{xx}, \epsilon_{xy}, \epsilon_{yy}, \epsilon_{yx}$ and μ_{zz} as seen in Eq.3.8. Under the orthogonality criteria of Eq. 3.15 and Eq. 3.1, the permittivity and permeability

tensors become

$$\overline{\overline{\epsilon'}} = \epsilon_0 \begin{pmatrix} \frac{\delta x'^2}{\delta x} & 0 \\ 0 & \frac{\delta y'^2}{\delta y} \end{pmatrix} / det(J) \tag{3.27}$$

$$\mu'_z = \mu_0 det(J)^{-1} \tag{3.28}$$

while $det(J) = (\delta x'/(\delta x).(\delta y')/(\delta y)$. The effective refractive index is now

$$n'^2 = n'_{xx} n'_{yy}/(\epsilon_0 \mu_0) = \sqrt{\epsilon'_{yy} \epsilon'_{xx} \mu'_z/(\epsilon_0 \mu_0)} \tag{3.29}$$

It can be easily checked that $\epsilon'_{xx}\epsilon'_{yy} \simeq \epsilon_0^2$ is true and thus the effective refractive index in this case is dependent on the chosen mesh as in Eq. 3.24

$$n'^2 \simeq \mu'_z/\mu_0 = \frac{1}{det(J)} \tag{3.30}$$

The analysis for the H-polarization indicates that a properly selected magnetic material can control these waves, similar to how a dielectric material can control the E-polarized waves. Therefore we have shown here that the designer can generate a mesh under the assumptions specified in this section. One must calculate the refractive index distribution from Eq. 3.26 and choosing either tuning ϵ or μ to operate over the E-polarization or H-polarization.

Discrete transformation optics devices can be simplified from a complex inhomogeneous and anisotropic material into a simpler and more easily fabricated one by using a lower resolution of materials (1). Researchers have simplification material parameters from 100's of blocks of different permittivity to tens of blocks without sacrificing performance. This uses effective material theory in order to average the permittivity values in a region using the Maxwell-Garnet theorem

$$\sum \delta \frac{\sigma_i - \sigma_e}{\sigma_i + (n-1)\sigma_e} = 0 \tag{3.31}$$

This formula applies to circular inclusions where n is the spatial dimension, δ_i and σ_i are

respectively the fraction of permittivity of each component and σ_e is the effective permittivity of the medium. This averaging process was applied to fabrication of discrete coordinate transformation medium using spherical 'holey' dielectrics. Each sphere was a different size to enable a different permittivity at that point in the material.

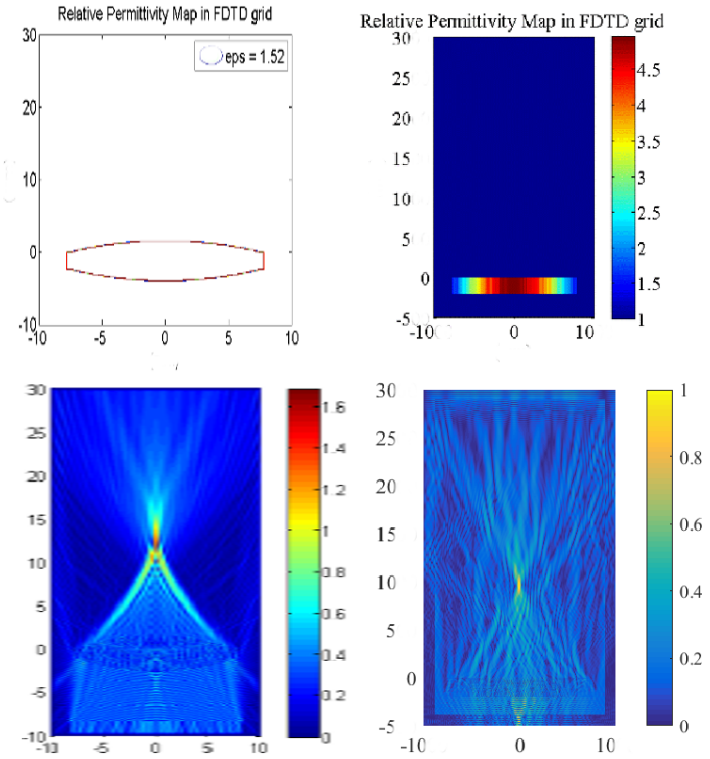

Figure 3.6: The single original lens is in the FDTD simulation on the top left. The flat lens permittivity map on the top right. The electromagnetic field distribution of the single lens and the TO lens is shown in the figure below. The simulation domain units are in cm. The lens is 16 cm wide and 2 cm thick for 8 GHz centre frequency.

The design method also allows us to set the right hand corner of the transformation grid to whatever we want. It makes sense here to make it equivalent to free space. This means that the wave entering at this position features very few reflections. This impedance matching of the transformation media to free space where the incident radiation enters to material immediately improves the performance of the device significantly compared with

traditional devices in terms of reflections and consequently transmission. It also allows the designer to use more easily accessible range of material parameters for the permittivity of the device.

fig. 3.6 shows the single lens taken from the Zemax image library on the top left. The figure in the top right shows the permittivity map in the the flat TO lens using the mathematical machinery described in this section. We can see that it is matched to free space at the edge and features a high permittivity in the centre due to compression of the lens in the centre. The bottom panels show the FDTD grid along with the field calculation for the original single lens and the transformed TO lens. The operating frequency is 8 GHz and the simulation domain is terminated with PML. According to the approximate discrete coordinate transformation method the incident radiation must be E-polarised therefore a TE mode incident wave is used and the focus of the original lens was 11.69 cm and the focus of the transformed lens is 10.19 cm. The focal length of the original lens is 11.69 cm measured from the back surface of the lens to the maximum intensity perpendicular to the centre of the lens and the focal length for the transformed lens is measured from the back surface of the lens which is now flat to the maximum intensity perpendicular to the centre of the lens at 10.19 cm. The original lens is 1.7 cm wide or 3.4 cm in diameter where the center of the original lens is at -0.5 cm making the focal length from the centre 11.19 cm. The width of the flat lens is 1 cm making the focal length from the centre of the lens 9.19 cm for the flat lens. The difference in focal length might be that the flat lens does not exactly match the condition that the transformed grid is not exactly isotropic.

3.2 Conclusion

In this section we have shown that a single lens can be designed using Transformation Optics and serves as a test of our methodology for the application to a more complex object. The

field distribution due to the FDTD simulation validates our approach in using Discrete Coordinate Transformation. In the next section we will apply this to the design of our MTM Cooke Triplet. The ability to create conformal flat surfaces allows simplification of optical systems while maintaining the original optical performance and is a key principle of us proceeding with the Discrete Coordinate Transformation method. The focal length is close to the original lens to verify the DCT method. The transformed lens has a variation in its permittivity values and a flat surface and benefits from being impedance matched to free space reducing reflections at the initial surface.

Bibliography

[1] Q. Wu, J. P. Turpin, X. Wang, D. H. Werner, A. Pogrebnyakov, A. Swisher, and T. S. Mayer, "Flat transformation optics graded-index (to-grin) lenses," in *Antennas and Propagation (EUCAP), 2012 6th European Conference on*. IEEE, 2012, pp. 1701–1705.

[2] F. Kong, B.-I. Wu, J. au Kong, J. Huangfu, S. Xi, and H. Chen, ""Planar focusing antenna design by using coordinate transformation technology"," *Applied physics letters*, 2007.

[3] Wenxuan Tang, Christos Argyropoulos, Efthymios Kallos, W. Song, and Y. Hao, ""Discrete Coordinate Transformation for Designing All-dielectric Flat Antennas"," *IEEE Transactions on Antenna and Propagation*, 2010.

[4] N. K. D. A. Roberts and D. R. Smith, ""Optical lens compression via transformation optic"," *Optics express*, 2009.

[5] "Kymeta delivers on the promise of what connectivity is supposed to be. Its removing barriers, spurring new waves of innovation and helping realize the power of a truly connected future through the use of a first-of-its-kind satellite antenna that can connect

anything that moves., howpublished = http://www.kymetacorp.com/, note = Accessed: 2015-09-23."

[6] R. Mittra and Y. Zhang, "A low-reflection flat-lens design for microwave imaging system," in *Antennas and Propagation (EUCAP), Proceedings of the 5th European Conference on.* IEEE, 2011, pp. 851–852.

[7] N. Yu and F. Capasso, "Flat optics with designer metasurfaces," *Nature materials*, vol. 13, no. 2, pp. 139–150, 2014.

Chapter 4

FDTD Analysis of A MTM and DCT Cooke Triplet

In this chapter we look at an overview of the design of the Cooke Triplet using a grid generation software package which forms the basis for the geometry generation and then the discrete coordinate transformation which yields permittivity and permeability values to insert into an FDTD grid for electromagnetic modelling. In the first subsection an explanation of the Cooke triplet, what it does, how it does it and what makes it unique in terms of minimizing the five Seidel aberrations is presented. In the next section we explain how the Cooke triplet is modeled in virtual space and mapped using ray tracing in order to generate a grid from which to transform into our flat TO Cooke Triplet. The method for calculating the permittivity values for the TO Triplet is explained in the next section including how a reduced map might be fabricated using readily available dielectric materials only. In the final section the FDTD method is used to model the TO Cooke Triplet and the mechanisms such as PML boundary conditions and FDTD modeling of dispersive materials is explained in the context of modeling the TO Cooke triplet to verify the operation of the design.

4.1 A Cooke Triplet

The Cooke triplet was first designed and patented in 1893 by Dennis Taylor who sold the patent to TT&H Cooke and sons of York which still makes the lenses under the name Cooke Optics in Thurmaston near Leicester. The Cooke Triplet eliminates five of the third-order Seidel aberrations (Spherical, Coma, Astigmatism, Distortion and Field Curvature) and in addition the frequency dependent aberration Chromatic aberration. The Cooke Triplet minimizes the aberrations in an image (1) by using a combination of two converging lenses surrounding a diverging lens. Multiple lenses are used to reduced spherical and coma aberrations, field curvature is flattened, astigmatism is reduced and distortion minimized by tailoring the lens surface curvatures, distances and lens powers. The chromatic aberration is minimized by using different refractive index materials; a combination of Crown and Flint glass for the different glass elements. Spherical aberration can be reduced using a combination of concave and convex lenses, off axis aberrations: coma and astigmatism can be reduced by tailoring the lens spacing and field curvature can be reduced by adjusting the lens spacing and use of a stop, whereas distortion can be controlled by use of a symmetrical system. The TT&H Cooke lens catalogue of 1897 states: "Lack of sharp definition at the margins, and blackness and lack of detail in the shadows, are among the commonest defects of photographs. The introduction of lenses which, without the use of stops, yield definition uniformly fine throughout their plates, marks quite a new era in photography." The Cooke Triplet is still used to capture images and reduce optical aberrations in a variety of applications today from cheap mass-produced cameras to expensive ones used by the film industry. A Cooke triplet design, undertaken using the optical software package Zemax, is shown in Figure 4.1.

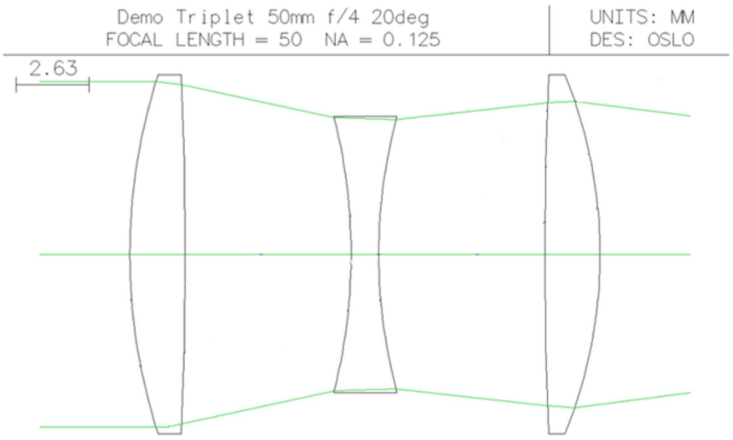

Surface		Radius	Thickness	Glass Type	Semi-diameter
1	Standard	2.2014	0.3259	SK16	0.95
2	Standard	-43.576	0.6008		0.95
3	Standard	-2.2213	0.1	F2	05
4	Standard	2.0292	0.475		0.5
5	Standard	7.9684	0.2952	SK16	0.75
6	Standard	-1.8395	4.2208		0.75

Figure 4.1: The Cooke Triplet with accompanying glass types, curvatures and thicknesses with meridonal and paraxial rays. The key optics data is taken from the triplet lens library in Zemax. The focal length of this device is 50 mm, NA is 0.125 and the scale is given. This is the specification of the lens designed using the transformation optics method. Glass type SK16 and F2 are crown glass and flint glass types.

Optimisation is the process where the performance of a lens system is improved by changing the values of some of the lens variables such that the measure of lens performance is improved. The measure of lens performance is recorded in the merit function. The merit function is a list of targets that Zemax minimizes during the operation of the lens design. The initial lens used in terms of surface curvature, lens thickness and glasses is given in (1). No optimization process is done on this Cooke Triplet taken from this source and then used hereafter in this thesis. We will in the following section describe the creation of the Cooke Triplet in Zemax.These lens parameters are given in Fig. 4.1. The lens used was the standard lens in the Zemax lens library.

The Cooke Triplet can be designed with the following tailoring parameters to find an optical combination of parameters for the three lenses (2)

$$K = K1 + \frac{h2K2}{h2} + \frac{h3K3}{h1} \tag{4.1}$$

$$P = \frac{K1}{n1} + \frac{K2}{n2} + \frac{K2}{n3} \tag{4.2}$$

$$C1 = \frac{h2^2K1}{V1} + \frac{h2^2K2}{V2} + \frac{h3^2K3}{V3} \tag{4.3}$$

$$C2 = \frac{h1\bar{h1}K1}{V1} + \frac{h2\bar{h2}K}{V2} + \frac{h3\bar{h3}K3}{V1} \tag{4.4}$$

Where K is the power, P is the Petzval sum and C_1 and C_2 are the longitudinal and transverse chromatic aberrations. K1, n1, h1, V1 is the power, refractive index, height and Abbe or V-value of lens 1 (2). h is the height of the lens for the marginal ray and $\bar{h}$ is the height for the chief ray. These variables govern all the parameters of the optical system which can be altered by the designer in order to minimize the optical aberrations in the system of lenses. As we have explained the single lens features significant spherical aberration and coma which can be reduced by the use of additional lenses. In tailoring these additional lenses we can control the overall properties of the system of lenses in terms of the overall power and also the chromatic aberrations C_1, C_2 which can be reduced using the correct selection of materials which refractive indices. P is the Petzval sum which determines the amount of field curvature in the overall system of lenses. It is possible to have positive or negative aberrations C_1 and C_2 and the optimal system will have a value closest to zero.

The Cooke triplet is tailored using these equations containing the independent variables: distances between the lenses d_1 and d_2, six curvatures of the lenses which can be considered as three powers K_1, K_2 and K_3 and three shape factors. Usually a glass type is chosen first, there is no unique solution and typically an estimate is made and then optimized for a given merit function. It is an achromatic lens in that it minimizes chromatic aberration by

balancing the powers of two converging lenses with a central diverging lens. A Cooke Triplet comprises a negative flint glass element in the centre with a crown element on each side.

Optical designers has been reducing the aberrations in an image to create good photographic equipment for centuries by adding more lenses to a system giving them the ability to tailor the aberrations in the final image to give a better image. The novel feature of the Cooke Triplet is that it uses a fair amount of symmetry and different materials to achieve a significant reduction in optical aberrations using only 3 lenses as opposed to using 8 or 10. This results in a reduction in cost, size and weight of the system. Cooke triplets are still used today in many low cost disposable cameras to produce low aberration images.

4.2 Grid Generation of the Virtual Coordinate Space

Grid generation is the process where a geometric shape is approximated using a mesh. Grid generation is an important part of engineering fluid flows and designing structures such as airplane aerofoils among other things. We use mesh generation software Pointwise to take the geometry of rays in the Cooke Triplet and utilize their smoothing function to generate a quasi-orthogonal mesh. The details of this smoothing process using Elliptic PDE smoothing with the Laplace function describes how a quasi-orthogonal mesh which describes the Cooke triplet was arrived at. The Cooke Triplet is a multi-block structure requiring multiple meshes to be generated. This mesh is then feed into the discrete coordinate transformation optics solver and FDTD grid in Matlab and this method is described in this section.

Ray tracing is carried out on the Cooke Triplet and these form the basis for the boundaries of the grid, see Fig. 4.2. The straight ray can be imagined entering the Cooke Triplet,

being deflected towards the centre by the initial concave lens, it is then focused back to the centre by the central diverging lens and the focused again at the final peak by the second converging lens before reaching a focus. The rays are cut off before the final focus is reached. The rays are presumed to travel in a straight line when they leave the transformation optics device.

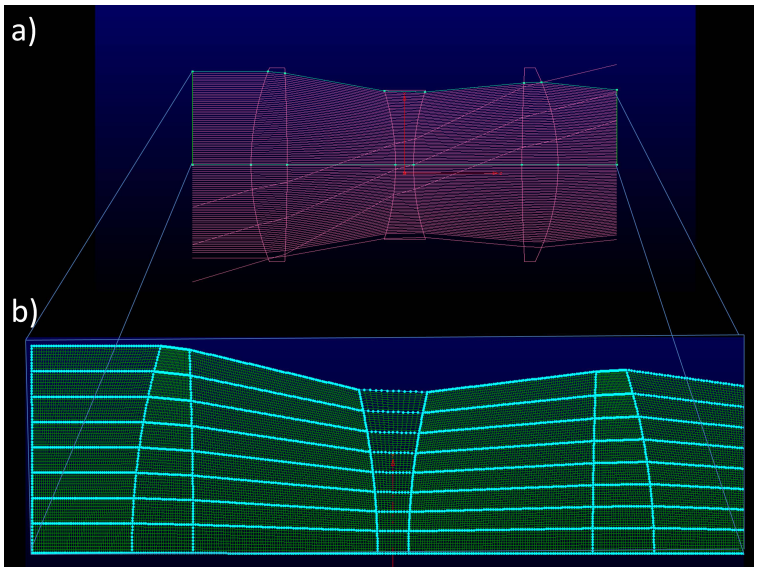

Figure 4.2: Panel (a) shows the results from the numerical grid generation software Pointwise for the Cooke Triplet. The lateral lines are the rays and the structure of the lens is visible. In panel (b) only the top half is modelled to space and the design will be copied later in Matlab using symmetry considerations for the triplet.

The Laplace equation is a good one to use because it is inherently a smooth function which results from the calculation.

$$\nabla\phi = 0 \tag{4.5}$$

The Pointwise generated grid, Fig. 4.3 is made orthogonal using a smoothing function. Only the top half is modelled and the design will be copied later in Matlab using symmetry consideration for the triplet. The grid size between the grid boundary nodes is 0.14 mm for an

operating wavelength of 37.5 mm (8 GHz). This involves the commercial program solving a set of partial differential equations. The Laplace smoothing functions create quasi-orthogonal grids by optimizing the distribution of cells. The grid is optimised for a discrete coordinate transformation limit for orthogonality using this smoothing function on the grid.

The mesh generation is achieved using iterations of an elliptic Partial Differential Equation (PDE) (4) which is of the form

$$Au_{xx} + 2Bu_{xy} + Cu_{yy} + Du_x + Eu_y + F = 0 \tag{4.6}$$

This generates a mesh with equally space grid points at the edge and a consistent number of points in the x and y axis along a distorted boundary region in which the individual cells are optimized for orthogonality.

The modified Liao functional was used in the smoothing of the grid for the carpet cloak in (5) and in the design of this Triplet.

$$I_{ml} = \int \int_{g'} (\frac{g_{11} + g_{22}}{\sqrt{g}})^2 d\zeta d\nu \tag{4.7}$$

It is used with the slipping condition at the boundaries which allows a quasi-orthogonal grid to be generated with the condition that the boundary grid points are allowed to slip. The slipping boundary condition means that each of the four boundary edges of the virtual domain must be mapped to the four boundaries of the real space only up to sliding freedom. The no slip condition in computational fluid dynamics is that the fluid flow parallel to the surface at the boundary is assumed to be zero. Allowing slipping in this calculation means that the field at the boundaries are not held to this condition that they must be zero.

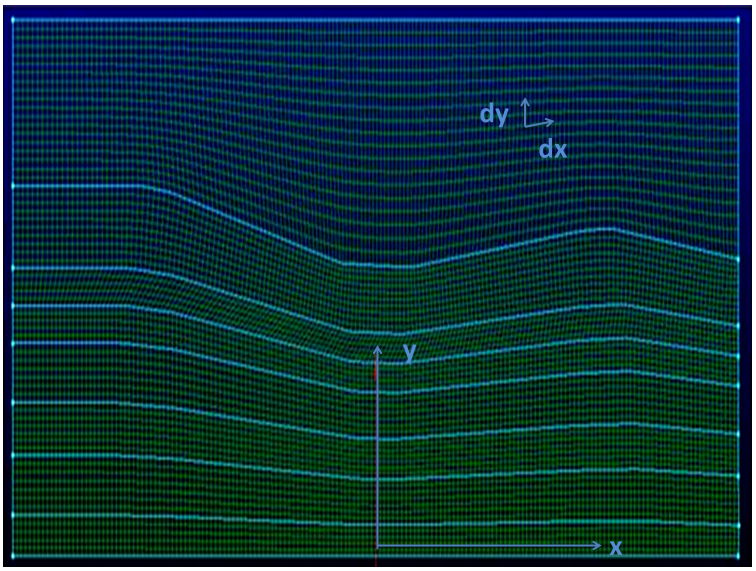

Figure 4.3: This shows the grid generated in Pointwise. The curved lines are the boundaries of the grids taken from the ray tracing data of the Cooke Triplet together with having to place the device is a box to create the edges of the device. Elliptic grid generation is then applied to the grids for a grid cell spacing of 0.14 mm. Laplace smoothing is applied to the grids following this to achieve the smoothest possible grid to allow for the quasi-orthogonal approximation to be met on the MTM Triplet. x and y show the x and y axis in the grid coordinate system and dy and dx show the coordinate system for the individual grid cell.

Great care is taken in the creation of the final grid. This acts at the virtual distorted space for the Cooke Triplet upon which coordinate transformation is applied. The Laplace smoothing function ensures orthogonality of the grid and non-slipping boundary conditions are used to create a smooth flat orthogonal map. Cartesian coordinates are used to create cells which are rectangular which allows us to apply co-ordinate transformation and the calculation of the metric tensor easier.

4.3 The Discrete Transformation Optics Calculation

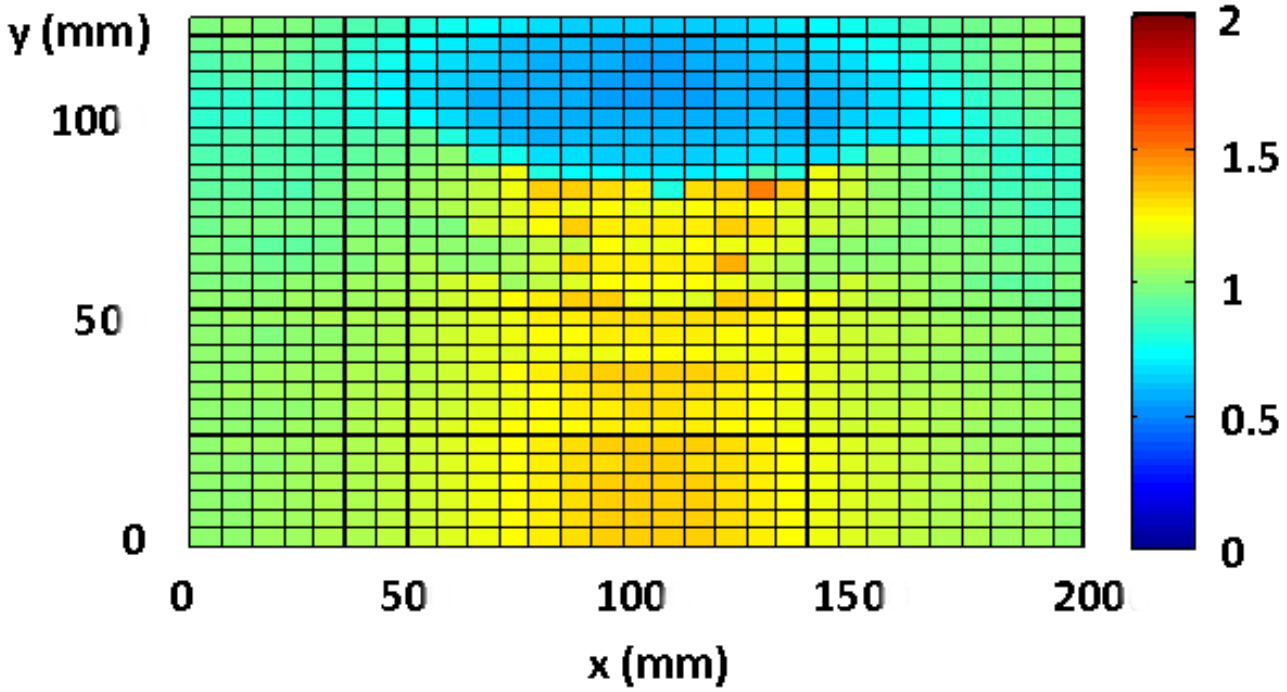

Figure 4.4: The Permittivity map obtained using TO which shows the values of Permittivity for a flat implementation of the Triplet. The FDTD simulation domain before a signal is launched contains this discretised Permittivity map. The blue areas are those with a Permittivity less than one generated from regions of the virtual space which are larger than the real flat space. Notice only the top half of the Permittivity map is shown as only the top half of the Cooke Triplet was meshed and this is copied according to symmetry for the final FDTD simulation.

The permittivity map, Fig. 4.4, was generated by the DCT design algorithm. A simplified map is also created where all MTMs are removed and replaced with index real dielectric material of 1.0. The relative permittivity of the transformation optics lens is between 1.5 and 0.8. The method used is that described in the chapter 3. Only the top half of the triplet is shown and symmetry used when placed into the FDTD grid to simulate the bottom half of the lens. The blue regions are those where the grid cells are stretched in virtual space compared with the flat real space resulting in a result with the permittivity less than one i.e. a MTMs implementation which are shown in blue. The reduced map has these region

removed so that an dielectric device can be created.

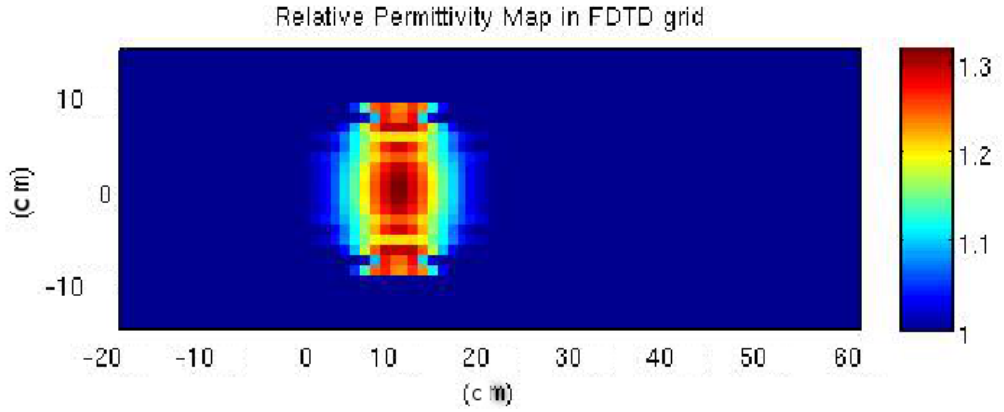

Figure 4.5: The permittivity map for the reduced map in the FDTD grid. The lens is 20 cm by 20 cm where the grid is larger due to the scaling which we did to reduce the size of the simulation domain to allow for fast simulation of the device. It is surrounded by free space and is also matched to free space to reduce reflections. The highest Permittivity relative to free space is $1.3\epsilon_0$ in the centre.

The reduced map is shown in fig. 4.5 in the FDTD grid. A reduced map may be implemented due to discrete coordinate transformation optics in this case so long at the device is impedance matched. The permeability is one as described in previous chapters which allows fabrication with a material with a permeability of unity of which all naturally occurring elements are and we might fabricate a real device. Using the discrete transformation method we can represent the transformation solely in terms of permittivity and the map of this transformation optics lens is given in Fig. 4.5 where the metamaterial cells in Fig. 4.4 have been removed, the permittivity rotated due to symmetry in the y axis and placed in an FDTD grid .

4.4 The FDTD Method for Modelling Metamaterials

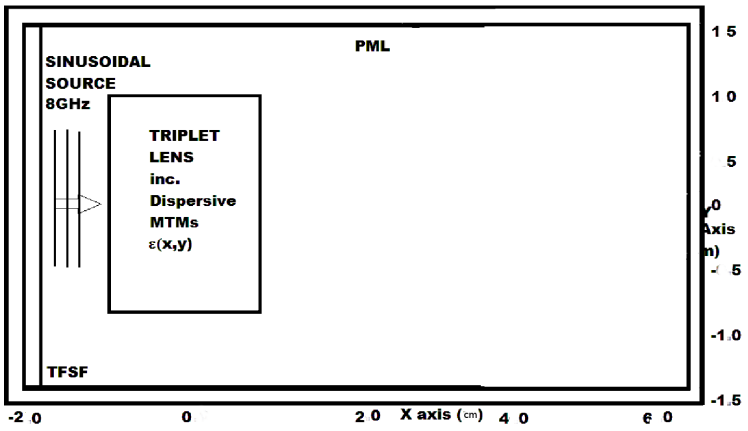

Figure 4.6: The Cooke Triplet is centered at zero and extends 20 cm by 20 cm. A sinusoidal plane wave is launched and controlled using Total Field / Scattered Field (TF/SF) formulation. The simulation domain is terminated using a Perfectly Matched Layer (PML). The dispersive MTM values in the triplet are modelled using the ADE approach.

FDTD modelling stands for Finite Difference Time Domain (FDTD) and it is a highly effective technique for modelling the electromagnetic field giving time domain results. There follows a brief introduction to the FDTD method (13; 14) which is used to model the MTM Triplet map and the All-Dielectric map lens. The permittivity map calculated in the previous section is placed in an FDTD grid according to the Fig. 4.6. FDTD has been used to model antennas as well as other standard antenna modelling methods such as the Method of Moments (MoM) (15). The FDTD method is a numerical method which solves Maxwell's equations in the time domain and can be used to simulate the 3D electromagnetic field in the presence of a 3D dielectric material (16). This method has been used successfully many times in the study of the cloaking devices (17; 18) and in the MTMs (19). For MTM based devices the boundary conditioned have to be modified in order for the left hand behaviour to be modelled. Backwards wave propagation can be seen in simulations of such devices as expected as well as negative refraction (20).

FDTD is chosen to model the lens over other methods such as plane wave expansion or finite element methods in modelling MTMs (21) because it allows the easy implementation of dispersive and anisotropic materials. Finite element time domain methods also allows a time domain simulation which is more intuitive to grasp compared to frequency domain methods. The Finite Difference Time Domain (FDTD) method allows simulation of structures with anisotropic and inhomogeneous values of complex permittivity matrices and simulation. The FDTD method can also be extended to parallel architectures to increase simulation domain size and accuracy of modelling results which allows parallelisation and the computation of very electrically large structures. FDTD codes can also be written in C rather than MATLAB to improve computational execution time.

A Yee grid, named after the author of the original paper (22), is used to place the field components, see Fig. 4.7. The magnetic field components are staggered compared to the electric so the code can leap-frog from magnetic to electric. The Yee grid gives a structure to the simulation domain which allows Discretization in space where the unit cell is a Yee grid and this separation of the simulation domain allows a mathematical solution to Maxwell's equations. This staggered arrangement means it is possible to solve for the **E** field and then use these values to supplement the calculation of the adjacent **B** fields.

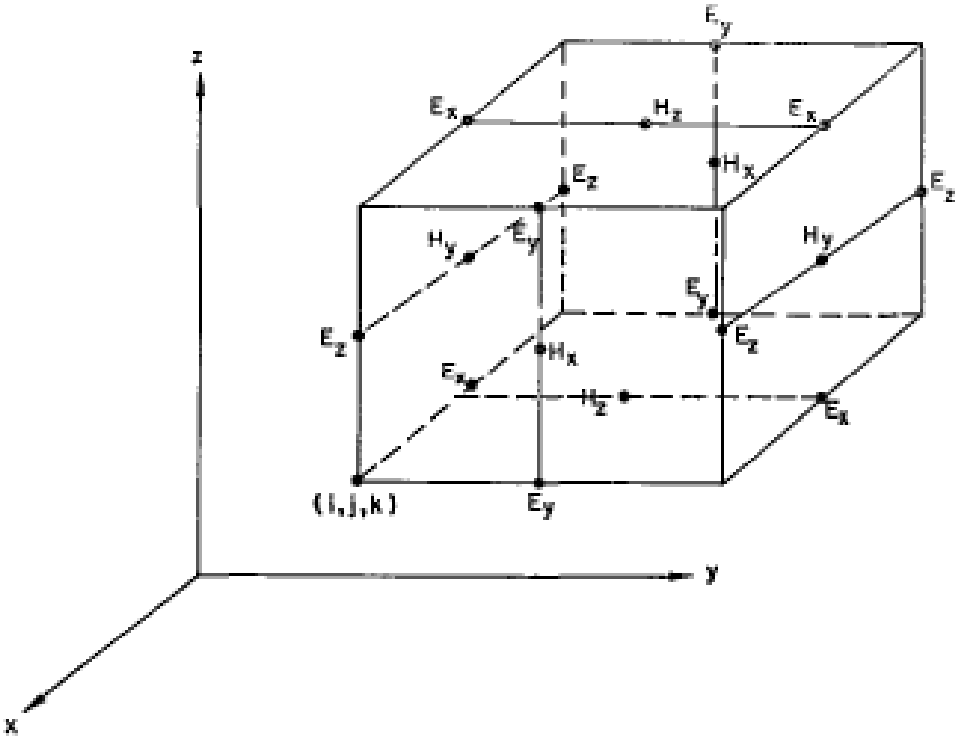

Figure 4.7: The Yee grid unit cell in 3D where magnetic and electric fields are placed in a staggered arrangement to allow the solution of Maxwell's equations for each grid cell (i,j,k).

In FDTD, for the simulation to remain stable the Courant stability condition

$$c\triangle t \leq \triangle x \tag{4.8}$$

must be satisfied. The physical interpretation of this equation is that information can travel in the grid no faster than the speed of light. Therefore when the Courant condition is satisfied, the grid is causally connected and the results are stable solutions. This is achieved when the Yee grid cell spacing is less than a tenth of the wavelength and less than one thirtieth when dispersive FDTD is used (18). At this size the radiation does not interfere with the structure in terms of diffraction or refraction as the radiation does not typically resolve structures less than a tenth of the wavelength. At this level the wave perceives a continuous refractive index and allows for smooth control of the radiation.

The FDTD method is a solution to Maxwell's equations which describe electromagnetic fields:

$$\nabla \cdot E = 4\pi\rho \tag{4.9}$$

$$\nabla \cdot B = 0 \tag{4.10}$$

$$\nabla \times E = -\frac{1}{c}\frac{\delta B}{\delta t} \tag{4.11}$$

$$\nabla \times B = \frac{1}{c}(4\pi J + \frac{\delta D}{\delta t}) \tag{4.12}$$

Solutions can be split into TE and TM mode solutions which do not interact as they are separate modes which can be split and analysed in order to simplify the equations, for the TE mode we have

$$\epsilon_0 \frac{\delta E_x}{\delta t} = \frac{\delta H_z}{\delta y} \tag{4.13}$$

$$\epsilon_0 \frac{\delta E_y}{\delta t} = -\frac{\delta H_z}{\delta x} \tag{4.14}$$

$$\mu_0 \frac{\delta H_z}{\delta t} = \frac{\delta E_x}{\delta y} - \frac{\delta E_y}{\delta x} \tag{4.15}$$

where the component E_x, E_y and H_z are non-zero.

The finite-difference approximation allows the solution of the differential equations to be solved leads to Maxwell's equations in TE mode with a finite difference where how the field are split according to the Yee grid cell structure where the grid cells are $\triangle x$ by $\triangle(y)$ in dimension and split into integer number i and j in the x and y axes

$$\epsilon_0 E_x(i + \frac{1}{2}, j) = \frac{H_z(i + \frac{1}{2}, j + \frac{1}{2} - H_z(i + \frac{1}{2}.j - \frac{1}{2})}{\triangle y} \tag{4.16}$$

$$\epsilon_0 E_y(i, j + \frac{1}{2}) = \frac{H_z(i + \frac{1}{2}, j + \frac{1}{2} - H_z(i - \frac{1}{2}.j + \frac{1}{2})}{\triangle x} \tag{4.17}$$

$$\mu_0 H_z(i+\frac{1}{2}, j+\frac{1}{2}) = \frac{E_x(i+\frac{1}{2}, j+\frac{1}{2}) - E_x(i+\frac{1}{2}.j)}{\triangle y} - \frac{E_y(i+1, j+\frac{1}{2} - E_y(i, j+\frac{1}{2})}{\triangle x} \quad (4.18)$$

The time-stepping equations, fig. 4.8, are where n is the time step. The separation of the time field into discrete units is known as the leap-frog method. The space and time stepping grid is arranged in a leap-frog arrangement where one component is calculated and then used recursively in the next calculation. The electromagnetic field components calculated on the previous iteration are the only input in calculating the field components for the next successive field component. The electric and magnetic field componants are staggered at half intervals and solved alternatively each result feeding into the calculation of the next

$$E^n = E^{n-1} + \frac{\triangle t}{\epsilon_0} \triangle x H^{n-1/2} \quad (4.19)$$

$$H^{n+1/2} = H^{n-1/2} - \frac{\triangle t}{\mu_0} \triangle x E^n \quad (4.20)$$

This is a very convenient set of equations for computational calculations using iterations. This provides a differential solution to Maxwell's equations which is time dependent. This means that the simulation results are inherently time dependant and can be represented as a movie. In this thesis simulations are presented once the simulation results have converged where the electric field component changes less than 1% compared to the previous time step.

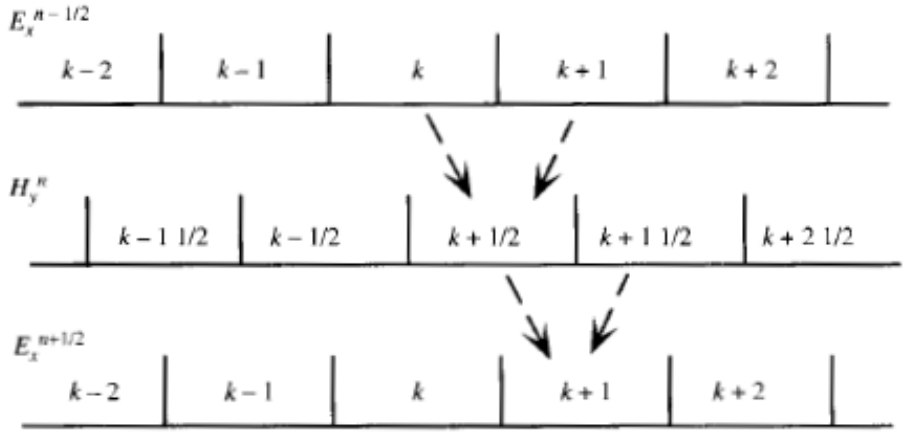

Figure 4.8: A schematic of the time-stepping method for the calculation of the FDTD simulations. Time is split into integer time steps n-1, n and n+1, k is the grid cell number where the magnetic field, H_y, is at every half integer and the electric field E_x is at every whole integer. The two adjacent field components from the dual field vector are used to calculate the next field vector. This gives the possibility of time domain movie animations in FDTD for algorithm execution.

To model the interaction with conventional dielectrics in the simulation using FDTD the finite difference equations, here in 2D, material properties such as conductivity σ and permittivity ϵ and permeability μ are combined into variables C_a, C_b, D_a, D_b Where the coefficients are given by

$$C_a|_{i,j,k} = (1 - \frac{\sigma_{i,j,k}\triangle t}{2\epsilon_{i,j,k}})/(1 + \frac{\sigma_{i,j,k}\triangle t}{2\epsilon_{i,j,k}}) \tag{4.21}$$

$$C_{b_1}|_{i,j,k} = (\frac{\triangle t}{\epsilon_{i,j,k}\triangle_1})/(1 + \frac{\sigma_{i,j,k}\triangle t}{2\epsilon_{i,j,k}}) \tag{4.22}$$

$$C_{b_2}|_{i,j,k} = (\frac{\triangle t}{\epsilon_{i,j,k}\triangle_2})/(1 + \frac{\sigma_{i,j,k}\triangle t}{2\epsilon_{i,j,k}}) \tag{4.23}$$

$$D_a|_{i,j,k} = (1 - \frac{\rho'_{i,j,k}\triangle t}{2\mu_{i,j,k}})/(1 + \frac{\rho'_{i,j,k}\triangle t}{2\mu_{i,j,k}}) \tag{4.24}$$

$$D_{b_1}|_{i,j,k} = (\frac{\triangle t}{\mu_{i,j,k}\triangle_1})/(1 + \frac{\rho'_{i,j,k}\triangle t}{2\mu_{i,j,k}}) \tag{4.25}$$

$$D_{b_2}|_{i,j,k} = (\frac{\triangle t}{\mu_{i,j,k}\triangle_2})/(1 + \frac{\rho'_{i,j,k}\triangle t}{2\mu_{i,j,k}}) \tag{4.26}$$

where $\triangle_1$ and $\triangle_2$ denote two possible lattice increments and for a cubic lattice $\triangle x = \triangle y = \triangle z$. In this case $C_{b_1} = C_{b_2}$ and $D_{b_1} = D_{b_2}$.

The time stepping equations including the C and D coefficients are as follows:

$$Ez^{n+\frac{1}{2}}_{i-\frac{1}{2},j+\frac{1}{2}} = C_a Ez^{n-\frac{1}{2}}_{i-\frac{1}{2},j+\frac{1}{2}} + C_b(Hy^n_{i,j+\frac{1}{2}} - Hy^n_{i-1,j+\frac{1}{2}} + Hx^n_{i-\frac{1}{2},j} - Hx^n_{i-\frac{1}{2},j+1}) \tag{4.27}$$

$$Hx^{n+1}_{i-\frac{1}{2},j+1} = D_a Hx^n_{i-\frac{1}{2},j+1} + D_b(Ez^{n+\frac{1}{2}}_{i-\frac{1}{2},j+\frac{1}{2}} - Ez^{n+\frac{1}{2}}_{i-\frac{1}{2},j+\frac{3}{2}}) \tag{4.28}$$

$$Hy^{n+1}_{i,j+\frac{1}{2}} = D_a Hy^n_{i,j+\frac{1}{2}} + D_b(Ez^{n+\frac{1}{2}}_{i+\frac{1}{2},j+\frac{1}{2}} - Ez^{n+\frac{1}{2}}_{i-\frac{1}{2},j+\frac{1}{2}}) \tag{4.29}$$

4.4.1 PML and TF/SF Boundary Conditions

Boundary conditions that avoid reflections at the edges of the problem space, obscuring the electromagnetic solution, are available using a Perfectly Matched Layer PML (23). The boundary conditions to the simulation domain are a rectangular PML

$$\mu_2\frac{\delta H_x}{\delta t} + \sigma_y H_x = \frac{-\delta E_z}{\delta y} \tag{4.30}$$

$$\mu_2\frac{\delta H_y}{\delta t} + \sigma_x H_y = \frac{\delta E_z}{\delta x} \tag{4.31}$$

$$\epsilon_2\frac{\delta E_{zx}}{\delta t} + \sigma_x E_{zx} = \frac{\delta H_y}{\delta x} \tag{4.32}$$

$$\epsilon_2\frac{\delta E_{zy}}{\delta t} + \sigma y E_{zy} = \frac{-\delta H_x}{\delta y} \tag{4.33}$$

which acts as an absorbing layer to the incident radiation from all angles of incidence and reduces the reflection intensity to zero.

For this lens simulation the frequency of the incidence field is 8 GHz which is in the

microwave regime and therefore the geometric approximation used for ray tracing remains valid. The resolution is $\lambda/20$ satisfying the stability condition. A high quality sinusoidal source is launched using the Total-Field Scattered Field formulation

$$H_{total} = H_{scat} + H_{inc} \tag{4.34}$$

for TM mode(H_x, H_y and E_z). In the TFSF formulation the field is split into the total field which contains the incident field plus any scattered field and the scattered field which features only the scattered field. The total field is contained inside a box placed around the FDTD simulation domain at 30 grid cells from the edge and 10 grid cells beyond the PML and the lens is placed in the centre of the total field region. The source, $H_{inc}$is then emitted from a line along the boundary between the scattered and total fields and the scattered field, H_{scat} is that visible outside of this.

4.4.2 The FDTD Method for Dispersive Materials

A simulation was carried out on the MTM Triplet where for areas with permittivity less than one a Drude medium is used to model the MTM (24). The Auxiliary Differential Equation (ADE) method is used with the FDTD method to calculate the electromagnetic response for the MTM Triplet whichas has been shown to give more accurate results in the modelling of left-handed media (25). The full MTM Triplet is modelled accurately using the ADE method outlined in this section.

A dispersive medium can be modelled by the Lorentz-Drude model with a relative permittivity and permeability given by (26):

$$\epsilon(\omega) = \epsilon_0(1 - \frac{\omega_{pe}^2}{\omega^2 - j\omega\gamma_e}) \tag{4.35}$$

$$\mu(\omega) = \mu_0(1 - \frac{\omega_{pm}^2}{\omega^2 - j\omega\gamma_m}) \tag{4.36}$$

where ω_{pe} and ω_{pm} are the electric and magnetic plasma frequencies and γ_e and γ_m are the electric and magnetic collision frequencies. The method for solving the FDTD equations used is called the (E,D,H,B) scheme according to these components being solved in the time stepping algorithm. It is based on Faraday's and Ampere's Laws, see eq. (4.11) and eq. (4.12). The constituent relations are

$$\mathbf{D} = \epsilon\mathbf{E} \tag{4.37}$$

$$\mathbf{B} = \mu\mathbf{H} \tag{4.38}$$

where ϵ and μ are expressed as eq. (4.35) and eq. (4.36). We discretise eq. (4.11) and eq. (4.12) to give Maxwell's equations in a form which allows use to solve them in a discrete time and space grid.

$$\mathbf{B}^{n+1} = \mathbf{B}^n - \triangle t \cdot curl(\mathbf{E}^{n+\frac{1}{2}}) \tag{4.39}$$

$$\mathbf{D}^{n+1} = \mathbf{D}^n + \triangle t \cdot curl(\mathbf{H}^{n+\frac{1}{2}}) \tag{4.40}$$

where curl is the discrete operator, $\triangle$ is the FDTD time step and n is the number of time steps. The constitutive relations are discretised in the following way

$$(\omega^2 - j\omega\gamma_e)\mathbf{D} = \epsilon_o(\omega^2 - j\omega\gamma_e - \omega_{pe}^2)\mathbf{E} \tag{4.41}$$

The inverse of the Fourier transform gives the following rule

$$j\omega \rightarrow \frac{\delta}{\delta t}, \omega^2 \rightarrow -\frac{\delta^2}{\delta t^2} \tag{4.42}$$

therefore we re-write the constitutive equation as

$$(\frac{\delta^2}{\delta t + \frac{\delta}{\delta t}\gamma_e})\mathbf{D} = \epsilon_o(\frac{\delta^2}{\delta t^2} + \frac{\delta^2}{\delta t}\gamma_e + \omega_{pe}^2)\mathbf{E} \tag{4.43}$$

The FDTD simulation grid is spaced equally in 2 Dimensions with periods of $\triangle$x and $\triangle$y and for further discretisation we use central finite difference operators in time (δ_t and δ_t^2 and central average oeprator with respect to time (μ_t and μ_t^2)

$$\frac{\delta^2}{\delta t^2} \rightarrow \frac{\delta_t^2}{(\triangle t)^2}, \frac{\delta}{\delta t} \rightarrow \frac{\delta_t}{(\triangle t)^2}, \omega_{pe}^2 \rightarrow \omega_{pe}^2 \mu_t^2 \tag{4.44}$$

where the operators δ_t, δ_t^2, μ_t and μ_t^2 are defined as

$$\delta \mathbf{F}|_{m_x,m_y,m_z}^n \equiv \mathbf{F}|_{m_x,m_y,m_z}^{n+\frac{1}{2}} - \mathbf{F}|_{m_x,m_y,m_z}^{n-\frac{1}{2}} \tag{4.45}$$

$$\delta_t^2 \mathbf{F}|_{m_x,m_y,m_z}^n \equiv \mathbf{F}|_{m_x,m_y,m_z}^{n+1} - 2\mathbf{F}|_{m_x,m_y,m_z}^n + \mathbf{F}|_{m_x,m_y,m_z}^{n-1} \tag{4.46}$$

$$\mu_t \mathbf{F}|_{m_x,m_y,m_z}^n \equiv \frac{\mathbf{F}|_{m_x,m_y,m_z}^{n+\frac{1}{2}} + \mathbf{F}|_{m_x,m_y,m_z}^{n-\frac{1}{2}}}{2} \tag{4.47}$$

$$\mu_t^2 \mathbf{F}|_{m_x,m_y,m_z}^n \equiv \frac{F|_{m_x,m_y,m_z}^{n+1} + 2\mathbf{F}|_{m_x,m_y,m_z}^n + \mathbf{F}|_{m_x,m_y,m_z}^{n-1}}{4} \tag{4.48}$$

where $\mathbf{F}$ represents the field components and m_x, m_y, m_z are the indices for certain discretisation points in the FDTD domain. The constituent equation is now discrised are is in the form:

$$[\frac{\delta_t^2}{(\triangle t)^2)} + \frac{\delta_t}{\triangle t \mu_t \gamma_e}]\mathbf{D} = \epsilon_o[\frac{\delta_t^2}{(\triangle t)^2} + \frac{\delta_t}{\triangle t}\mu_t\gamma_e + \omega_{pe}^2\mu_t^2]\mathbf{E} \tag{4.49}$$

noting that the discretisation of term ω_{pe}^2 is performed using the central average operator μ_t^2 in order to guarantee improved stability and the central average operator μ_t is used for the term containing γ_e to preserve second-order feature of the equation. We now write the equation

$$\begin{aligned} &\frac{\mathbf{D}|_{m_x,m_y,m_z}^{n+1} - 2\mathbf{D}|_{m_x,m_y,m_z}^n + \mathbf{D}|_{m_x,m_y,m_z}^{n-1}}{(\triangle t)^2} + \gamma_e \frac{\mathbf{D}|_{m_x,m_y,m_z}^{n+1} - \mathbf{D}|_{m_x,m_y,m_z}^{n-1}}{s\triangle t} \\ &= \epsilon_o[\frac{\mathbf{E}|_{m_x,m_y,m_z}^{n+1} - 2\mathbf{E}|_{m_x,m_y,m_z}^n + \mathbf{E}|_{m_x,m_y,m_z}^{n-1}}{(\triangle t)^2} + \gamma_e \frac{\mathbf{E}|_{m_x,m_y,m_z}^{n+1} - \mathbf{E}_{m_x,m_y,m_z}^{n-1}}{2\triangle t} \\ &\qquad + \omega_{pe}^2 \frac{E|_{m_x,m_y,m_z}^{n+1} + 2\mathbf{E}|_{m_x,m_y,m_z}^n + \mathbf{E}|_{m_x,m_y,m_z}^{n-1}}{4}] \end{aligned} \tag{4.50}$$

Therefore the updating equation for $\mathbf{E}$ in terms of $\mathbf{E}$ and $\mathbf{D}$ at the previous time step is:

$$\begin{aligned}\mathbf{E}^{n+1} = [\frac{1}{\epsilon_0(\triangle t)^2} + \frac{\gamma_e}{2\epsilon_o \triangle t}]\mathbf{D}^{n+1} = \frac{2}{\epsilon(\triangle t)^2}\mathbf{D}^2 \\ [\frac{2}{(\triangle t)^2} - \frac{\omega_{pe}^2}{2}]\mathbf{E}^2 - [\frac{1}{(\triangle t)^2} - \frac{\gamma_e}{2\triangle t} + \frac{\omega_{pe}^2}{4}]\mathbf{E}^{n-1} \\ +[\frac{1}{\epsilon_o(\triangle t)^2} - \frac{\gamma_e}{2\epsilon_o \triangle t}]\mathbf{D}^{n-1} \\ /[\frac{1}{(\triangle t)^2} + \frac{\gamma_e}{2\triangle t} + \frac{\omega_{pe}^2}{2}]\end{aligned} \tag{4.51}$$

The updating equation for $\mathbf{H}$ has the same form by replacing $\mathbf{E}$, $\mathbf{D}$, ω_{pe}^2 and γ_e by $\mathbf{H}$, $\mathbf{B}$, ω_{pm}^2 and γ_m respectively

$$\begin{aligned}\mathbf{H}^{n+1} = [\frac{1}{\epsilon_o(\triangle t)^2} + \frac{\gamma_m}{2\epsilon_o \triangle t}]\mathbf{B}^{n+1} - \frac{2}{\epsilon_o(\triangle t)^2}\mathbf{B}^2 \\ +[\frac{2}{(\triangle t)^2} - \frac{\omega_{pm}^2}{2}]\mathbf{H}^n - [\frac{1}{\triangle t^2} - \frac{\gamma_m}{2\triangle t} + \frac{\omega_{pm}^2}{4}]\mathbf{H}^{n-1} \\ +[\frac{1}{\epsilon_0(\triangle t)^2} - \frac{\gamma_m}{2\epsilon_o \triangle t}]\mathbf{B}^{n-1} \\ /[\frac{1}{(\triangle t)^2} + \frac{\gamma_m}{2\triangle t} + \frac{\omega_{pm}^2}{4}]\end{aligned} \tag{4.52}$$

The results of simulations are dependent on the resolution of the Yee grid cell. The typical limit is $\frac{\lambda}{10}$ (14). In dispersive FDTD modelling of metamaterials this increases to $\frac{\lambda}{30}$ (17). The simulation was run at $\frac{\lambda}{20}$, at $\lambda/30$ however the domain was too large and the simulation too computationally expensive on a computer with four dual core 3 GHz Opterons. The convergence study was conducted as shown in the figure. The resolution at $\lambda/20$ was found to be the optimum for reliable results offering a reasonable computation time.

4.5 Summary

In this section The MTM Cooke Triplet was designed using the DCT method and simulated using the FDTD method. The ray tracing and design of the Cooke Triplet has been presented using commercial software package Zemax where the Seidel aberrations were minimised using the merit function. In addition to this the virtual space for the MTM triplet was generated using commercial grid generation software Pointwise and GenGrid where Laplace smoothing functions were used to increase cell orthogonality. The DCT approach was used to design the MTM triplet using a calculation on a cell by cell basis and the All-Dielectric Triplet also derived. In the following section we look at the results to the FDTD simulation.

The Finite Difference Time Domain method is one of the most popular computational electromagnetic solvers which are used. It is a differential equation solver which solves in the time domain which allows time series results to be produced. The lens is placed in the FDTD domain and a plane wave source at 8 GHz launched at the lens. The simulation area is terminated by PML and the MTM regions are modelled using the Drude model. The Finite Difference Method used to model the Transformation Optics lens is formulated in this chapter. MTMs are dispersive and therefore require use of the auxiliary differential equation formulation. The boundary areas are closed using PML and the transformation optics lens is placed in the centre of the simulation domain. The simulation is stable so long as the Courant condition is satisfied. The results of the simulation are given in the next chapter.

Bibliography

[1] R. Kingslake, *Lens design fundamentals*. academic press, 1978.

[2] M. J. Kidger, "Fundamental optical design." SPIE, 2001.

[3] M. Born and E. Wolf, *Principles of optics: electromagnetic theory of propagation, interference and diffraction of light*. Cambridge university press, 1999.

[4] J. F. Thompson, B. K. Soni, and N. P. Weatherill, *Handbook of grid generation*. CRC press, 1998.

[5] J. Li and J. B. Pendry, ""Hiding under the carpet: a new strategy for cloaking"," *ArXiv*, 2008.

[6] "Gridgen - Pointwise's Legacy Meshing Software, howpublished = http://www.pointwise.com/gridgen/, note = Accessed: 2013-09-30."

[7] F. Kong, B.-I. Wu, J. au Kong, J. Huangfu, S. Xi, and H. Chen, ""Planar focusing antenna design by using coordinate transformation technology"," *Applied physics letters*, 2007.

[8] Wenxuan Tang, Christos Argyropoulos, Efthymios Kallos, W. Song, and Y. Hao, ""Discrete Coordinate Transformation for Designing All-dielectric Flat Antennas"," *IEEE Transactions on Antenna and Propagation*, 2010.

[9] N. K. D. A. Roberts and D. R. Smith, ""Optical lens compression via transformation optic"," *Optics express*, 2009.

[10] R. Mittra and Y. Zhang, "A low-reflection flat-lens design for microwave imaging system," in *Antennas and Propagation (EUCAP), Proceedings of the 5th European Conference on*. IEEE, 2011, pp. 851–852.

[11] N. Yu and F. Capasso, "Flat optics with designer metasurfaces," *Nature materials*, vol. 13, no. 2, pp. 139–150, 2014.

[12] Q. Wu, J. P. Turpin, X. Wang, D. H. Werner, A. Pogrebnyakov, A. Swisher, and T. S. Mayer, "Flat transformation optics graded-index (to-grin) lenses," in *Antennas and Propagation (EUCAP), 2012 6th European Conference on*. IEEE, 2012, pp. 1701–1705.

[13] A. F. Peterson, S. L. Ray, and R. Mittra, *"Computational methods for electromagnetics"*. IEEE Press, 1998.

[14] A. Taflove and S. C. Hagness, *"Computational Electrodynamics: the finite difference time-domain method"*. Artech House, 2005.

[15] H. A. El-Raouf, V. Prakash, J. Yeo, and R. Mittra, "Fdtd simulation of a microstrip phased array with a coaxial feed," *IEE Proceedings-Microwaves, Antennas and Propagation*, vol. 151, no. 3, pp. 193–198, 2004.

[16] D. M. Sullivan, *Electromagnetic simulation using the FDTD method*. Wiley-IEEE Press, 2013.

[17] Christos Argyropoulos, Efthymios Kallos, and Yang Hao, ""FDTD analysis of the optical black hole"," *J. Opt. Soc. Am. B*, 2010.

[18] Y. H. Christos Argyropoulos, Yan Zhao, ""A radially-dependant dispersive finite-difference time-domain method for the evaluation of electromagnetic cloaks"," *IEEE Transactions of Antennas and Propagation*, 2009.

[19] *"FDTD Modeling of Metamaterials: Theory and Applications"*. Artech house, 2009.

[20] C. Argyropoulos, N. M. Estakhri, F. Monticone, and A. Alù, "Negative refraction, gain and nonlinear effects in hyperbolic metamaterials," *Optics express*, vol. 21, no. 12, pp. 15 037–15 047, 2013.

[21] Y. Hao and R. Mittra, *FDTD modeling of metamaterials: theory and applications*. Artech house, 2008.

[22] K. S. Yee, ""Numerical solution of inital boundary value problems involving maxwells equations in isotropic media"," *IEEE Transactions on antennas and propagation*, 1966.

[23] J.-P. Berenger, "Three-dimensional perfectly matched layer for the absorption of electromagnetic waves," *Journal of computational physics*, vol. 127, no. 2, pp. 363–379, 1996.

[24] S. Zhang, W. Fan, N. Panoiu, K. Malloy, R. Osgood, and S. Brueck, "Experimental demonstration of near-infrared negative-index metamaterials," *Physical review letters*, vol. 95, no. 13, p. 137404, 2005.

[25] Y. Zhao, C. Argyropoulos, and Y. Hao, ""Full-wave finite-difference time-domain simulation of electromagnetic cloaking structures"," *Opt. Express*, vol. 16, no. 9, pp. 6717–6730, Apr 2008. [Online]. Available: http://www.opticsexpress.org/abstract.cfm?URI=oe-16-9-6717

[26] Y. Zhao, P. Belov, and Y. Hao, "Accurate modelling of left-handed metamaterials using a finite-difference time-domain method with spatial averaging at the boundaries," *Journal of Optics A: Pure and Applied Optics*, vol. 9, no. 9, p. S468, 2007.

Chapter 5

The Analysis of The Primary Seidel Aberrations

This chapter presents the analysis of the conventional Cooke triplet and the MTM and reduced maps based on FDTD simulations to find the Seidel aberrations of each of the lenses. The simulation results are in the form of electric field components. A typical analysis will look at the five primary Seidel aberrations: Spherical, Coma, Astigmatism, Field Curvature and Distortion. The Spherical aberration can be investigated using a plane wave source. The Coma and remaining Seidel aberrations can be examined using a source placed at an angle to the lens. The Chromatic aberration will also be examined using the FDTD results where the source is a Gaussian pulse. The FDTD Simulations of the Single Concave Lens, The Cooke Triplet, MTM Triplet and Dielectric Triplet will be compared in terms of these aberrations in order to determine the imaging performance of the MTM and Dielectric only lenses compared to the original Cooke Triplet.

5.1 FDTD Results

5.1.1 The Cooke Triplet and Single Lens Results

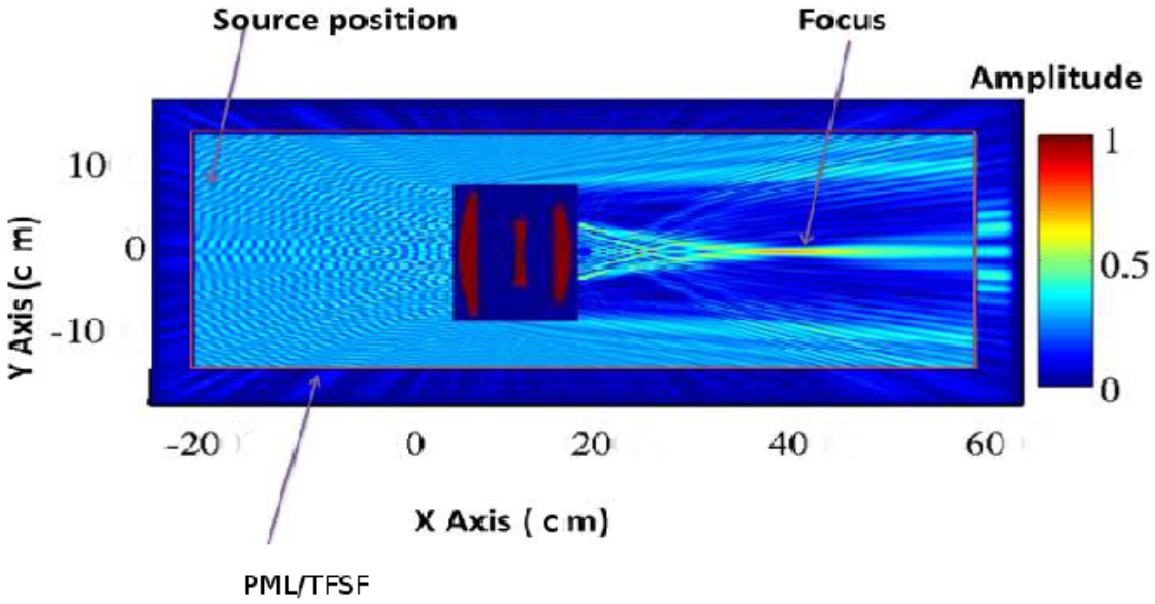

Figure 5.1: The results of the field amplitude, abs(Ez), for the FDTD simulation results for the Cooke Triplet at 8 GHz. The field amplitude is normalised to the maximum value in the computation space. The source is a sinusoidal wave launched from the left of the domain. The permittivity map for the Cooke Triplet and single lens is placed on the simulation results where they were located in the MATLAB simulation. The focus is signified by an arrow and the Perfectly Matched Layer (PML) which acts as the boundary conditions for the numerical technique are shown as a red line.

fig. 5.1 shows the FDTD simulation results of the original Cooke Triplet with the lens permittivity superimposed onto the FDTD simulation domain. This is the field which we will compare the results for the designed MTM and DCT Triplet's with. The results for the FDTD simulation of the Cooke Triplet, fig. 5.1, show reflections in the field from the initial surface which would reduce the power of the lens. In the field distribution for the Cooke Triplet the focal region is very clean of energy due to little scattering from inside the lens. You would expect there to be more reflections from the Cooke Triplet because there are 6

refractive index boundaries rather than two for the single lens. The electromagnetic field in the focal region beyond lens is very well focused toward the focal point so the refraction due to the lenses in Cooke Triplet is doing an excellent job focusing the energy beyond the lens to the focal point. That being said there is a small region in front of the focal point which contains an area which is scattered visible in the TFSF region.

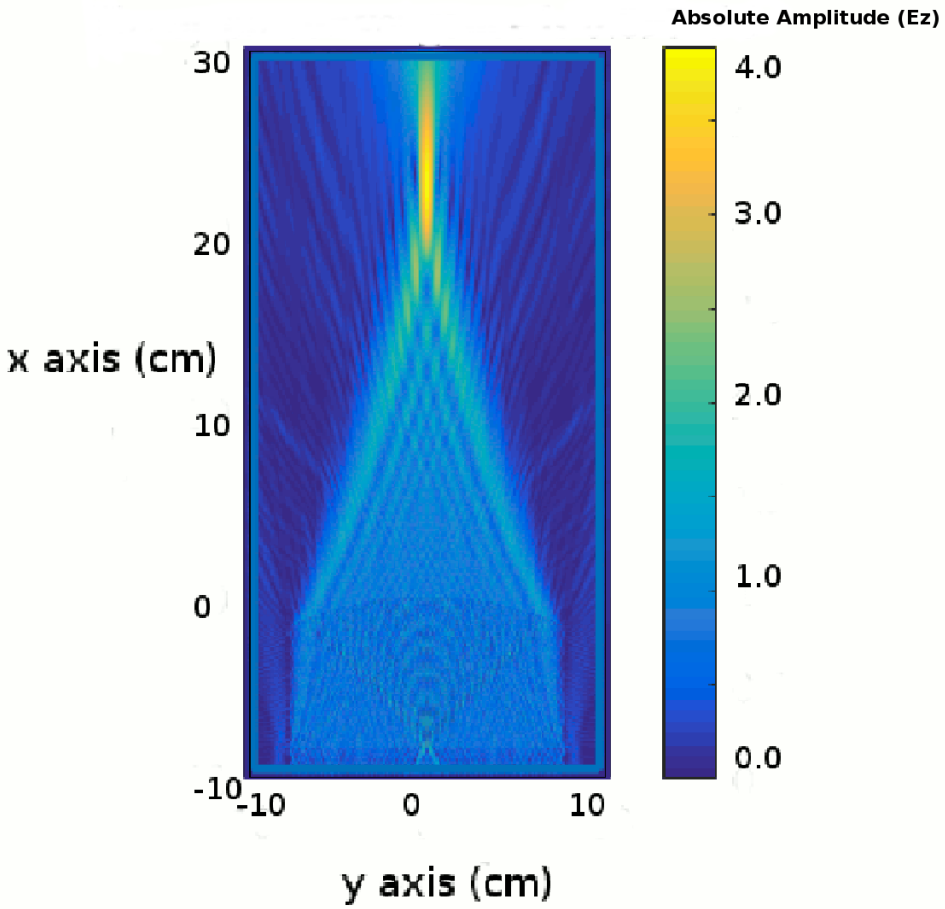

Figure 5.2: The results of the field amplitude for the FDTD simulation results for the Single Lens at 8 GHz. The simulation was set to converge for E_z amplitude maximum divergence being less than 0.1.

The Single Lens, see fig. 5.2, has large energy wave reflected from the system compared to the Cooke Triplet. The reflection parameter is greater for the single lens when compared

to the Cooke Triplet. The far field is also more scattered according to our FDTD simulations when compared to the FDTD simulation of the Cooke Triplet lens. In this field distribution for the single lens the focal point is wider in both both longitudinal and transverse directions. The lens used for the single lens is in the same place which can be seen from the lens structures superimposed onto the FDTD grid results. The focusing is not as tightly constrained as the Cooke Triplet as you would expect. The single lens has very low scattering as a single lens has only two surfaces to refract the incident wave. The focus of the Concave Lens is slightly more diffuse than that of the Cooke Triplet. The Cooke Triplet is more highly engineered to control the flow of radiation through the system so you would expect a more controlled and focused focal region for the Cooke Triplet. There is however more scattering in front of the lens compared with the original lens.

5.1.2 The MTM Triplet and All-Dielectric Triplet Results

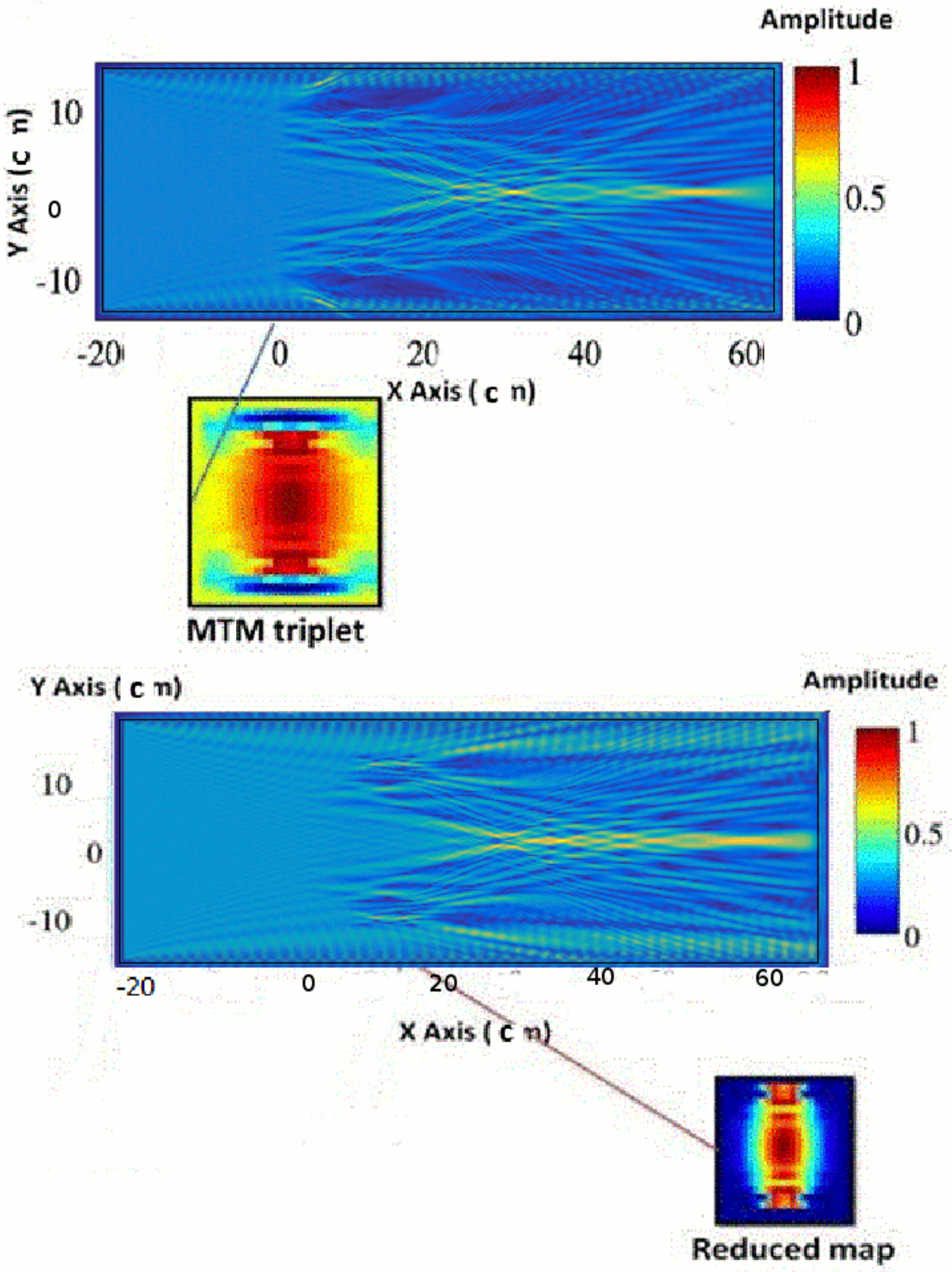

Figure 5.3: The results of the field amplitude for the FDTD simulation results for the MTM (top-panel) and reduced map (bottom-panel). The red lines show the location of the PML and the permittivity boundaries on the top, left, right and bottom and the simulation domain. The central red square signifies the location of the lens in the FDTD simulation. The field amplitude is normalised to the maximum value. The source is a sinusoidal wave launched from the left of the domain. The permittivity map is shown superimposed onto the bounded structure for MTM and reduced lenses.

fig. 5.3 shows the simulation FDTD results for the MTM Triplet and Dielectric Triplet. The MTM Triplet is a focusing lens and field distribution results show that the focusing is not as perfect as the Cooke Triplet but it does feature a sharp focus in the place you would expect. There is more scattering through-out the simulation domain: forward scattering, side scattering and back scattering, compared to the Cooke Triplet. The MTM Triple features two regions of sharp, dark blue losses where the Metamaterial regions are where the energy is being absorbed by the MTM elements as well as scattered away from the less of into the PML region. The electromagnetic field for the MTM Triplet is more diffuse in the focal region exiting the lens compared to the original Triplet due to more scattering caused in the lens.

The simulation results for the DCT Triplet, see 5.3 show that the focal region is a lot more diffuse and spread out along the optical axis than either the original Triplet or the MTM Triplet which would suggest more focusing ability. There is a large amount of scattering which occurs in the lens and leaving a lot of unfocused electromagnetic energy in the region following the lens. In both the MTM region and the reduced map there is a sharp spike of energy before the actual focal region which is not the truth focal point and a worsening in the performance characteristics of these lenses in terms of gain or focusing power. There is alot more side scattering in the dielectric Triplet. There is very little back scattering for both MTM and Dielectric Triplets due to the lens impedance matching.

5.2 The Primary Seidel Abberations

The most basic optical aberrations in a lens are Spherical aberration, Coma, Astigmatism, Field Curvature and Distortion. These are monochromatic aberrations which means that they are aberrations at a single frequency. They are due to the geometry of the lenses system and the inherent limitations using systems of lenses to control the flow of light through the

system. A perfect image and can be achieved using device such as a Luneburg lens where the effective refractive index is varied within the single lens. A real system of lenses however features many areas where this ideal behaviour is not possible. In this chapter we analyse the Primary aberrations of the lenses and yield a conclusion to the imaging ability of the MTM and Dielectric maps in terms of there Primary Seidel aberrations.

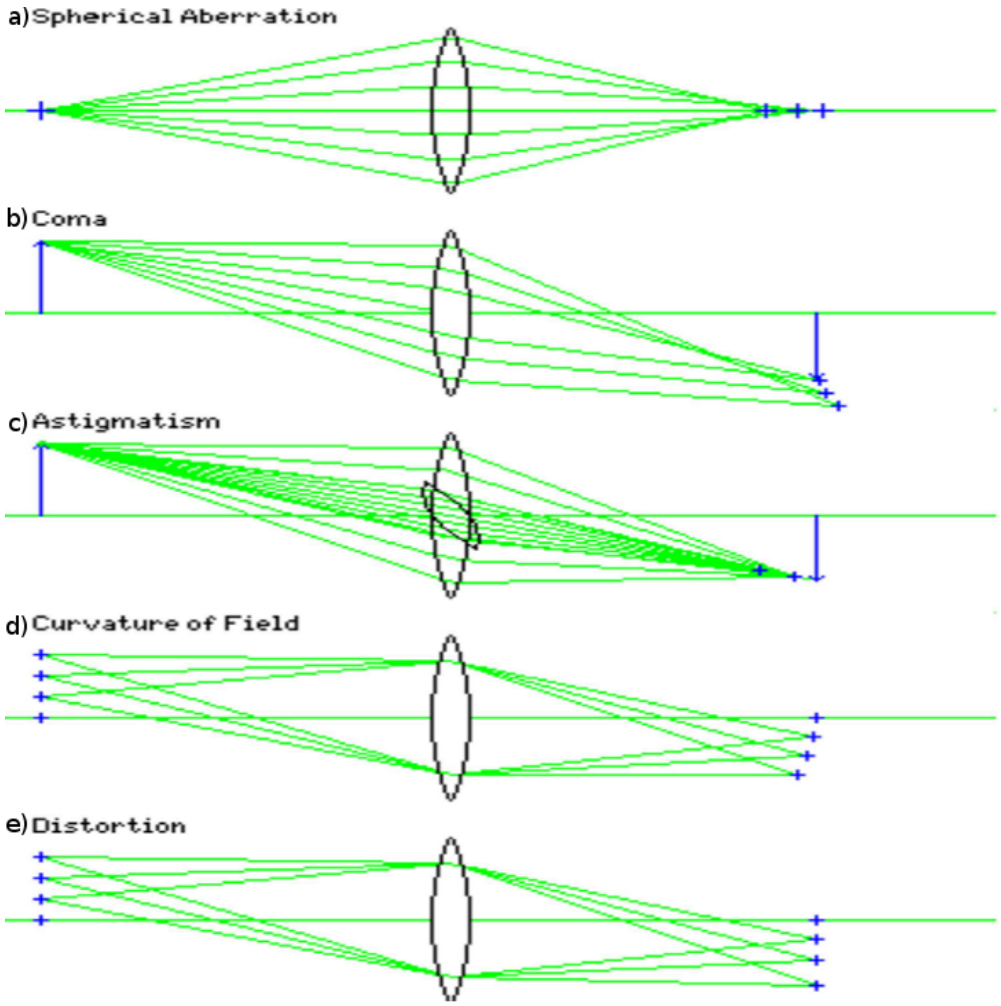

Figure 5.4: The ray tracing demonstrating the five Seidel aberrations: Spherical, Coma, Astigmatism, Field Curvature and Distortion. Spherical aberration is caused by rays having larger angles of incidence on the lens surface being focused at different point. Coma is caused by an off-axis ray having different paths through the lens and being focused at different points causing a comet-like pattern. Astigmatism is caused by rays having different ray paths due to hitting different planes of the lens and Field Curvature is an aberration from flat image plane to curved image plane. The Distortion is an aberration where the power of the lens causes the image to appear stretched in the vertical direction.

In order to explain each of these aberrations in detail we will first look at Spherical Aberration (SA), see the top panel of fig.5.4. The SA occurs when light rays leaving a point on the object converges after travelling through the system of lenses or a single combination lens at different focal lengths. The distance in the longitudinal direction is called longitudinal spherical aberration and the distance in the transverse direction is called the transverse spherical

aberration. In the figure we have an example of the longitudinal spherical aberration where light rays which hit different heights on the lens surface are diffracted by a different amount compared to the rays which are incident on the lens at a narrower angle of incidence. These light rays converge at the focus at a different focal length resulting in a blurring of the image known as longitudinal spherical aberration.

The second monochromatic aberration is Coma. It is so named because it looks like a comet shape with a tail which is either left or right which is defined by a positive or negative result in the value or the coma. A picture of the Coma can be seen in panel 2 of fig.5.4. The coma is caused due to light rays leaving the object having different angles of incidence on the lens surface. This results in different diffraction angles and a convergence on the final image location which has a dispersion of light rays incident resulting in a blurry image.

Next is Astigmatism which is caused due to the 3 dimensional nature of the lens rather than it being 2 dimensional as in the simple ray-path lens drawings, see fig. 5.4. This means there are two planes axial and transverse where the rays leave the object refract on the lens and come to a focus. The angle of refraction for the rays are different depending on which plane they hit. This results in the aberration known as Astigmatism as shown in panel 3 of fig. 5.4. Any real optical system is three dimensional and will feature this aberration in the image plane.

The Field Curvature and Distortion are focal aberrations rather than image aberrations. This means that if an object is placed at a different position the image created will be a distorted position. This is valid because most objects are modelled as points of light being emitted from every point on its surface, see panel 4 and 5 in Fig. 5.4. The field curvature is when these different focal point are created not on a flat image plane but on a curved one. The distortion is when the image focal positions are not equally spaced as on the object but

elongated by a scale magnitude factor. These result in the aberrations in the image known as Field Curvature and Distortion.

These aberrations can be explained in terms of the Seidel equation.

$$W(\rho,\theta) = s(\rho d)^4 + c\alpha(\rho d)^3 cos + a\alpha^2(\rho d)^2 cos2\theta + u\alpha^2(\rho d)^2 + g\alpha^3(\rho d)cos\theta \tag{5.1}$$

where s, c, a, u and g are the Seidel coefficients for spherical, coma, astigmatism, field curvature and distortion. α is the field angle, ρd is the height in the pupil, with d being the nominal pupil radius and ρ the relative (0 to 1) height in the pupil, and θ the pupil angle (**?**).

The Chromatic Aberration is due to different refraction occurring for different frequencies of which white light is made from. The Cooke Triplet is able to reduce the chromatic aberrations in an image using a combination of different refractive index lenses. This combination of two materials: Flint and Crown Glass minimises the dispersion of the rays with different frequencies. The Cooke Triplet is one of the simplest and most effective methods of reducing Chromatic Aberration in lens images.

The Cooke Triplet to be used in this thesis was designed in Zemax. This meant taking an initial estimate of the lens shapes. The traditional Flint and Crown glass was used for the material. A diverging lens in the middle surrounded by two concave lenses. The lens structure was then optimized to minimized the five Seidel aberration and longitudinal and transverse chromatic aberration, see Fig. 4.1. The ray paths were then exported to MATLAB. The rays used in the grid were shortened so they finished somewhere between the final lens surface and the focal point so the device terminates the ray paths before reaching the focal point. The Cooke triplet designed is shown with parameters in Fig. 4.1 and this is the design used in the fabrication of the TO device in the next sections.

5.3 Focal Length

The focal point in a lens is where the rays converge. This is given by the lens makers equation for a lens or system of lenses. In the FDTD simulation it is the point of maximum intensity along the optical axis where the most electromagnetic field has been focused to. The optical axis is the line along the centre of the optical system and as our system of lenses are symmetrical the focus will be along this axis. We compare the results for the focal point for the MTM Lens, Dielectric Lens, Triplet and Single Lens, table 5.1

	Singlet	Triplet	MTM	Reduced
Focal Length (cm)	33.1750	37.0375	38.7985	37.2625

Table 5.1: The fundamental performance metrics for the lenses. This table shows the Back focal length from the final surface of the lens to to focal point along the longitudinal axis. The gain is the amplitude of the focal region and the beamwidth is the FWHM of the beam at the focal region. The results are shown for the FDTD simulations of the single lens, Cooke Triplet and the MTM lens and reduced map.

The focal length of the reduced map and MTM lens designed using our transformation optics method closely matches that of the original Cooke Triplet. The focal length is defined as the distance from the centre of a lens to its focal point. We measured the focal length in the FDTD Simulations for the Single Concave Lens, the Cooke Triplet, the MTM lens and the Dielectric Triplet, see Tab 5.1. A comparison of the focal length is a typical way to verify the correct application of transformation optics (1) to lenses. We confirm that the Dielectric-only Triplet has almost the same focal length as the MTM Triplet and original Triplet verifying the method used to design the lens.

The focal lengths for the MTM Triplet and Dielectric only Triplet match that of the original Cooke Triplet. This confirms that the method used to design the Cooke Triplet gives an accurate recreation of the original Cooke Triplet lens. We would expect to see the

same focal length. The focal length for the single lens is slightly less than the other three. This is because it is because it is a single lens taken from a different optical instrument. The focal length is important in validating the transformation optics method used which should produce the same electromagnetic field response and also that the calculation has been correct and validated in our FDTD simulation.

5.4 Spherical Aberration

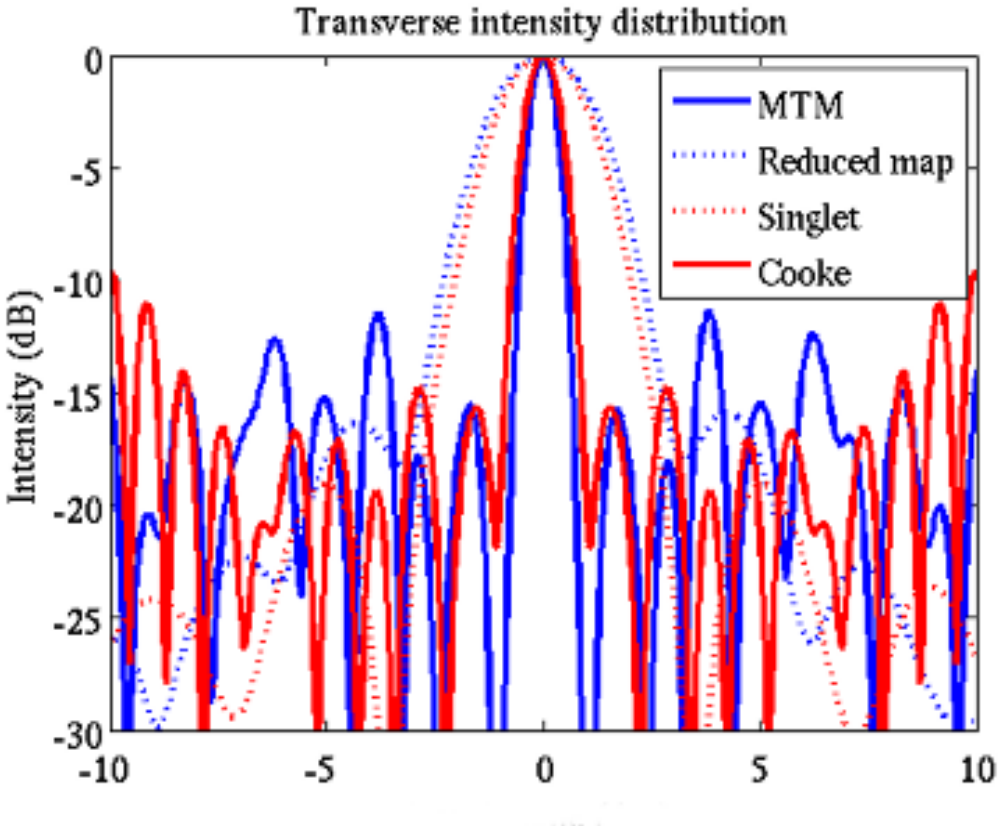

Figure 5.5: The Spherical Aberration for the Concave, Cooke, MTM and Reduced map centred at the focus.

To analyse the performance of the lenses we start with the first primary Seidel aberration, Spherical aberration which can be split up into longitudinal spherical aberration and transverse spherical aberration. The transverse Spherical Aberration (tSA) is the spherical

aberration of the lens along the transverse axis. The difference is that the width of the beam in the transverse plane is measured and again we want this to be as small as possible to generate the better image by the lens. tSA was measured by plotting the field amplitude (Ez) for all 4 lenses along the transverse axis at the focal point, as shown in fig. 5.5. The focal point being taken as the point of maximum intensity along the optical or x axis.

The transverse spherical aberration (tSA) of the MTM triplet is smaller than the Cooke Triplet, see Fig. 5.5. The tSA of the reduced map and single lens are much larger, almost double. This would suggest that the resolution and imaging performance of the MTM lens is slightly better than the conventional Cooke triplet with the reduced far out lobe amplitude of the field , the reduced map and single lens being much worse. This should be caveated by saying that this would certainly be a benefit in some specific applications for example where you wanted to focus power in a small area such as high gain applications and this property has been reported in the literature (2). In more complicated optical systems however the imaging system as a whole is considered and the depth of field in this imaging system would be less for the MTM lens. Regarding the specific focusing ability then the MTM lens performs better than the Cooke triplet.

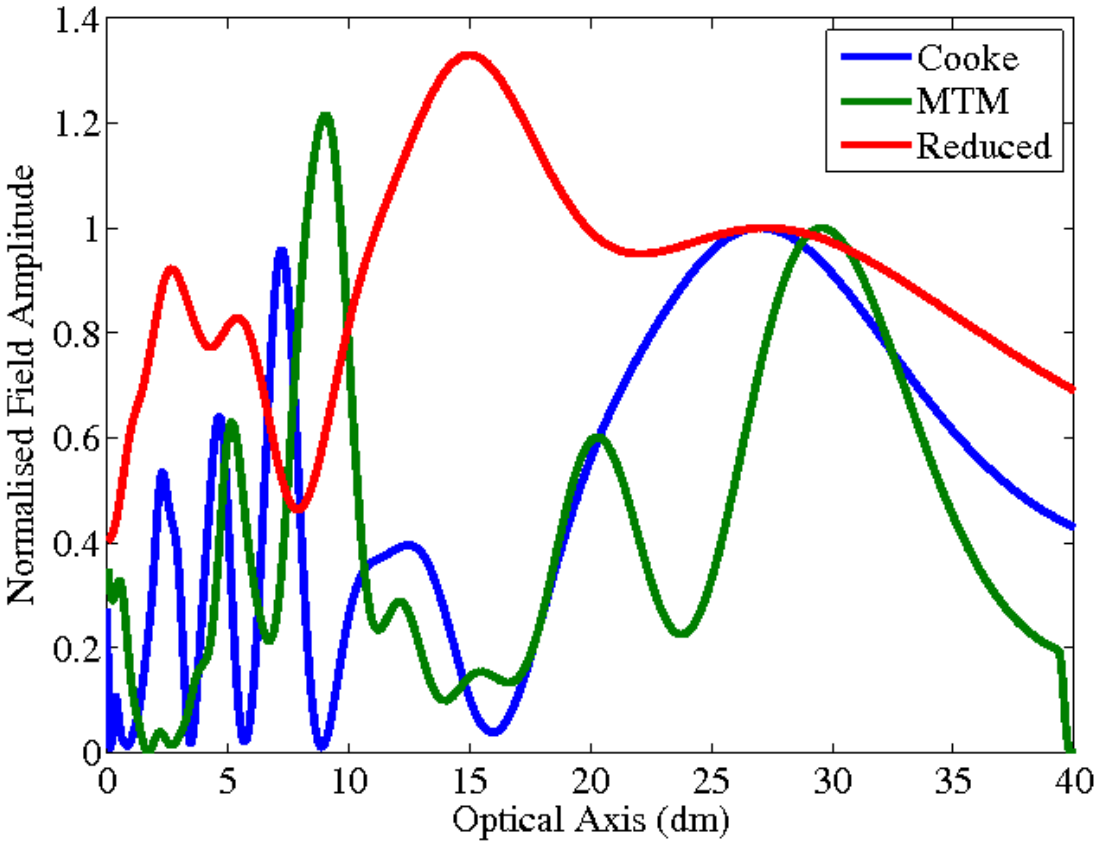

Figure 5.6: The longitudinal intensity distribution for the single, Cooke, MTM and reduced map measured from the back surface of each lens. The focus of each lens is visible. There is a large peak in intensity before the focus for the MTM due to scattering effects from the Metamaterial. The focal length is similar for each lenses. The reduced map suffered from a large aberrations before the main focus which is also suffered but to a lesser extent by the Metamaterial lens.

The performance of a lensing system is also quantified in terms of the longitudinal spherical aberration (lSA), see fig. 5.6 which is the spread of the intensity in the focal region in the longitudinal or optical axis. The MTM lens has a much sharper and therefore smaller lSA than the conventional Cooke Triplet. This agrees with our assertion that the Cooke Triplet has smaller aberrations than the single lens. It would provide evidence for the conclusion that the MTM lens has a similar reduction in terms of lSA as the Cooke Triplet. The re-

duced map features alot of scattering as is evident in the large amount of energy preceding the focal point compared to the other two. The MTM Triplet is good however does have a bump in intensity before the focus. The Cooke Triplet has a smooth intensity build up to the focal region resulting in a clearer focal region which would fade more gradually making it a better imager.

5.5 Coma

The Coma aberration is the next Primary Seidel aberration. The Cooke Triplet, the MTM lens, the reduced map and the single lens were also simulated using the FDTD method where the source a line source was placed at an angle to the lenses without using the TFSF method. This was done in order to look at the off axis aberrations of the lens such as Coma. The Coma aberration is the peaks where Coma is a set of smaller peaks after the main peak. It appears when the wave is incident at an angle to the lenses and the focal point is split into regions of decreasing size trailing the main peak.

The Coma is found by taking a cut is taken along the longitudinal axis at the focus when a source is incident at a angle off the four lenses, see Fig. 5.7. The Cooke Triplet has a small and well defined coma with a couple of equally spaced peaks disappearing to the left of the main peak. The simulation results here show that the Coma in the MTM lens is much more narrow therefore resulting in a better imaging property for the MTM lens, see fig. 5.7. It has a larger maximum intensity due to the stronger focusing ability of the MTM lens. The width of the coma in the MTM lens is less than the Cooke Triplet. The Coma is also to the right of the main peak rather than the left in the original lens. We are unable to explain this change in side of the Coma aberration but I would speculate that it is because the MTM lens is designed considering only rays incident on it at normal to the lens without taking into account of these off axis rays.

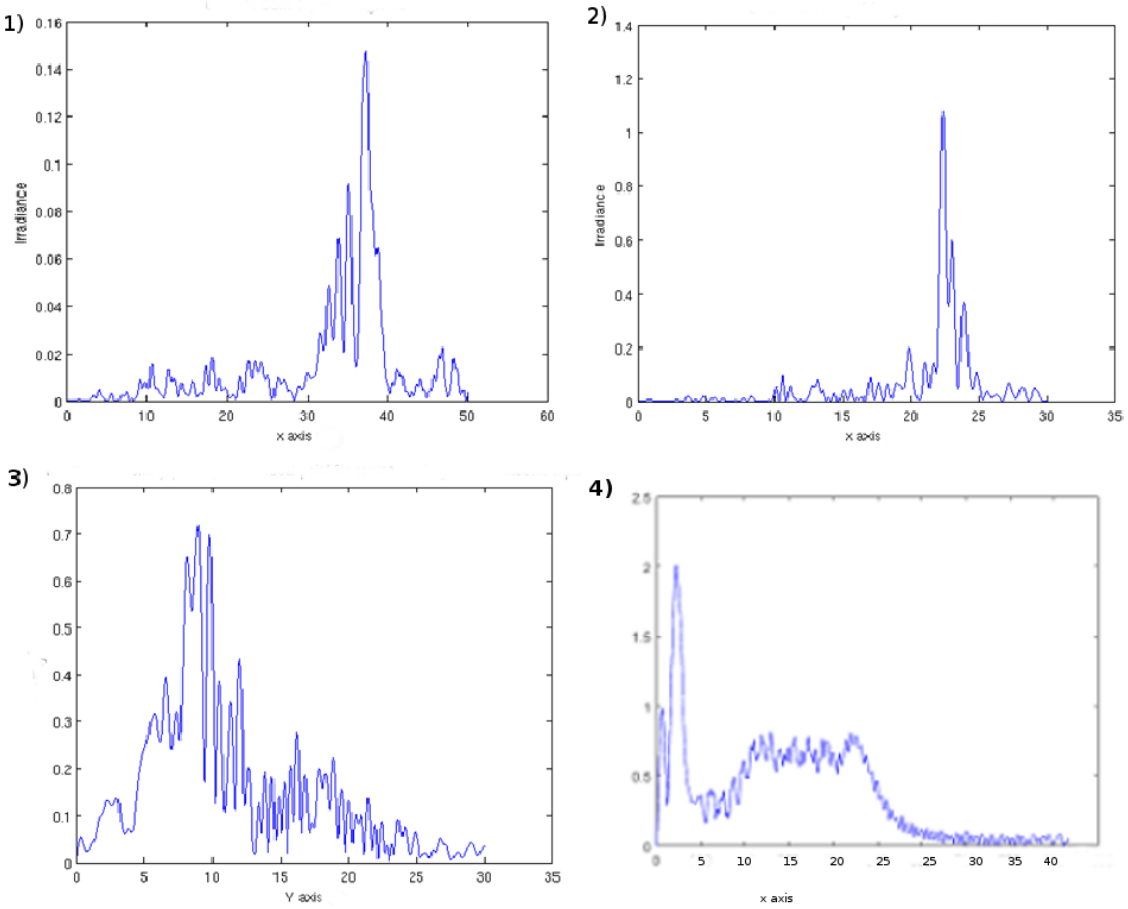

Figure 5.7: The Coma or off-axis source incident at 14 degrees (1) on the conventional lens (2) the MTM lens (3) the reduced triplet and (4) the single lens. The angle of the source is 18 degrees in each case. The irradiance or intensity is a square of the absolute electric field component in the z axis. For the conventional lens the intensity at the focal region is smaller than the MTM and reduced map due to fewer reflections from the TO Triplet resulting in a higher intensity at the focus compared to the original triplet lens.

The reduced map has a very poor aberration with many Coma spikes. The reduced map has a very large spread of intensity spikes compared to the other two lenses suggesting a much greater Coma in this lens compared to the original Cooke Triplet and the MTM Triplet. It is the same side as the MTM lens but however is much more distorted, therefore I would conclude that the reduced map has much worse Coma aberrations than the MTM lens. The Single lens has a Coma which is the same side as the original Cooke Triplet and is of a similar order.

The Coma is the smallest for the simulation of the Cooke Triplet peaking at 0.15, The MTM Triplet peaks at just above 1.0 and the Reduced Map about 0.7 with additional scattering and Coma spread over a larger area. This tells us that the MTM lens and reduced map are both much worse in terms of coma than the Cooke Triplet. We see significant electromagnetic scattering in the MTM lens. The Coma for the MTM lens is large and spread and the reduced map is comparable to the MTM triplet but less pronounced due to less focusing of light rays away from the lens at the edges of the device as in the Cooke and MTM lenses.

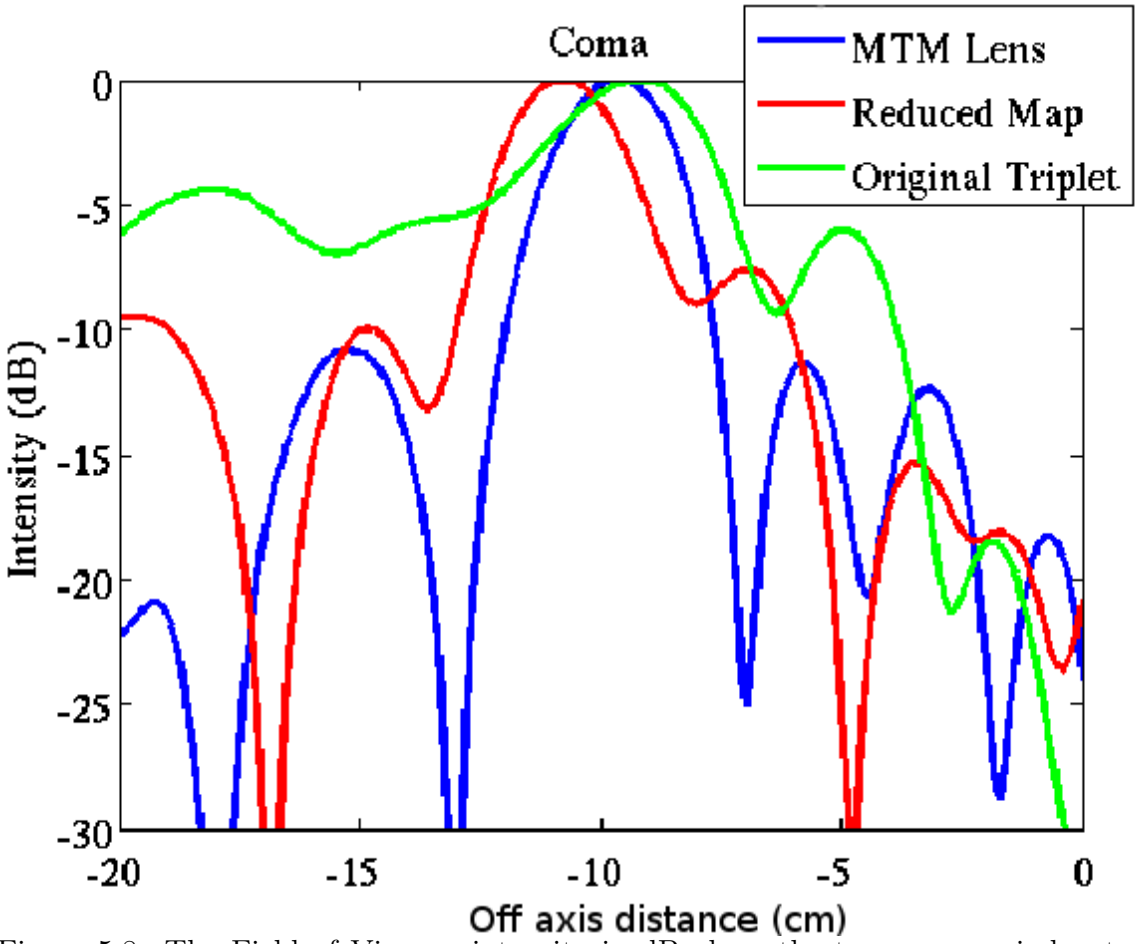

Figure 5.8: The Field of View or intensity in dB along the transverse axis located at the focus where the coma is located at an angle of incidence is 27 degrees. The Cooke Triplet has no large beam being formed at the centre and small coma to the right as this is larger than its field of view. The side lobes to the right of the MTM lens being slightly more pronounced than the dielectric-only map.

The FDTD simulation done at an angle of 27 degrees was beyond the field of view of the original Cooke Triplet however we have included the result here to show that the MTM Triplet and reduced maps are unlike the conventional lens still able to form a focus at this wide angle of view. The MTM lens design has a larger field of view than the standard Cooke Triplet, see fig. 5.8. This behaviour is present in the FDTD simulations of the MTM triplet at large angles of incidence suggesting that the MTM triplet has a larger field of view not unlike other wide angle lens antennas such as the Luneburg lens. Another example of a

lens which is used because of its large field of view is the Rotman lens (3) and this facility is a valuable ability to have in enhancing communications systems. For standard optical systems the Cooke Triplet has a field of view at 20 degrees yet the MTM triplet is still able to form a focus at 27 degrees, fig. 5.8. Wide angle beam scanning is a desirable feature for dielectric lenses (4; 5) to compare with the performance of alternative reflector antennas. Dielectric lens antennas might have applications in millimetre communications instead of reflector antennas (6). Fig. 5.8 shows that the Cooke Triplet can not focus at 27 degrees but the MTM and reduced maps are able to. This confirms that transformation optics designed dielectric lenses provide good performance in wide-angle scanning roles such as intelligent car management systems or microwave dielectric lenses for satellite communications. The MTM lens and reduced lens is able to produce a focus at angles far beyond that available to the original Cooke Triplet design. This extension in field of view is due to the nature of its construction of controlling the flow of light which means there is not a cut off angle of incidence at which the lens terminates its ability to image an object.

5.6 Field Curvature, Distortion and Astigmatism

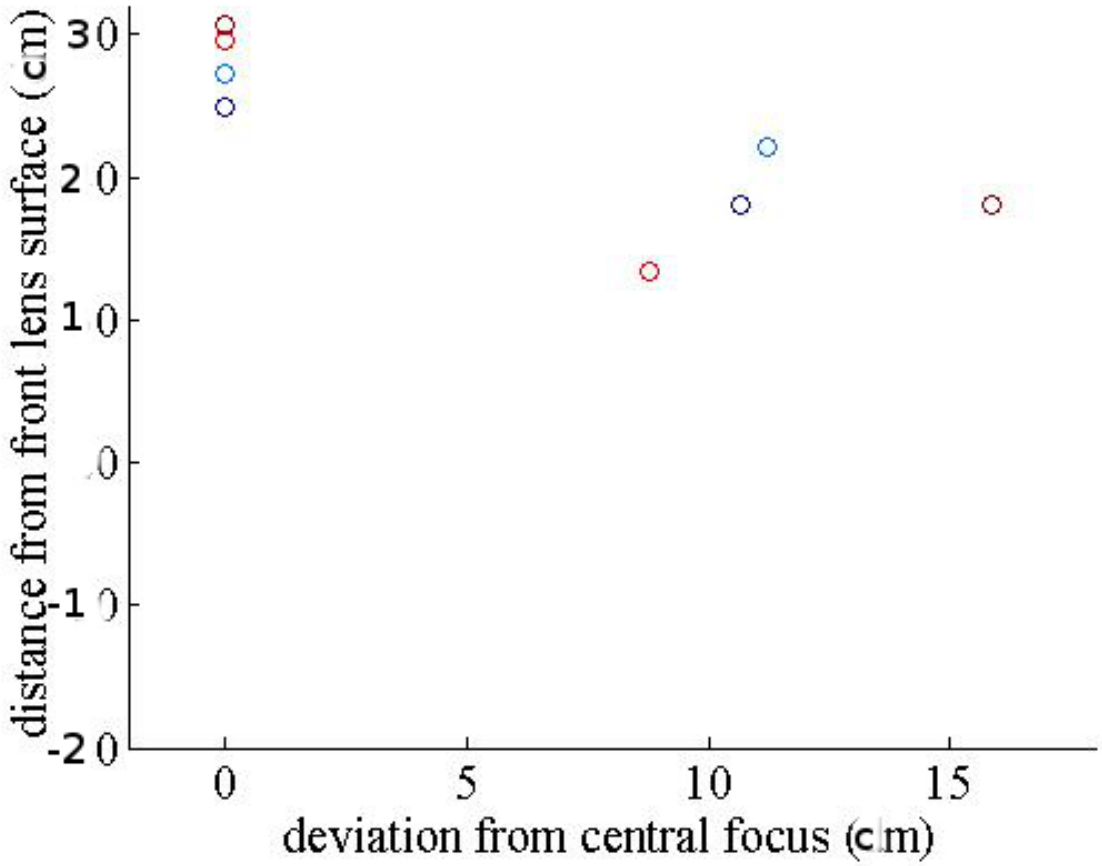

Figure 5.9: The Field Curvature and Distortion or focal points of the single lens (brown), Cooke Triplet (cyan), MTM triplet (red) and reduced map (navy). The results are the focal points from the on and off axis FDTD simulations. The Field Curvature is the deviation between focal points in the y-axis and Distortion in the x-axis.

The Field Curvature is a Seidel aberration which is results in a curvature in the focal plane with a variation of angle of incidence, see Fig. 5.9. An ideal lens would have the same focal distance for a ray angle at incident to the lens from 0 degrees to 90 degrees however in reality this is not the case resulting in a blur in the image called field curvature (7). The variation in position of the focus was calculated from measuring the focus for each of the four lenses for a plane wave at 0 degrees, 14 degrees, 18 degrees and 27 degrees. The Field Curvature

and Distortion are quantified in the variation in the focal point for the source at an angle of incidence and this variation in focal point is plotted in Fig. 5.9. The Field Curvature and Distortion are aberrations in the position of the focus rather than in the spread of the intensity distribution in the focal region.

The field curvature for the Cooke Triplet is the smallest. This is the difference in lateral distance between the two focal points, see Fig. 5.9. The reduced map Field Curvature is larger, then the single lens and the Metamaterial lens is the worst as shown in fig. 5.9. I would speculate that this is due to the fact that the MTM lens was designed considering only on axis rays meaning that its off axis aberrations such as field curvature are therefore worse compared to the original Cooke Triplet. Here the Cooke Triplet remains the standard in terms of performance with the other lenses fairing worse.

The Distortion is a variation of the focal position in the lateral direction , see Fig. 5.9. The Distortion is an aberration which is manifested as a stretching of the image towards the edge of the image. Barrel distortion is where the image magnification increases with transverse distance from the central optical axis and pincushion distortion where it decreases with distance from the optical axis. The single lens has greater Distortion, the MTM lens has a smaller Distortion and the reduced map has a slightly smaller Distortion compared to the Cooke Triplet. This would suggest that the MTM Triplet and Dielectric map has a smaller distortion than the original Cooke Triplet lens. I would hazard a guess that this may be to do with the field angle results where the Transformation Optics lens is able to image objects at wider field of views. This fact has been reported on in the literature by other researchers and may account for this finding which gives the MTM Triplet and Dielectric-only Triplet a smaller distortion than the Cooke Triplet.

The Astigmatism of the lens is the final of the Primary Seidel aberrations. Astigma-

tism occurs when the focal region is shifted for rays passing through different axis in a 3D lens called the Sagital and tangential fields. It is not possible to analysis this aberration without using a 3D model. The results for Astigmatism for the four lenses therefore could not be analyzed. A full analysis of Astigmatism would require both Sagital and tangential planes modelled simultaneously which could be achieved using the Body of Revolution (BoR) FDTD or a 3D FDTD simulation which would be computationally too large to simulate.

5.7 The Chromatic Aberration

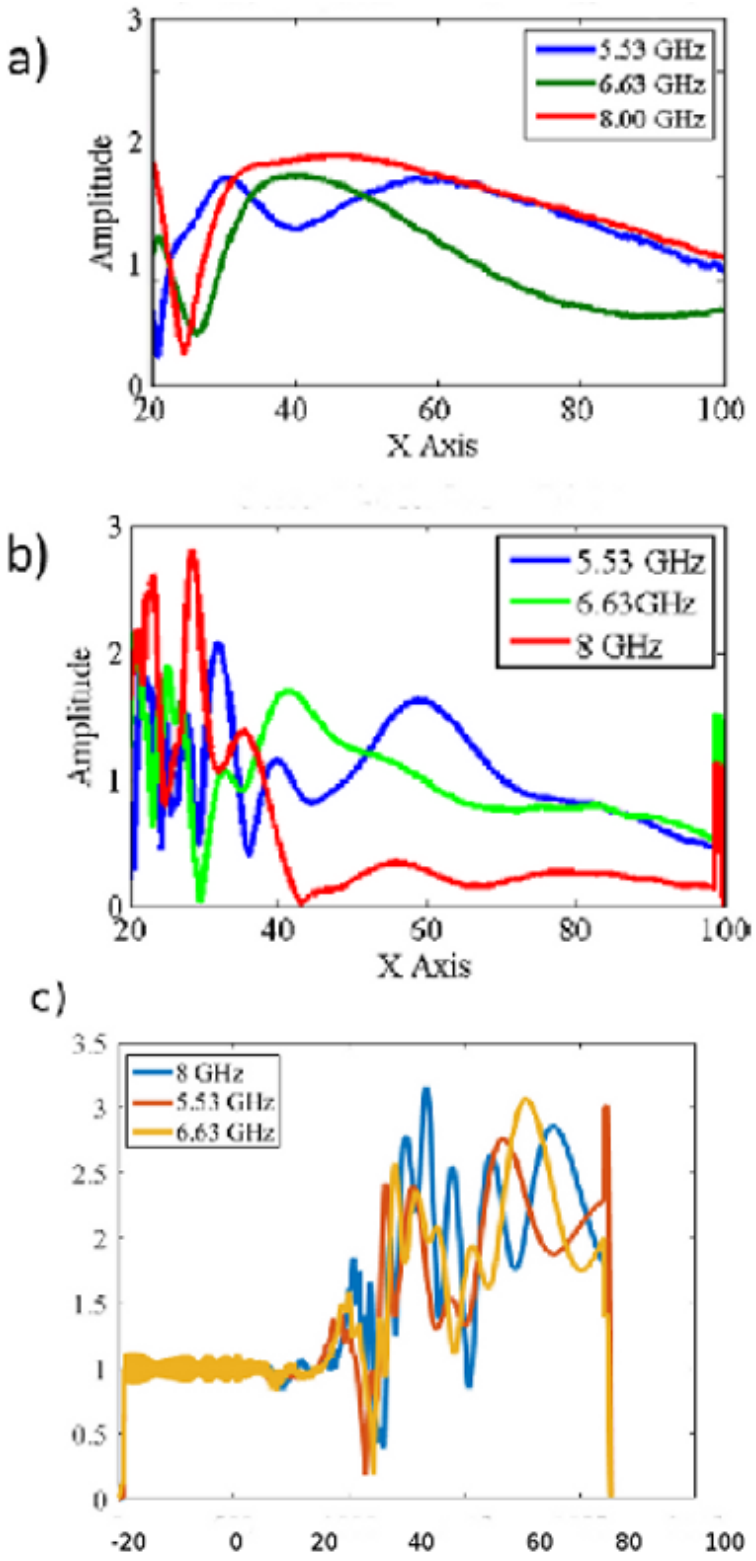

Figure 5.10: The Chromatic Aberration or longitudinal electric field distribution along the optical axis for the Cooke Triplet (top) and the MTM lens (middle) and Dielectric lens (bottom) at 5.53 GHz, 6.63 GHz and 8.00 GHz.

The Chromatic aberration is on of the most important aberrations which optical designers use to quantify the performance of any system of lenses. The Chromatic Aberration is due to the dispersion in a medium refracting light by differing amounts depending on the frequency of the incident light ray. It results is a different focal length for light frequencies with a different frequency.

The Chromatic aberration (C) for the four lenses is calculated using a Gaussian pulse which was launched at 0 degrees incidence fig. 5.10 which included frequencies 5.53 GHz, 6.63 GHz and 8 GHz. These are the equivalent at microwave frequencies to the frequencies for blue, green and red light at optical frequencies. The longitudinal chromatic aberration (lCA) is quantified as the difference in focal length or maximum intensity of the lenses at the three different frequencies. The results of the Gaussian pulse FDTD simulation yield a result for C similar to the results for lSA but for a range of frequencies.

Fig. 5.10 shows the intensity of the field along the longitudinal axis at three different frequencies. The Cooke triplet has a larger range of operation as expected and as before in the lSA result where the focal region is spread over a large range resulting in a smooth and wide focal region improving the imaging performance of the lens. If we compare this with the MTM lens we know that it suffers from a narrow bandwidth which is due to the lossy and dispersive nature of its Metamaterial and it is evident that the focal region is narrow and at 6.63 GHz the focus is shifted far back and at 8 GHz it fails to form a focus at all. The MTM Triplet fails to function as a lens outside of a narrow frequency range.

The Dielectric map is an interesting one as this is designed specifically to operate across a wide range of frequencies. The reduced map shows focusing after the lens which is an improvement on the MTM Triplet. The radiation is however highly scattered as we can see from the original FDTD simulation in the region beyond the lens. The Dielectric lens does

show a focus which is not shifted much by a change in frequency confirming our expectation that the all-dielectric map works well across a range of frequencies. The focus is not a smooth one however like the original Cooke Triplet and like the lSA measurement there is a significant amount of energy disbursed before the actual focal point. The dielectric-only Triplet does work across a range of frequencies but it still performs poorly in terms of imaging ability compared to the original Triplet with huge problems introduced from internal forward scattering.

5.8 Conclusion and Discussion

The job of the optical designer is filled with trade-offs and in this section we have seen that the MTM Triplet and reduced map might find applications where it is better than the original Triplet and applications where it would be worse. Different lenses are better suited for different purposes and lenses are usually designed for a specific purpose in mind so making an absolute comparison to say one lens is better than another is practically impossible. We try to analyse the results in this section by looking at the potential use cases of each lens where a certain feature might be beneficial or detrimental. In this way we hope to give an idea of the general properties displayed by the MTM Triplet and Dielectric Triplet. The results contained in the previous chapter are varied for different lenses and each requires analysis and requires an attempt to understand the underlying processes going on. Lenses are usually tailored with a specific application in mind and each of the properties in this chapter requires a different understanding in terms of the nature of the MTM Triplet.

In terms of Chromatic aberration, Distortion and Field Curvature the Cooke Triplet is the best performing lens with the MTM and reduced maps performing less well. The spherical aberration for the MTM lens is smaller for the MTM lens than the original lens. The coma for the MTM lens features a reversed sign. The reduced map has a much more

distorted focal region than the MTM lens and therefore a worse coma than the MTM lens and the original triplet. The distortion for the reduced map is slightly worse than the Cooke triplet and much worse in the MTM triplet. The Astigmatism could not be measured. The field curvature was slightly worse than the original lens in the reduced map and much worse for the MTM lens. The chromatic aberration is much worse in the MTM lens when compared with the Cooke triplet. The Cooke Triplet remains the gold standard in terms of Seidel aberrations with the MTM and reduced maps performing less well overall. We have analysed the primary aberrations (Spherical, Coma, Astigmatism, Field Curvature and Distortion) and the Chromatic aberration from the FDTD simulation of the MTM Triplet, Cooke Triplet, Reduced Map and Single Lens. The focal lengths of the MTM and reduced map are very close to the focal length of the original Cooke triplet. The reduced lens being the worse performer of the three in terms of spherical aberration.

The MTM lens shows excellent performance in terms of wide angle incidence focusing. This is because the MTM Triplet more easily controls the flow of radiation allowing a reduction in monochromatic aberrations when compared with the traditional Cooke Triplet and Reduced Map. The MTM lens does allow more accurate control over the flow of radiation and therefore might allow a greater reduction in spherical aberration in an image. The MTM Triplet does not provide a good replacement for the Cooke Triplet in terms of its ability to correct Chromatic Aberration. In terms of chromatic aberrations the results are much worse for the MTM lenses because of the losses associated with the dispersive MTM region. There are losses associated with the MTM lens which contributes to this smaller focal region. The effect of dispersion on the MTM lens is very strong in reducing any benefits to image quality over a large bandwidth. One of the primary function of the Cooke triplet design is to minimise the chromatic aberration in an image. The advice would be to use the MTM lens to minimize aberrations for a narrow band of frequencies such as the primary Seidel aberrations: Spherical, Coma, Field Curvature, Distortion and Astigmatism. These benefits would

largely be lost if you wanted to implement a wide bandwidth solution as traditional optical lenses in photography are. The MTM triplet might be an improvement in terms of directivity compared to the traditional Cooke Triplet. the MTM and reduced maps have a wider angle of incidence which is a benefit of using transformation optics to design wide angle imaging lenses or antennas. This is in agreement with papers published on using transformation optics for wide angle beam scanning. The reduced map has been matched to free space and the reduction in reflections is a significant feature of this lens when compared to the conventional case. The gain of the MTM lens is much greater than the conventional lens which also agrees with results published on high gain antennas using transformation optics. The improvement is not supported when the reduced map is used. The improvement in wide angle focusing ability means that the distortion for the MTM Triplet is less than the Cooke Triplet.

The reduced map is designed to work over a range of frequencies and is able to form a focus resulting in a good result for chromatic aberration. The reduced map here does suffer from a lot of forward scattering resulting in a poor Spherical Aberration and Coma and Chromatic aberration resulting in worse results than both the original Triplet and MTM Triplet. The reduced map also have improved angle of operation resulting in a better distortion parameter than the original Triplet and in fact MTM Triplet. This is due to the field not being absorbed in the MTM regions which is an improvement.

The job of the optical designer is to design a lens for a purpose. We can say that the Cooke Triplet performs better across the Seidel aberrations and would produce the best image on its own. One might also envisage a situation where the features displayed for the MTM Triplet might be useful. One could also envisage situations were the results for the reduced map might be useful. It would be unproductive to write off any of them completely. This section serves to look more closely at the Seidel aberrations of each of the lenses to explore features shown rather than say one is categorical a better lens for all situations.

Bibliography

[1] Q. Wu, J. P. Turpin, X. Wang, D. H. Werner, A. Pogrebnyakov, A. Swisher, and T. S. Mayer, "Flat transformation optics graded-index (to-grin) lenses," in *Antennas and Propagation (EUCAP), 2012 6th European Conference on*. IEEE, 2012, pp. 1701–1705.

[2] W. X. Jiang, T. J. Cui, H. F. Ma, X. M. Yang, and Q. Cheng, "Layered high-gain lens antennas via discrete optical transformation," *Applied Physics Letters*, vol. 93, no. 22, p. 221906, 2008.

[3] W. Rotman and R. Turner, "Wide-angle microwave lens for line source applications," *Antennas and Propagation, IEEE Transactions on*, vol. 11, no. 6, pp. 623–632, 1963.

[4] F. Friedlander, "A dielectric-lens aerial for wide-angle beam scanning," *Electrical Engineers-Part IIIA: Radiolocation, Journal of the Institution of*, vol. 93, no. 4, pp. 658–662, 1946.

[5] W. Rotman, "Analysis of an ehf aplanatic zoned dielectric lens antenna," *Antennas and Propagation, IEEE Transactions on*, vol. 32, no. 6, pp. 611–617, 1984.

[6] R. Shavit, "Dielectric spherical lens antenna for wireless millimeter-wave communications," *Microwave and Optical Technology Letters*, vol. 39, no. 1, pp. 28–33, 2003.

[7] T. A. Milligan, *Modern antenna design*. John Wiley & Sons, 2005.

Chapter 6

Zernike Image Evaluation for the MTM Triplet

Zernike aberrations are an additional way to characterise the aberrations in an optical system on top of Seidel aberrations. Zernike aberrations are derived from the distorted wavefront aberration and can be used to build a modulation transfer function for a lens which provides a resolution of the lens in terms of spatial frequencies. In order to analyse the wavefront aberrations a point source is placed at the focus of the lenses in the FDTD simulation and the wave exiting the lens is analysed. The Zernike aberrations provide an orthogonal measure of aberration coefficients which don't overlap like Seidel aberrations. The MTM, Dielectric Triplet and Cooke Triplet are analysed and results on there imaging quality derived.

6.1 Zernike Aberrations

The Zernike aberration is an alternative way to characterise the performance of an optical system. Zernike aberrations are a set of polynomials which are summed together to characterise, to a desired degree of accuracy, a deviation of a wavefront from an ideal zero deviation from a wavefront. In this chapter we analyse the MTM, reduced map and original Cooke Triplet as an optical system using waves and wavefront aberrations to build on our

understanding of the optical performance of the device. We investigate the RMS Wavefront Error, the Modulation Transfer Function (MTF) and the Zernike Aberration Coefficients: Piston, Defocus, Spherical Aberration and Secondary SA. In this way we aim to get a better understanding of the optical performance of our MTM and Discrete TO Cooke Triplet.

The mathematical functions that describe wavefront aberrations were described by Frits Zernike in 1934. Frits Zernike went on to win the Nobel prize in 1953 in Physics for the development of Phase Contrast Microscopy. Zernike aberration analysis is commonly used by opticians for fitting spectacles and contact lenses (1). Zernike aberration coefficients are the standard way to quantify wavefront aberrations (2) where each aberration coefficient is independent of the others. It is an innovation on the traditional Seidel aberrations so much so that it is widespread in the optical industry for aberration measurements in the eye (3). Zernike aberrations are used in astronomy, optics, optometry, and ophthalmology. It has also yielded some interesting results in experiments on the performance in how well an object is hidden in optical cloaking (4).

The wavefront aberration function, W, can be decomposed into a sum of Zernike polynomials which form an orthogonal set of order m and n

$$W(\rho,\theta) = \sum_{n=0}^{\infty}\sum_{m=0}^{n} z_{nm}\sqrt{\frac{2(n+1)}{(1+\delta_{m0})}}V_n^m \rho cos(m\theta) \tag{6.1}$$

Where V_m^n is the radial variable with the constants n (radial degree) and m (azimuthal degree) which determine the individual aberrations in Zernike aberrations and z_{nm} is the weighting of each Zernike polynomial . Primary spherical aberration is m=0 n=4 where a chart of the Zernike polynomials are shown in fig. 6.1. n can go on to infinity and m is limited by the order n of the set. The δ_{m0} function is the Kronecker delta which is equal to one when m equals zero and zero when m does not equal one. The $\rho cos(m\theta)$ is the angular part of the

function radius ρ and angle θ with the integer m.

In the following sections we will characterize a lens using the wavefront aberration function which we will measure from the FDTD simulation to yield results on the Modulation Transfer Function (MTF) and Zernike aberrations for each of the lenses. The wavefront aberration function of the lenses calculated from the FDTD simulation where a source is places at the focus and a plane wave exits the final surface. The MTF and Zernike aberration coefficients give a more detailed picture of the aberrations created by the MTM lens and the discrete TO lens.

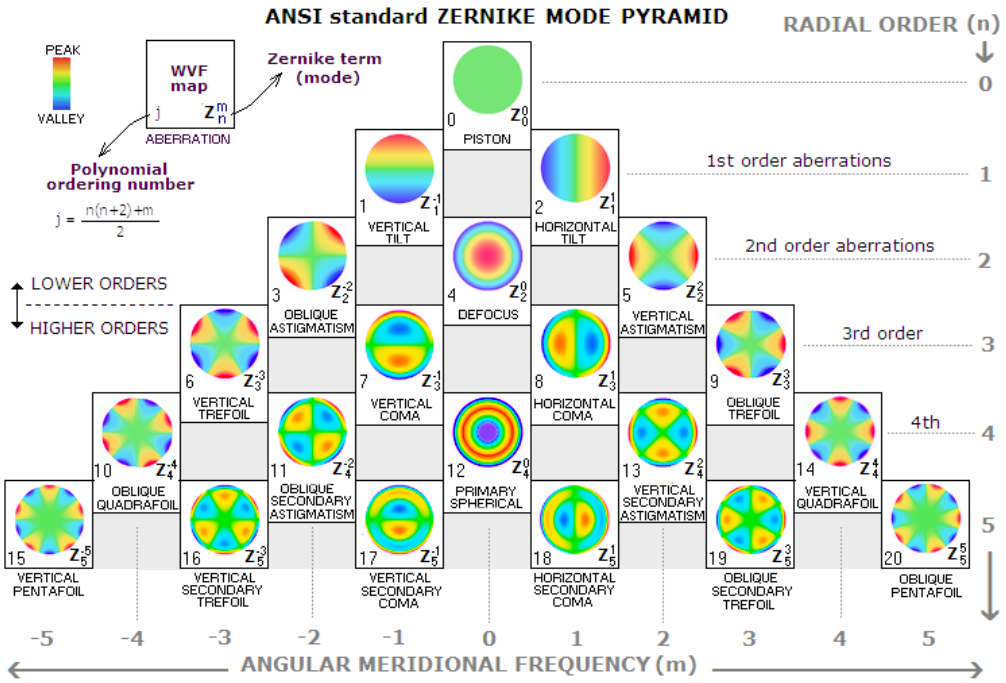

Figure 6.1: The Zernike aberration pyramid with radial order on the right hand side in ascending order going down and the m order along the bottom. Each figure of the pyramid shows the picture of the distorted wavefront for that aberration, its polynomial number j on the left of the insert and its Zernike mode of the form Z_n^m to the right of the insert. The Peak and Valley are in read and blue and the equation for polynomial ordering j is given as well as the distinction between lower order and higher order aberrations.

6.2 The Wavefront Aberration Function

In this section we derive the distorted wavefront function from the FDTD simulation of the lens in order to extract the Zernike aberration coefficients. We use the lenses derived in previous sections of the thesis for the TO Triplet, reduced map triplet and original Cooke Triplet and the FDTD simulation of these devices. We extract a wavefront aberration function from these simulations by placing the source at the focus. The wavefront exiting each of the lenses is then measured. This distorted wavefront is them compared between the MTM Triplet, Dielectric Triplet and Cooke Triplet to yield results for the performance of the lenses.

The wavefront aberration function was extracted from the FDTD simulation, see fig. 6.2 using tools available in Matlab such as a scatter plot, the matrix grid nature of Matlab and cubic spline interpolation. To find the contour of the wavefront in the FDTD simulations we take the point where Ez was zero for the region one wavelength beyond the lens was used to map an iso contour of the edge of a wave. This was found to produce the most stable wavefront with which to extract and compare the lenses. The final wavefront in the FDTD Simulation domain is sampled from the simulation results. The program was written in Matlab and sampled at every grid cell in the transverse axis. The wavefront was fitted to a polynomial to yield an analytical result in terms of x which can be mathematically treated in the preceding sections and split into Zernike aberration coefficients. Fitting a cubic spline gives the best result for interpolation of the sampled data points for reconstructing the wavefront. Cubic spline interpolation is a method of taking distinct points and fitting a line function to them in the process known as interpolation where the polynomial is selected where the residual amount is the lowest for this order. This resulted in an analytical function for each of the lenses which closer fitted the points on the wavefront.

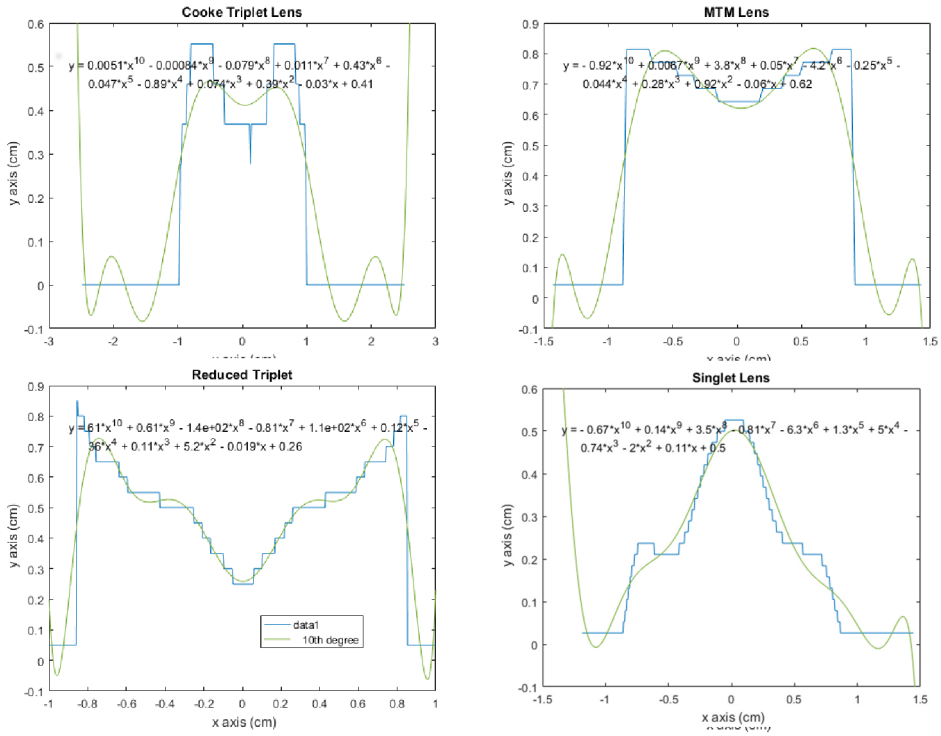

Figure 6.2: The sampled wavefront and the fitted polynomial for the MTM lens, the Cooke Triplet, the reduced map and the single lens. These are the polynomials which are used in the calculation of the Zernike Coefficients.

The wavefront polynomial is computed from the sampled wavefront for each of the lenses. The results show the Cooke Triplet has the smallest wavefront aberration function with the MTM Triplet and then reduced Triplet being the worst performing result. We might expect the Cooke Triplet design to have the smallest wavefront error and it does. A Greater PV Ratio in the MTM lens are most likely due to lossy regions of meta-materials at the edges. The reduced map is also significantly worse in the PV ratio compared to the original Cooke Triplet and a slight improvement on the MTM Lens. The higher PV ratio for the reduced lens compared to the Cooke Triplet could be due to the isotropic approximation not being exactly met in the design of the reduced lenses and the wavefront aberration looks alot more distorted potentially due to reflections and scattering inside the lens. Overall the Cooke Triplet has the smallest PV Ratio, which measures the magnitude of the wavefront aberration function, compared with the two Dielectric and MTM lenses.

The Root Mean Squared (RMS) error gives the average deviation from an ideal surface across the whole wavefront. The smaller the wavefront aberration the better the performance. The root mean squared wavefront deviation gives a performance of each lens. The average deviation of the wavefront from a plane surface yields the root mean squared optical path difference, see table 6.1 and is usually measured in units of wavelength. The PV ratio is the difference between maximum and minimum values of the wavefront however RMS is a better measure as it gives an average measure across the lens.

	MTM Lens	DCT Triplet	Cooke Triplet	Singlet
RMS Error	0.16	0.1	0.05	0.1554
PV Ratio	0.72	0.41	0.125	0.5

Table 6.1: The RMS wavefront error and PV ratio in units of unit wavelength of the wavefront aberration function sampled for the MTM lens, DCT lens and the Cooke Triplet lenses.

The MTM lens possesses the largest PV Ratio however the reduced map has the largest wavefront RMS error which is an average deviation from a flat plane wave. The Cooke Triplet has a lower RMS error in its wavefront aberration function than the MTM and reduced map which you might expect. The Cooke triplet is within the level you would expect for an optical instrument whereas the MTM lens and reduced lens are much larger making them a poor choice as an optical lens when compared to the Triplet in respect of raw image aberrations. The reduced map appears to be a slightly better option than the MTM lens in terms of wavefront aberration function making it a potential option for imaging in this situation so long as you realise the imaging performance will be less than the original Triplet.

6.3 The Radial Zernike Coefficients

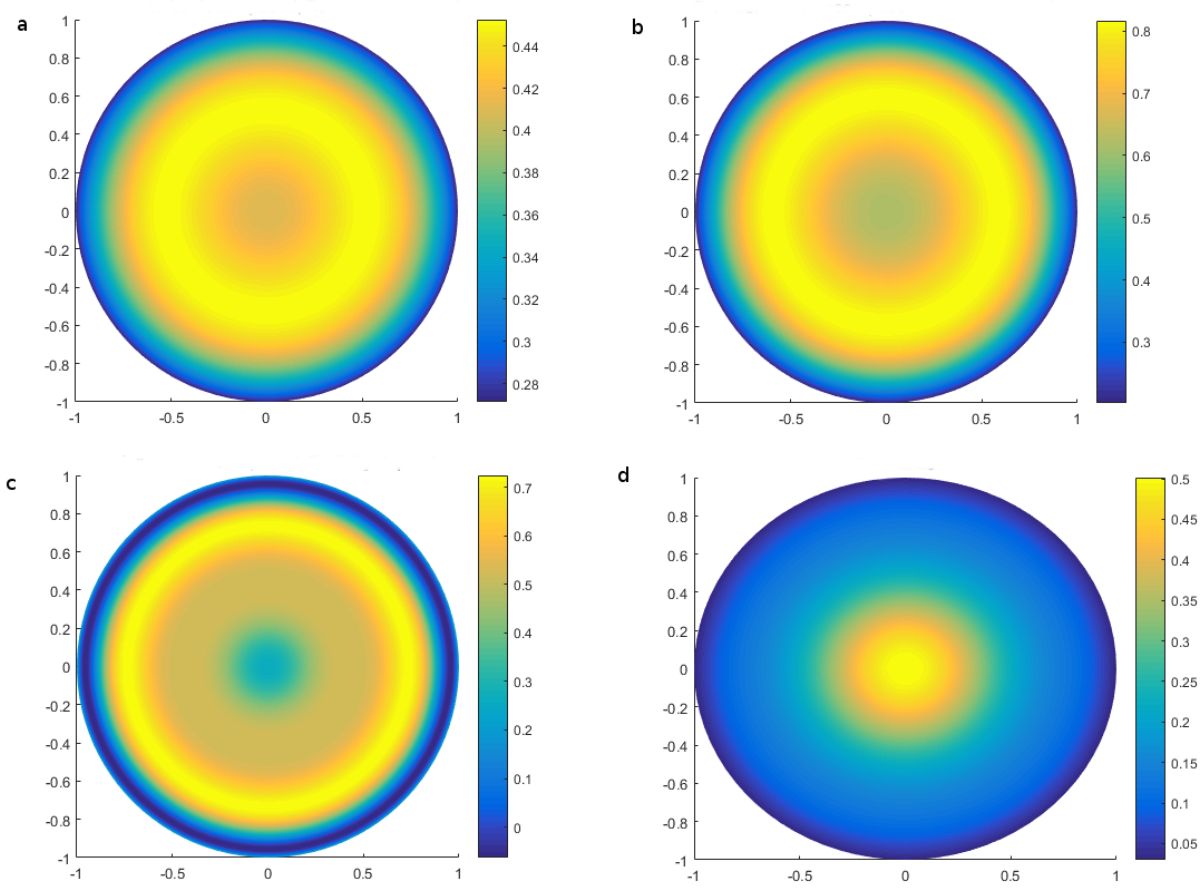

Figure 6.3: The wavefront aberration on a Zernike unit disk for (a) the Cooke lens, (b) the MTM map and (c) the reduced Triplet and (d) a single lens.

In this section we will use the wavefront aberration function as an input for a deconvolution into orthogonal Zernike polynomials. In the previous section we have extracted a polynomial for each lens, is derived from the curve fitting of the distorted wavefront. This is the input to a MATLAB script called deco.m which deconvolves the polynomial into its constituent Zernike coefficients for each aberration. These polynomials will yield Zernike coefficients which will tell us more detail on the imaging properties and wavefront aberrations present in the MTM, reduced and Cooke triplet. The wavefront aberrations are rotated on a unit disk as is typical for the calculation of Zernike aberrations, see Fig. 6.3. The wavefront

aberration function is taken as a polynomial for each lens, rotated on a unit disk and then fitted to a set of Zernike polynomials where the radial polynomials are the strongest because there is no angular component in our simulation. In order to derive the Zernike aberrations from the wavefront aberration function a Matlab program is used which takes a function as an input and calculates it as a sum of the Zernike polynomials. This program computes the Zernike functions $Z_{nm}(r,\theta)$ for modes n and m evaluated at positions (R,θ) using the scale of a unit circle. The normalization factor $\sqrt{((2-\delta(m,0))*(n+1)/\pi)}$ is used with the Kronecker delta $\delta(m,0)$ so that the integral over the unit circle (from r=0 to r=1, and θ=0 to theta=2π) is unity. The wavefronts fitted to a unit Zernike disk are scaled to a maximum value.

n	m	Zernike function	Normalization
0	0	1	$1/\sqrt{(\pi)}$
1	1	r * cos(theta)	$2/\sqrt{(\pi)}$
1	-1	r * sin(theta)	$2/\sqrt{(\pi)}$
2	2	r^2 * cos(2*θ)	$\sqrt{(6/\pi)}$
2	0	($2r^2$ - 1)	$\sqrt{(3/\pi)}$
2	-2	$r^2 * sin(2*\theta)$	$\sqrt{(6/\pi)}$
3	3	$r^3 * cos(3*\theta)$	$\sqrt{(8/\pi)}$
3	1	$(3*r^3-2*r)*cos(\theta)$	$\sqrt{(8/\pi)}$
3	-1	$(3*r^3-2*r)*sin(\theta)$	$\sqrt{(8/\pi)}$
3	-3	$r^3 * sin(3*\theta)$	$\sqrt{(8/\pi)}$
4	4	$r^4 * cos(4*\theta)$	$\sqrt{(10/\pi)}$
4	2	$(4*r^4-3*r^2)*cos(2*\theta)$	$\sqrt{(10/\pi)}$
4	0	$6r^4-6r^2+1$	$\sqrt{(5/\pi)}$
4	-2	$(4*r^4-3*r^2)*sin(2*\theta)$	$\sqrt{(10/\pi)}$
4	-4	$r^4 * sin(4*\theta)$	$\sqrt{(10/\pi)}$
6	0	$20r^6-30r^4+12r^2-1$	$\sqrt{(7/\pi)}$

Table 6.2: This table shows the first radial Zernike aberrations up to secondary spherical aberration. The wavefront aberration function is only radially dependant therefore of all first 36 Zernike coefficients only these radial aberrations are non-negligible.

The Zernike functions are products of the Zernike radial coefficients and sine and cosine

functions

$$\begin{matrix} Z_n^m(r,\theta) \\ Z_n^{-m}(r,\theta) \end{matrix} = R_n^m(r) \begin{matrix} sin(m\theta) \\ cos(n\theta) \end{matrix} \tag{6.2}$$

The index n is called the degree of the function defined as n=0,1,2.. while m is called the order and while m= -n ... 0 ... n with the condition that (n-m) must be an even number and k = 0,1,2,... . The radial polynomials are defined using a series representation of a sum of multiples of r^2

$$R_n^m(r) = \sum_{k=0}^{(n-m)/2} \frac{(-1)^k(n-k)!}{k!(\frac{n+m}{2}-k)!(\frac{n-m}{2}-k)!} r^{n-2k} \tag{6.3}$$

The principle of orthogonality states that any function f(r,θ) can be expressed as a sum of Zernike modes.

$$f(r,\theta) = \sum_{n=0}^{\infty} \sum_{m=-n}^{n} a_{nm} Z_n^m(r,\theta) \tag{6.4}$$

This is the same principle used in sine and cosine functions for Fourier analysis of waves. The coefficient of these modes a_{nm} are the Zernike coefficients which quantify the amount of Zernike aberration is contained in a function.

$$a_{nm} = \int \int_{circle} f(r,\theta) Z_n^m(r,\theta) r dr d\theta \tag{6.5}$$

by representing data in this way we can decompose a complicated structural aberration in terms of a small number of coefficients associated with Zernike modes. a_{nm} can be determined from the integral of the the function f(r,θ). This is the aberration function which we calculated in the previous section for the MTM, reduced map and Cooke Triplet. The integrals are solved using a numerical quadrature routine to produce results for the Zernike coefficients.

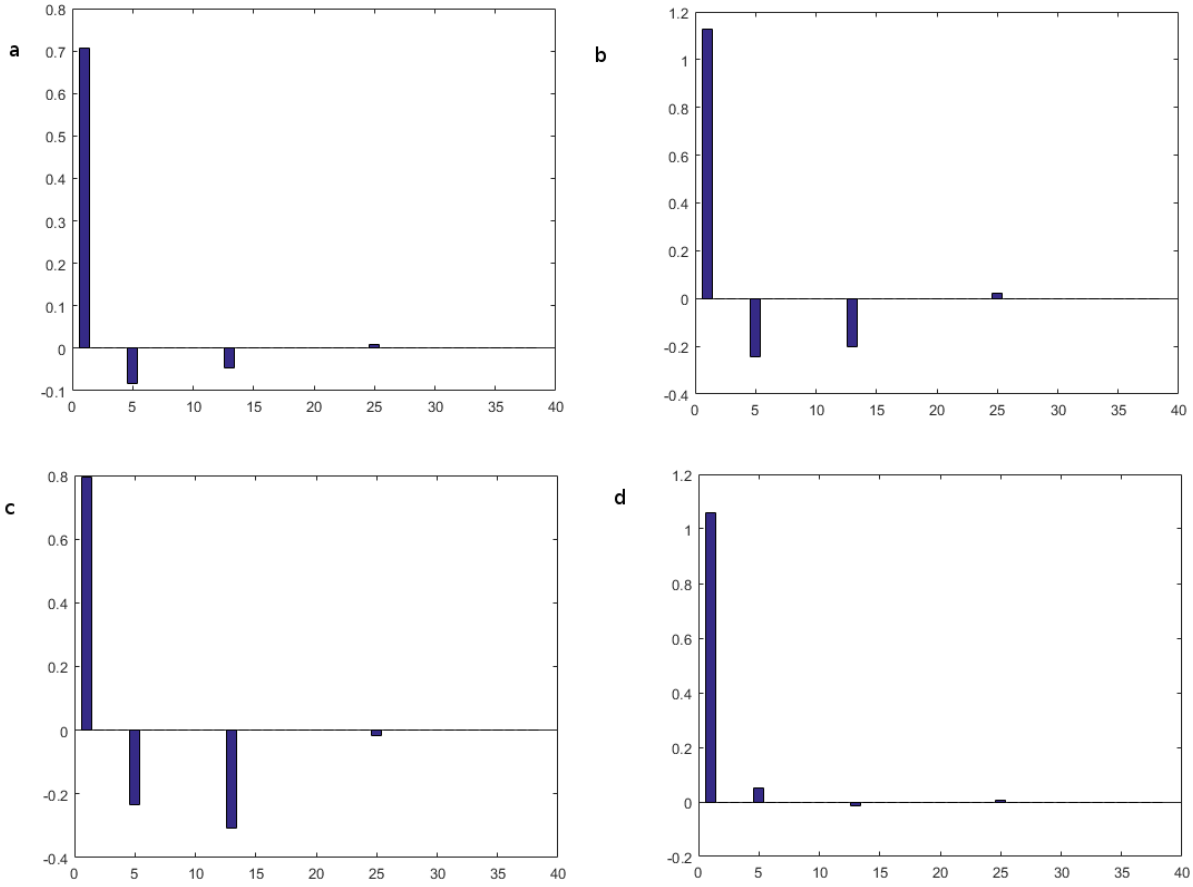

Figure 6.4: A bar chart of the Zernike aberration coefficients for the Cooke Triplet (a), the MTM Triplet in (b) and All-Dielectric lens (c) and the single lens (d).

The Piston, see Fig. 6.4 is the first radial Zernike coefficient Z_0^0, using the notation Z_m^n and is the lowest for the Cooke Triplet as expected, see table 6.3. Piston Z_0^0 is transverse defocus so transverse scattering which we know occurs in the MTM lens would result in larger piston in the MTM and reduced maps. The second radial Zernike coefficient is tilt Z_{-1}^1 which was zero in our calculations because we only had data along one axis which was rotated about a point meaning that there was no tilt in the calculation. The defocus Z_0^2 is the third radial Zernike polynomial and for the Cooke Triplet which is around -0.1 is also the lowest compared to the MTM lens and the Dielectric implementation which are both around -0.2. The Single lens is used to compare the performance of the Cooke Triplet against

the others and we can see that it has the highest Piston, the MTM is about as high as a single lens and the reduced map is an improvement although not as good as the original which would lend weight to the importance of this measure in terms of imaging quality. The remaining aberrations are higher order deviations in the aberration function and may be due more to internal scattering in the lens and shape of the focus which is smaller in the single lens compared with the Triplets. The Dielectric map has a much larger Spherical Aberration compared to the other two Triplet maps which is the result of the more greatly distorted wavefront aberration function and unit Zernike disk suggesting more aberration from internal scattering and in the case of the MTM lens losses from Metamaterial regions.

Name	MTM lens	Reduced map	Cooke Triplet	Single Lens
Z_0^0 (Piston)	1.1285	0.7940	0.7080	1.0610
Z_0^2 (Defocus)	-0.2425	-0.2338	-0.0817	0.0496
Z_0^4 (Spherical)	-0.2005	-0.3071	-0.0471	-0.0135
Z_0^6 (Secondary SA)	0.0235	-0.0168	0.0083	0.0071
Z_0^8(Tertiary SA)	0.0001	0.0001	0.0000	0.0003

Table 6.3: The results for the radial Zernike aberration coefficients for the MTM lens, reduced map and the Cooke Triplet. The remaining radial Zernike coefficients calculated were smaller than 0.0001 where not included in this table and do not appear on the bar chart however values were recorded for these coefficients.

The wavefront aberration polynomial calculated for each lens in the previous section was validated by adjusting for Piston Z_0^0 and the efficacy of this calculation can be translated immediately into lenses performance by moving the lens according to this defocus and then looking if there is an improvement in the wavefront aberration when the lenses is focused. One of the major factors the wavefront polynomial depends on is the position of the source, which is placed at the focus. It should be able to correct these lenses for the focal length by moving them by the amount determined in the defocus in order to achieve better performance.

We performed simulations in FDTD for these lenses adjusted for defocus. These results were not included so as to not confuse the debate about different lenses one corrected for defocus and another not. Indeed since the results for all three lenses have very small defocus values and so all that happens is the Zernike parameters approximate the values shown in table 6.3.

6.4 The Modulation Transfer Function

The Modulation Transfer Function (MTF) gives the resolution of a lens in terms of spatial distance and in this chapter we use the wavefront aberration functions to calculate the MTF for the MTM lens, reduced map, singlet and Cooke Triplet. The MTF of a lens is a measure of its ability to resolve between light and dark in units of spatial frequency. In fig. 6.5 the spatial frequency along the bottom axis is how many black and white lines or cycles can fit in one mm and still be resolved by a lens. The higher the spatial frequency the more difficult a lens system has resolving between tightly spaced individual patterns or slits. In this section we present a method of calculating the Modulation Transfer Function using the wavefront aberration function as the input to compare this property of the lenses.

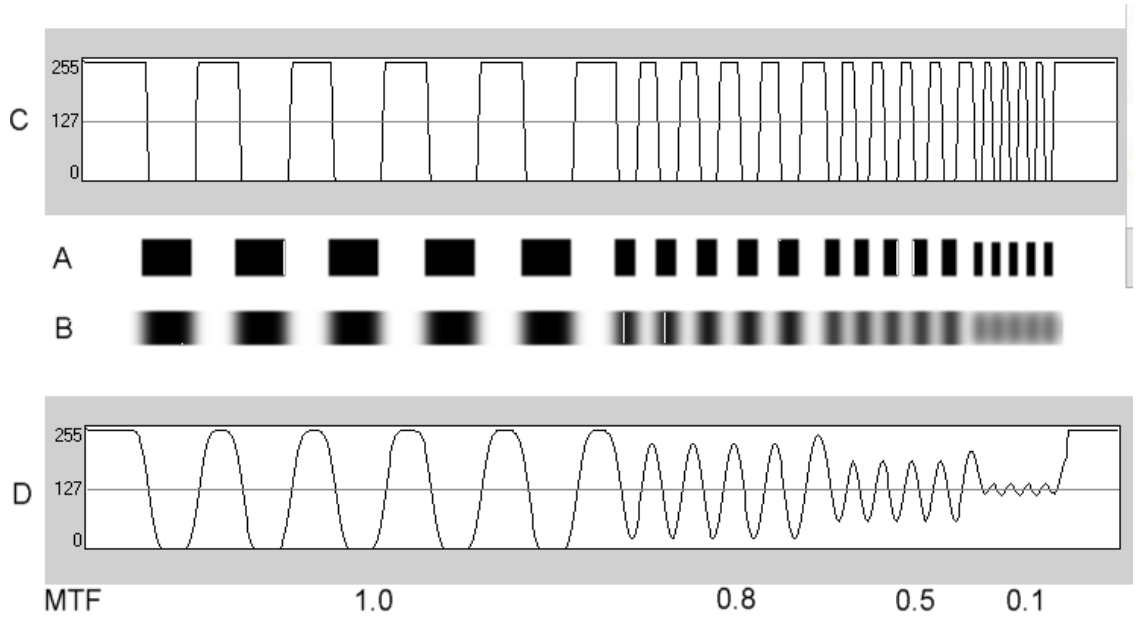

Figure 6.5: The MTF explained using 2 test patterns and 2 intensity distributions. The original test pattern is (A). B is the original test image of that pattern through an optical imaging system of lenses. C is the pattern of the original test pattern where 255 is completely black and 0 completely white. D is the line pattern of the test image (5).

The definition of MTF is

$$MTF = (maxintensity - minintensity)/(maxintensity + minintensity) \tag{6.6}$$

fig. 6.5 demonstrates this using a graph of colour white at 0 and black at 255 for a test pattern and the test image of the pattern. The blurring of the lines in the image is due to diffraction and the lens could be a perfect lens and these blurs due to diffraction would still occur, thus the diffraction limit is the best that a conventional lens could achieve. The test pattern shown in fig. 6.5 has an MTF of 1 in the initial section, 0.8 in the next section, 0.5 in the next and 0.1 in the last section.

This program calculates the MTF from the Zernike aberration coefficients. It plots the MTF of the Zernike Polynomial specified by: n = highest power or order of the radial

polynomial term, m = azimuthal frequency of the sinusoidal component, for a given n, m can take on the values -n, -n+2, -n+4,..., n-4, n-2, n, d = pupil diameter in mm, Wrms = rms wavefront error coefficient and lambda for wavelength. The wavefront aberration polynomial sampled in the previous section is used as the input to construct a wavefront aberration function made from Zernike polynomials. The radial Zernike polynomials shown in table 6.2 are modelled with the correct Zernike aberration coefficient. The derived MTF for the original Cooke triplet, singlet, MTM lens and all dielectric implementation is found using the following calculation using the Point Spread Function. The fitted polynomial coefficients are used to reconstruct a wavefront aberration from Zernike radial polynomials and then this wavefront is used to calculate the MTF.

The MTF is calculated in Matlab using a code which generates the results for fig. 6.6 which uses the results from the previous section for the Zernike coefficients to calculate the PSF, OTF and MTF for each of the lenses. The Point Spread Function (PSF) is a Fourier transform of the pupil function of an aberrated lens and can be described by a generalised pupil function, P, which is a circular aperture of value one. The unit spacing of the pupil function is 0.1 of a wavelength and a radius is 30 times the wavelength where the wavelength is 0.0375m. A combination of Zernike wavefront aberrations calculated from the previous section are then combined to make up the aberration function which is calculated as follows

$$\mathbf{P}(x,y) = P(x,y)exp[jkW(x,y)] \tag{6.7}$$

$$PSF_{(x,y)} = \frac{1}{(\lambda^2 d^2 A_p)} FT(p_{(x,y)})(e^{-i2\pi(W(x,y))\lambda})^2 \tag{6.8}$$

The MTF is related to the point spread function via Fourier transforms of the optical transfer function. The OTF is the Fourier transform of the Point Spread Function PSF

and the PSF is the square absolute of the inverse of the Fourier transformed pupil function then from convolution theorem

$$OTF(s_x, s_y) = \frac{FT(PSF)}{FT(PSF)_{s_x=0, s_y=0}} \tag{6.9}$$

and the MTF is the modulus of the OPF

$$MTF(s_x, s_y) = ||OTF_{(s_x, s_y)}|| \tag{6.10}$$

where s_x and s_y are the spatial frequencies in the x and y direction where the results for this calculation are presented in fig. 6.6.

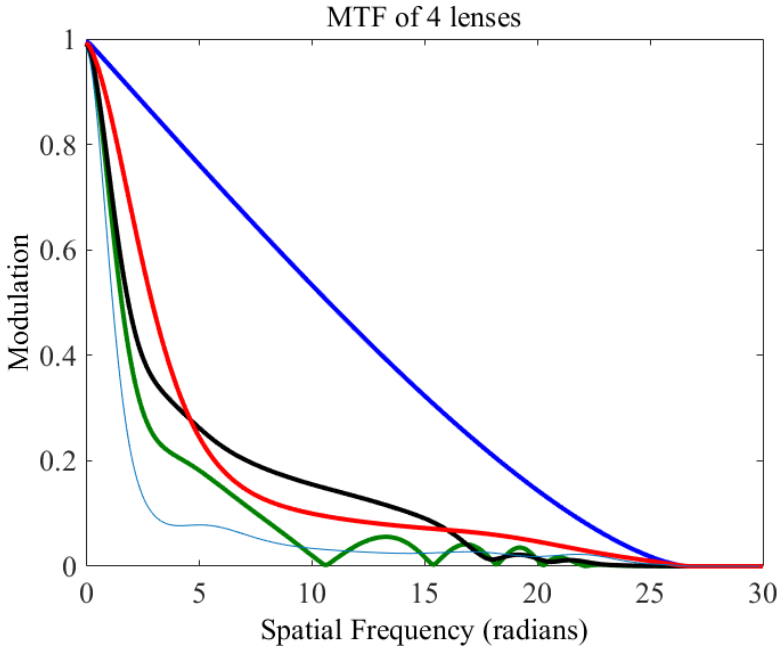

Figure 6.6: The MTF results of the Zernike aberration coefficients for the Cooke Triplet (black), the MTM triplet (green), the Singlet (light blue) and the Reduced map (red) and the aberration free case (dark blue). For the case of 1 the modulation of the lines from black to white would be perfect however for a case of zero no distinction between black and white lines would be possible.

The MTF results tell us that the Cooke Triplet has the best MTF across the majority of the spatial frequencies as expected from previous experimental results. The Metamaterial map appears to perform worse in terms of image evaluation, see fig. 6.6 which is due to the Metamaterial regions which are lossy, scattering and interfering with the image at low spatial frequencies. The reduced map is slightly better performing than the Metamaterials lens which is encouraging. It has better performance than The Cooke Triplet at the extremes of spatial frequency: at lower spatial frequencies (less than 1/5 units of wavelength) and then at greater than 1/16.5 units of spatial frequency. This would suggest that the reduced map while not performing overall as well as the original Cooke would not be a bad choice if there were size and weight constraints and a better choice than the full MTM lens. The MTM lens appears to have a few resonant frequencies were the MTF drops to zero highlighting the problems with its limited, narrowband operation inherent to the design. The single lens performs the worst in terms of MTF across the whole of the spatial frequency spectrum compared with the Cooke Triplet and transformed Triplets as you would expect. The Cooke triplet has the highest MTF in the majority of the spatial frequency range here from the range 5^{-1} λ to 16.5^{-1} λ suggesting that it is the best imaging lens with the MTM lens suffering from limiting bandwidth and the reduced map suffering slightly in terms of imaging due to scattering and reflections due to limitations from the quasi-orthogonal approximation however the performance is similar overall for both lenses.

6.5 Conclusion and Discussion

As with the previous chapter analysis the results between the MTM lens and the Cooke Triplet then results are encouragingly similar for our design approach and this can be seen in the results for the wavefront aberration function and the Zernike disk aberration function.

We can see that both the reduced map and MTM implementations of the Triplet do suffer from increased Zernike aberrations and lower MTF than the original Triplet. This is due to internal scattering from the quasi-orthogonal approximation in the reduced map and from losses from metamaterials in the MTM lens. The Triplet performs better than the sampled single lens. This is encouraging if you were considering using either of these approaches in designing an imaging lens.

In terms of the performance of the lenses this chapter has verified that the Cooke triplet is performing well and that the MTM lens and reduced map are performing poorer in terms of the PV ratio and RMS error which are measures of the wavefront. This validates analysing the lenses in terms of wavefront aberrations and gives further insight into the imaging properties of the MTM lens. The Spherical Aberration in the MTM lens is large and about the same as the Cooke Triplet with the reduced map being nearly an order of magnitude larger. The RMS error and Zernike aberrations is much lower for the Cooke Triplet than the MTM and reduced maps. This further validates the results that overall the Cooke Triplet has the lower aberrations. There are slight improvements such as the Dielectric lens has a better MTF over low and high spatial frequencies. This lens might make a better choice of lens than the original Cooke Triplet resolving lower and higher spatial frequencies, if this was the frequency range which matched the object you wanted to resolve. For the wavefront aberrations, Zernike aberrations and MTF the MTM lens and the Dielectric lenses are worse than the original Cooke Triplet. The MTF shows a measure for the spatial frequency resolution of the lens and shows the MTM lens performing worse than the conventional triplet across a wide range of spatial frequencies aside from very small spatial frequencies and a slight bounce at around 200 lp/cm.

Bibliography

[1] W. Charman, "Wavefront aberration of the eye: a review," *Optometry & Vision Science*, vol. 68, no. 8, pp. 574–583, 1991.

[2] D. R. Iskander, M. J. Collins, M. R. Morelande, and M. Zhu, "Analyzing the dynamic wavefront aberrations in the human eye," *Biomedical Engineering, IEEE Transactions on*, vol. 51, no. 11, pp. 1969–1980, 2004.

[3] J. Liang and D. R. Williams, "Aberrations and retinal image quality of the normal human eye," *JOSA A*, vol. 14, no. 11, pp. 2873–2883, 1997.

[4] T. Ergin, J. Fischer, and M. Wegener, "Optical phase cloaking of 700 nm light waves in the far field by a three-dimensional carpet cloak," *Phys. Rev. Lett.*, vol. 107, p. 173901, Oct 2011. [Online]. Available: http://link.aps.org/doi/10.1103/PhysRevLett.107.173901

[5] G. D. Boreman, *Modulation Transfer Function in Optical and Electro-Optical Systems*. SPIE Press, Bellingham, WA.

[6] J. Goodman, "Introduction to fourier optics," 2008.

Chapter 7

Conclusion and Further Work

7.1 Overall Conclusion

We have designed a MTM lens and reduced map using Dielectric-only Transformation Optics based on the Cooke Triplet which possessed the benefit of being made of a single block of dielectrics reducing size, weight and price for a variety of applications. This would have benefits in improving the ability to construct complicated optical systems which often uses many lenses to achieve a specific optical effect. Transformation optics also allows the opportunity to create compressed lenses which take up less space with comparable imaging properties. The imaging properties from the MTM Triplet such as focal length, wavefront aberration Error and Zernike aberrations are all comparable to the original Cooke Triplet.

The Cooke triplet minimizes Seidel aberrations in an image: Spherical, Coma, Astigmatism, Field curvature and Distortion better than our MTM and Dielectric only Triplets according to our results ever so slightly. A reduced map triplet would possess no metamaterials and is not subject to losses and narrow-band operation therefore is not effected strongly by Chromatic aberration however it's imaging ability is not as good as the original Triplet due to simplification of the material parameters resulting in poorer overall imaging ability.

The Coma and Spherical Aberration is worse for the MTM and Dielectric Triplet compared to the Cooke Triplet. This is due to the inherent losses of the metamaterials in the MTM Triplet. The limitation which yields a slight degradation in the Dieletric implementation Triplet in terms of imaging is that the quasi-orthogonal approximation is exactly an approximation resulting in internal scattering and interference.

While we can confirm that a MTM Cooke Triplet and reduced map can be designed using transformation optics the design is limited by its narrowband operation which results in losses. This is a problem in many transformation optics devices however we have employed the all-dielectric transformation optics approach to create a lens without Metamaterials. The reduced non-MTM map performs as well in many respects as the original Cooke Triplet and our results confirm this to be the case.

We do record other beneficial qualities from the Metamaterial Triplet such as a large wide angle scanning ability which has been recorded in the literature and an exact replication of focusing ability for on axis rays as the original design. This benefit of wide angle beam scanning for a wide band width has been used by commercial company Kymeta based on research showing that this Dielectric only lens could operate as a lightweight and compact satellite communications antenna. We also note that the MTM triplet can be matched to free space and reflections internally are less which improves the gain or power of the lens. This improvement in the Field of View results in the Distortion and Field Curvature being improved very slightly in the MTM Triplet and Dielectric Triplet compared with the Cooke Triplet. There are additioanl benefits of the lens created using transformation optics compared to the conventional Triplet lens.

7.1.1 Recommendations for Future Work

Arising from the research carried out during this work, areas of potential further research could include:

1 Demonstration of a prototype MTM Triplet is a requirement for further work. The device could be tested and fabricated using dielectrics in a antenna and or microwave laboratory. This would verify the results here and also provide a confirmation of the results in experiments. The experiment would be carried out on a 2D scanner fed by a waveguide with a probe measuring the field in a similar way to how the invisibility cloak was experimentally verified in the laboratory (1).

2 Research into GRIN optical materials is required. If the device is to be fabricated at optical frequencies then more research must be done on optical metamaterials and the limitations of current gradient index optical lenses. The current design would only function for microwaves and antennas but combined with the latest 3D printing techniques this would offer new configurations for high gain antennas not previously possible.

3 A 2D + body of revolution (BOR) or A 3D FDTD analysis so that all the Zernike terms could be calculated as suggested in the previous chapter. This would allow off axis Zernike aberrations to be calculated for the MTM lens, the dielectric map and the original Cooke triplet. This would show the full spectrum of Zernike aberration results for the lenses and give a more complete picture of the device performance in terms of wavefront aberrations.

4 Development of a ray tracing simulation in Matlab to calculate the spot diagrams and other imaging properties. Commercial software packages typically use ray tracing to calculate imaging properties of lenses however the ability to do this in gradient index lenses is limited. The ability to calculate the Seidel aberrations and chromatic aberration from a ray tracing calculation in inhomogeneous materials was initiated (2; 3; 4)

and the gradient index of the MTM and reduced Triplets applied to this calculation. A full ray tracing calculation would be advantageous to determine more imaging properties of the MTM Triplet and then compare those results with commercially available imaging properties for the Triplet such as spot diagrams and results for the Primary Seidel aberrations.

Additional work from the thesis includes the rectangular Luneburg lens design which was patented by BAE systems. This shows that a flat Luneburg lens has been fabricated using the ray tracing technique and grid generation software and the electromagnetic behaviour verified in electromagnetic experiment validating its ability. This results in a square luneberg lens which can be added conveniently as a component to an optical system. The Luneberg lens is a perfect imaging device similar to a Maxwell's Fish eye lens which has the limitation of being a sphere. I designed a flat Luneberg lens which is not contained in this thesis and was patented by BAE Systems for there internal usage.

Perfect Imaging using drains to allow sub-wavelength imaging was tested as a hypothesis and we find that drains artificially create the impression of a sub-wavelength image (5). Researchers debated if a sub-wavelength imaging might be possible using a drain at the focus of a transformation optics designed lens. We concluded that this drain would be an artefact of imposing the metallic drain in the simulation results rather than evidence of sub-wavelength imaging (6; 7; 8). The peak caused by wavelength imaging and focusing to a conductive tip create the same electromagnetic field pattern in FDTD. I completed my own simulations in Matlab to investigate the matter however the conclusion was that this metallic drain would damage the image. I implemented the field transformation lens and calculated the field distribution which demonstrates that a flat field transformation lens performs equally as well as one designed using transformation optics designed in this thesis. This validates the field transformation method for designing flat lenses. These results showed that an artificial drain did impose some interesting results in terms of the electromagnetic

field pattern but featuring a drain artificially can not be said to increase the ability of the lens to achieve sub-wavelength imaging. My conclusions were similar to those reported in the literature that introducing a drain at the focal point did not create wavelength imaging but rather simply the illusion of it due to the light being focused onto a metallic point and the research was discontinued. This being said the process of designing a sub-wavelength imaging device using Transformation Optics without Metamaterials is a fascinating topic with much potential avenues of research yet to be investigated.

Bibliography

[1] R. Liu, C. Ji, J. Mock, J. Chin, T. Cui, and D. Smith, "Broadband ground-plane cloak," *Science*, vol. 323, no. 5912, pp. 366–369, 2009.

[2] F. Bociort and J. Kross, "Seidel aberration coefficients for radial gradient-index lenses," *JOSA A*, vol. 11, no. 10, pp. 2647–2656, 1994.

[3] F. Bociort and M. van Turnhout, "Generating saddle points in the merit function landscape of optical systems," in *Optical Systems Design 2005*. International Society for Optics and Photonics, 2005, pp. 59 620S–59 620S.

[4] F. Bociort, "Chromatic paraxial aberration coefficients for radial gradient-index lenses," *JOSA A*, vol. 13, no. 6, pp. 1277–1284, 1996.

[5] U. Leonhardt, "Perfect imaging without negative refraction," *New Journal of Physics*, vol. 11, no. 9, p. 093040, 2009.

[6] F. Sun and S. He, "Can maxwell's fish eye lens really give perfect imaging?" *arXiv preprint arXiv:1009.4751*, 2010.

[7] R. Merlin, "Maxwells fish-eye lens and the mirage of perfect imaging," *Journal of Optics*, vol. 13, no. 2, p. 024017, 2011.

[8] R. Blaikie, "Comment on perfect imaging without negative refraction," *New Journal of Physics*, vol. 12, no. 5, p. 058001, 2010.